DESIGN AND IMPLEMENTATION OF A 0.6 GHz-0.9 GHz RF-SQUID READ-OUT SYSTEM AND INVESTIGATION OF RF-SQUID SIGNAL CHARACTERISTICS

A THESIS

SUBMITTED TO THE DEPARTMENT OF ELECTRICAL AND

ELECTRONICS ENGINEERING

AND THE INSTITUTE OF ENGINEERING AND SCIENCE

OF BILKENT UNIVERSITY

IN PARTIAL FULFILLMENT OF THE REQUIREMENTS

FOR THE DEGREE OF

MASTER OF SCIENCE

By
Taylan EKER
June, 2005

I certify that I have read this thesis and that in my opinion it is fully adequate, in scope and inquality, as a thesis for the degree of Master of Science.

Assist. Prof. Dr. Mehdi Fardmanesh (Supervisor)

I certify that I have read this thesis and that in my opinion it is fully adequate, in scope and inquality, as a thesis for the degree of Master of Science.

Assoc. Prof. Dr. Iman Askerzade

I certify that I have read this thesis and that in my opinion it is fully adequate, in scope and inquality, as a thesis for the degree of Master of Science.

Prof. Dr. Ziya Ider

Approved for the Institute of Engineering and Science:

Prof. Dr. Mehmet Baray

Director of Institute Engineering and Science

ABSTRACT

DESIGN AND IMPLEMENTATION OF A 0.6 GHz - 0.9 GHz RF-SQUID READ-OUT SYSTEM AND INVESTIGATION OF RF-SQUID SIGNAL CHARACTERISTICS

Taylan EKER

M. S. in Electrical and Electronics Engineering

Supervisor: Assist. Prof. Dr. Mehdi Fardmanesh

June 2005

Design and implementation of a transceiver system for rf-SQUID (Superconducting Quantum Interference Device) operation is investigated in this work. Besides, experiments to characterize the rf-SQUID have been performed using the implemented system.

The steps in system design and implementation are presented. The difficulties and drawbacks of the system are reported and alternative techniques required to overcome these problems are determined. Also, for the operation of the rf-SQUID at much higher frequencies, different transceiver architecture is proposed and possible drawbacks are stated.

Using implemented system, several experiments were performed on two high T_c rf-SQUID gradiometers with a tank-circuit resonating at 720 MHz. In these experiments, the frequency and amplitude of the applied rf signal were swept and output flux to voltage transfer signal (modulation added by rf-SQUID), V_{spp}, and incoming rf signal spectrum are reported and analyzed.

Keywords: Superconductor, rf-SQUID, Transceiver

ÖZET

0.6 GHz - 0.9 GHz FREKANS BANDINDA ÇALISAN RF-SQUID ÖLÇÜM SISTEMININ TASARIMI VE GERÇEKLENMESI, VE RF-SQUID SINYAL ÖZELLIKLERININ ARASTIRILMASI

Taylan EKER

Elektrik ve Elektronik Mühendisligi Bölümü Yüksek Lisans

Tez Yöneticisi: Yrd. Doç. Dr. Mehdi Fardmanesh

Haziran 2005

Rf-SQUID (Üstüniletken Kuantum Girisim Cihazi) çalismasi için bir verici-alici sistemi tasarlanip gerçeklenmistir. Bunun yani sira, gerçeklenen sistem kullanilarak, rf-SQUID tanimlamasina yönelik deneyler yapilmistir.

Sistemin tasarimi ve gerçeklenmesinde izlenen adimlar sunulmustur. Sistemde karsilasilan zorluklar ve dezavantajlar raporlanmis ve bu problemlerin asilmasi için gereken baska tekniklere belirlenmistir. Ayrica, rf-SQUID'in daha yüksek frekanslarda çalismasi için farkli bir verici-alici mimarisi önerilmis ve olasi dezavantajlar belirtilmistir.

Gerçeklenen sistem kullanilarak, 720 MHz frekansinda tinlayan bir depo devresiyle iki yüksek kritik sicaklikli rf-SQUID meyilölçer üzerinde çesitli deneyler yapildi. Bu deneylerde, uygulanan rf isaretin genlik ve frekansi kaydirilmis, çikista alinan V_{spp} (rf-SQUID tarafindan eklenen modülasyon) ve gelen rf isaretin tayfi raporlanip incelenmistir.

Anahtar Kelimeler: Üstüniletken, rf-SQUID, Verici-Alici

Acknowledgement

I would like to express my sincere gratitude to Dr. Mehdi Fardmanesh for his supervision, guidance, suggestions, and encouragement throughout my graduate study.

I would also like to thank my graduate committee members, Assoc. Prof. Dr. Iman Askerzade and Prof. Ziya Ider for reading and commenting on the thesis.

I would like to express my endless thanks to Ali Bozbey and Rizwan Akram for sharing their experiences with me and their essential help in performing the SQUID signal measurements. Also, I am thankful to my colleagues in Aselsan for their help.

Finally, I am so thankful to my wife, my parents and sisters, and my wife's family for their support.

Contents

List of Figures

LIST OF FIGURES

LIST OF FIGURES

LIST OF FIGURES

LIST OF FIGURES

List of Tables

To my beloved wife, Çigdem...

Chapter 1

INTRODUCTION AND LITERATURE SURVEY

1.1 Introduction

Superconductivity phenomenon was discovered in very early 20^{th} century. Before the discovery of superconductivity, the gradual decrease in the resistance of a cooled material had been known. After the success in liquefying helium and reaching temperatures below 4.2 K, several materials were found that showed a sharp drop in their resistance, going to the superconducting state later at some temperature, called the critical temperature, T_c. After the discovery of superconducting materials with higher critical temperatures, a new area was opened in the field. Besides, with the discovery of superconductivity, several theories about the principles of superconductivity mechanism were established [1].

Superconductivity is used in a variety of applications including power lines and cables, magnetic levitation trains, detection systems, microwave, biomedical systems, etc [1]. In this study, the focus is on Superconducting Quantum Interference Devices (SQUIDs) made of high temperature class of superconductors (detection systems).

SQUIDs are extremely sensitive magnetic flux detectors. The operation of them is based on the modulation created on the applied current caused by an externally applied

flux. They cover a wide range of applications such as biomagnetic systems, geophysics, commercial systems for measurement of magnetic properties of materials and non-destructive evaluation (NDE) of materials and electronic warfare [1], [2].

In this work, an experimental read-out system for rf-SQUIDs is designed and implemented. Following implementation of the system, several experiments are performed to investigate characteristics of rf-SQUID for different frequencies and amplitude levels. While explaining these works, several references are inserted for interested readers.

This thesis has three main parts. In the first part (LITERATURE SURVEY), background information about the basics of SQUID operation and the principles of typical read-out electronics are introduced. Second part (DESIGN AND IMPLEMENTATION OF AN EXPERIMENTAL RF-SQUID READ-OUT SYSTEM) contains the design and implementation of an rf-SQUID read-out system in details for each subsystem block. The third part (EXPERIMENTS AND RESULTS) consists of the experiments performed to characterize some rf-SQUIDs and the results.

Chapter 5 (CONCLUSIONS AND FUTURE WORK) describes the works to be done in the future to improve the performance of the implemented system and the strategy to be taken for higher frequency read-out systems.

1.2 Briefly Superconductivity

Superconductivity is a phenomenon displayed by some materials below a critical temperature, T_c. At this condition (below T_c), superconductors exhibit zero dc electrical resistance and perfect diamagnetism [1]. A very important characteristic of superconductivity is due to the properties of the junctions made out of these materials,

namely Josephson Junctions. The Josephson Junctions are the base of the very valuable devices such as super-sensitive magnetic sensors, SQUIDs (Superconductive Quantum Interference Devices), which are the base devices in this work and further studied in the following sections.

For years, several scientists put forward various theories about superconductivity, some of which are London Theory, Ginzburg Landau Theory, and the BCS theory (first letters of Bardeen, Cooper, and Schrieffer, who have modeled Type I superconductors). Of listed theories, the BCS theory greatly attracted attention of superconductivity societies. The BCS theory is out of the scope of this report and more information about it and other theories can be found in [4]-[8]. Superconductor materials can be grouped into two types, namely type I and type II superconductors. Characteristically, type I superconductors totally exclude magnetic fields below their T_c. If the applied magnetic field is of low amplitude, Type II superconductors can exclude it but they can only partially exclude high amplitude magnetic fields [1]. Interested readers may refer to [4]-[5] for more information on Type I and Type II superconductor properties and characteristics.

Another classification of superconductors can be made upon the critical temperature they exhibit. By 1973, metallic alloys having critical temperatures up to 23 K were found [4]. In 1986, Bernorz and Müller [6] showed the possibility of copper oxides to have higher critical temperatures (35 K). After this point, new materials having critical temperatures up to 136 K were found. As a result, superconductors with critical temperatures below 23 K are typically low-temperature superconductors (LTS), and that with critical temperatures above 23K are mostly high temperature superconductors (HTS) [4]. In Figure 1.1, critical temperatures of some superconductors are shown [4]. The study of this work is focused on HTS devices made of $YBa_2CO_3O_{7-x}$ material.

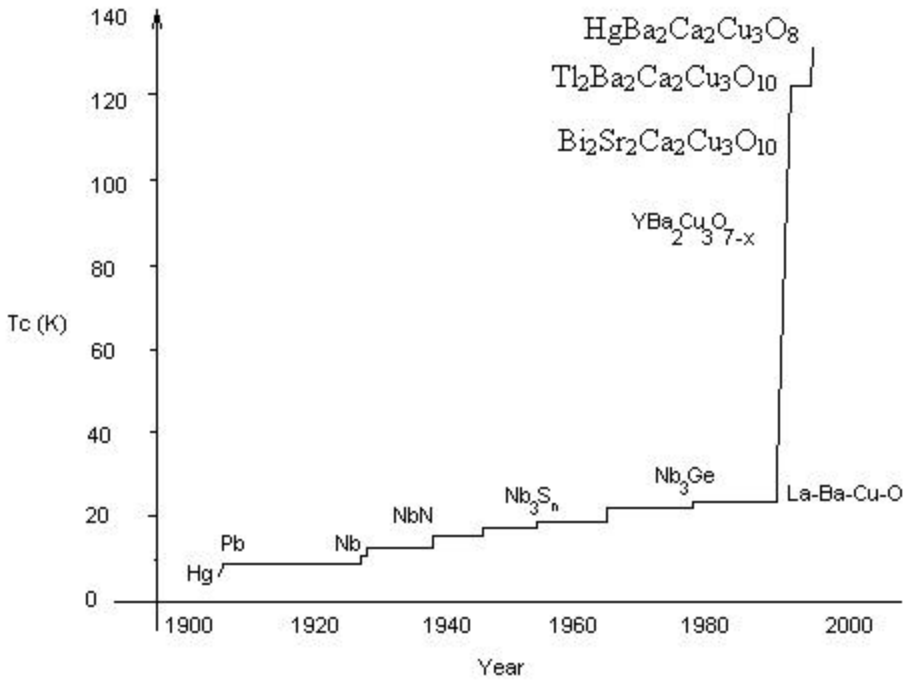

Figure 1.1 Critical temperature of various superconductors on years base

1.3 SQUID

SQUID is a sensitive flux to voltage transducer and has the sensitivity that makes it popular among all magnetic sensors. Main properties of SQUIDs include extremely high sensitivity (down to a few $fT/Hz^{-1/2}$), wide bandwidth (DC – 10kHz), broad dynamic range (>80dB), and quantative nature in terms of intercepted magnetic field [10]. These properties of SQUIDs allow engineers to design and implement efficient detectors working on wider bandwidths with higher dynamic ranges.

The principles of SQUIDs are based on the Josephson Junctions, which is reviewed in the following subsection.

1.3.1 Josephson Junction

Josephson Junctions are primary for the understanding of SQUIDs. Mainly, two superconductors having insulating barrier in between form a Josephson Junction. There are different types of Josephson Junctions such as S-N-S (Superconductor-Normal Conductor-Superconductor) and S-I-S (Superconductor-Insulator-Superconductor). In Figure 1.2, a basic figure of Josephson junction is shown. In this figure, sides 1 and 2 are superconductors, which are intercepted by an insulator (S-I-S).

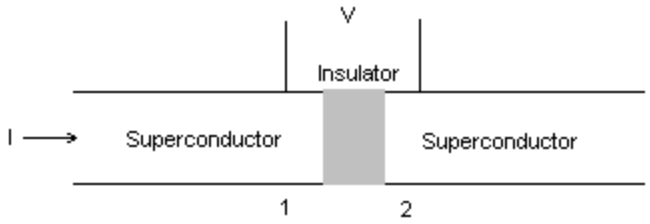

Figure 1.2 The Josephson Junction

The superconductivity wave function characterizing the condensed electron pairs (cooper pairs) assuming large separation between superconductors, can be defined as [4];

$$y = |y(\vec{r})| e^{\{i[q(r)-(2e_f/h)t]\}} \tag{1.1}$$

where $|y(r)|$ is square root of cooper pair density and $q(r)$ is the phase of the wave function of cooper pairs. For the two sides of the junction, the wave function of cooper

pairs has unlocked phases. Reduction of separation between the superconductors leads to penetration of y into the barrier and thus phases become locked (no energy reduction during cooper pair transition). An applied voltage can also accomplish pair tunneling. In this case, the phases are uncorrelated again, but the phase difference between the junctions evolves as a function of the applied voltage [3], [4].

Time evolution of wave functions for two sides of the junction can be described by,

$$\begin{aligned} i\hbar\frac{\partial y_1}{\partial t} &= U_1 y_1 + K y_2 \\ i\hbar\frac{\partial y_2}{\partial t} &= U_2 y_2 + K y_1 \end{aligned} \tag{1.2}$$

In this equation, y_1 is the wave function of pairs on side 1 and y_2 is the wave function for side 2. U_1 and U_2 are the energies of the wave functions on side 1 and side 2, respectively and, K is the coupling coefficient between the wave functions. It is assumed that a voltage (V) is applied on the junction and an energy difference of $U_2 - U_1$ is created between two sides of the junction. If the energies of the wave functions in the middle of the insulator is assumed to be zero, equation 1.2 becomes,

$$\begin{aligned} i\hbar\frac{\partial y_1}{\partial t} &= -\frac{e^* V}{2} y_1 + K y_2 \\ i\hbar\frac{\partial y_2}{\partial t} &= \frac{e^* V}{2} y_2 + K y_1 \end{aligned} \tag{1.3}$$

Besides, the wave functions at two sides of the insulator can be expressed by the electron pair densities, $y_k = \left(n_{sk}^*\right)^{\frac{1}{2}} e^{iq_k}$. Also, the phase difference between the two

sides of the junction can be introduced as $d = q_2 - q_1$. In the light of these equations, equation 1.3 can be reinterpreted as (by separating real and imaginary parts) [4]

$$\frac{\partial n_{s1}^{*}}{\partial t} = \frac{2}{\hbar} K (n_{s1}^{*} n_{s2}^{*})^{\frac{1}{2}} \sin d \tag{1.4}$$

$$\frac{\partial n_{s2}^{*}}{\partial t} = -\frac{2}{\hbar} K (n_{s1}^{*} n_{s2}^{*})^{\frac{1}{2}} \sin d \tag{1.5}$$

$$\frac{\partial q_1}{\partial t} = -\frac{K}{\hbar} \left(\frac{n_{s2}^{*}}{n_{s1}^{*}} \right)^{\frac{1}{2}} \cos d + \frac{e^{*} V}{2\hbar} \tag{1.6}$$

$$\frac{\partial q_2}{\partial t} = -\frac{K}{\hbar} \left(\frac{n_{s1}^{*}}{n_{s2}^{*}} \right)^{\frac{1}{2}} \cos d - \frac{e^{*} V}{2\hbar} \tag{1.7}$$

According to equations 1.4 and 1.5, there is a tendency of rate of change in pair densities in both sides of the junctions. This tendency is opposite for each side of the junction. This tendency is balanced by the current that flows through the circuit, which connects two junctions. If the phase gradient from side 1 to side 2 is positive, i.e. $d > 0$, the current density from side 2 to side 1 becomes positive. Thus, there should be transfer of electrons from side 1 to side 2 ($\frac{\partial n_{s1}^{*}}{\partial t} < 0, \frac{\partial n_{s2}^{*}}{\partial t} > 0$). This requires the coupling to be negative.

According to equation 1.4, the current density through the junction is,

$$J = J_c \sin d \tag{1.8}$$

where J_c is the current density whose derivation is out of the scope of this thesis. Also taking the difference between equation 1.6 and 1.7, and equating n_{s1}^{*} and n_{s2}^{*} to each

other, the time derivative of the phase difference between the two sides of the junction can be found.

$$\frac{\partial d}{\partial t} = \frac{2e}{\hbar} V \tag{1.9}$$

In equation 1.9, e^* is taken as $-2e$. Equations 1.8 and 1.9 are the Josephson relations, which express the electron pair behaviors [4], [10].

More details on Josephson Junctions can be found in [4], [5], [10], and [12].

1.3.2 SQUID Types

SQUIDs are fabricated by placing Josephson junctions on super-conducting loops. There are basically two types of SQUIDs which are of interest in this subsection namely rf-SQUID and dc-SQUID. They have different number of Josephson Junctions intercepting their loop as explained in the following parts.

- **dc-SQUID**

dc-SQUID is formed by a superconducting loop interrupted by two Josephson Junctions. In Figure 1.3, a sample plot of the dc-SQUID and its electrical equivalent schematic is shown.

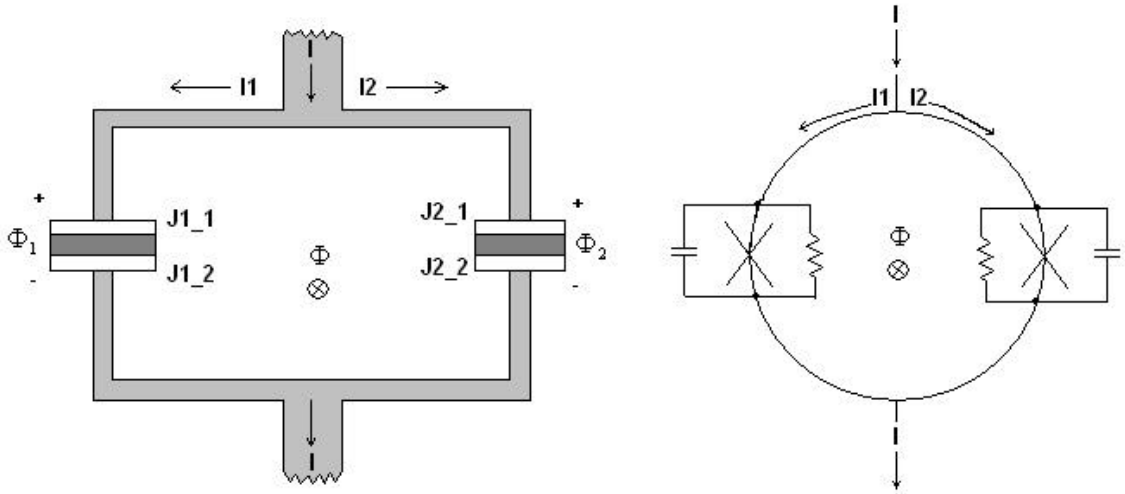

Figure 1.3: dc-SQUID and its equivalent schematic view

An externally applied magnetic flux creates a phase difference across the junctions where the phase difference is detected as voltage via electronics [4]. The logic in DC-SQUID operation is very similar to the logic in RF-SQUID operation in the sense that the detected voltage is a measure of the phase difference across the junctions.

The relation between the induced voltage and applied flux into SQUID at constant bias points is plotted in Figure 1.4. In this figure, y-axis is the applied current on the tank circuit and x-axis is the resulting voltage induced on the tank circuit. Besides, two extreme cases of applied flux on SQUID are plotted in the same figure. According to the figure, a constant current applied to DC-SQUID biases the SQUID at a fixed current on the y-axis. If the externally applied flux (an AC flux) exceeds the flux quanta, which is intercepted by SQUID, the output voltage would be a periodic function between the quanta points. So the output voltage would roughly be a sinusoidal [10] waveform

oscillating between V_{max} and V_{min}. By changing the current bias, the values of V_{min} and V_{max} can be changed; leading to higher signal levels at the output. A sample plot of the output waveform is shown in Figure 1.5 [10], [4].

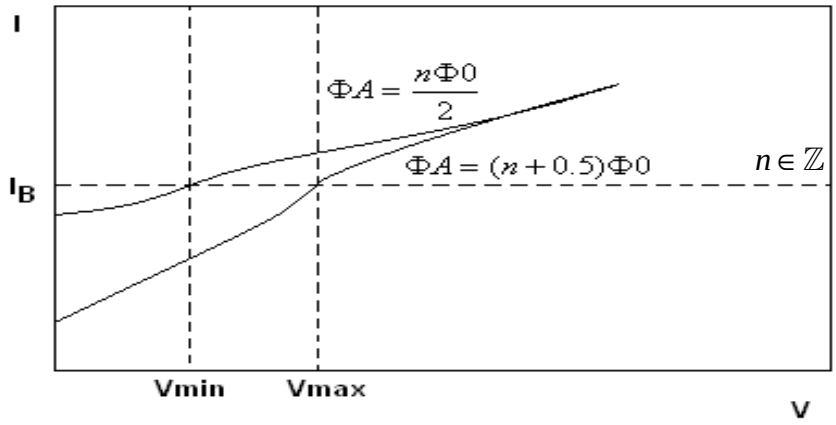

Figure 1.4: Voltage created in SQUID tank circuit versus applied current for changing flux.

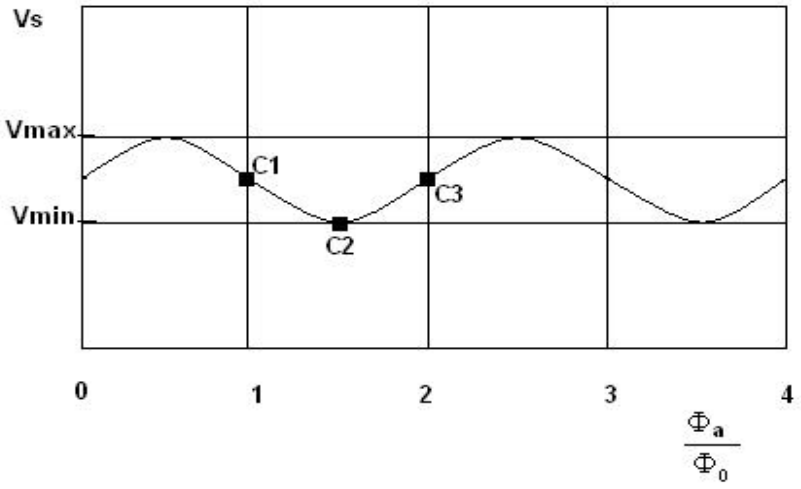

Figure 1.5: Output voltage of dc-SQUID for changing applied magnetic field

According to Figure 1.5, if we bias the SQUID at fixed currents, the SQUID can be in conditions C1, C2, or C3. Assume that the SQUID is biased at point C1. In this condition, the SQUID's response to the applied flux (can be rf-flux, which is the case in rf-SQUID) of frequency w would be at frequency of w again. If the SQUID were biased at point C3, the phase of the response would be reversed at frequency of w again. Lastly, if the SQUID is biased at point C2, there would be a phase transition of 180 degrees during an ac cycle, so the output voltage would have a frequency of $2w$ [10], [12], [13].

More details about the DC-SQUIDs will not be investigated in this report, since it is out of the scope of this thesis. Interested readers can find further information and related equations about DC SQUID in [4], [12], [15], and [16].

- **rf-SQUID**

rf-SQUID is a superconducting loop similar to DC SQUID, but it is interrupted by only one Josephson Junction. A plot of rf-SQUID and its equivalent electrical schematic is demonstrated in Figure 1.6.

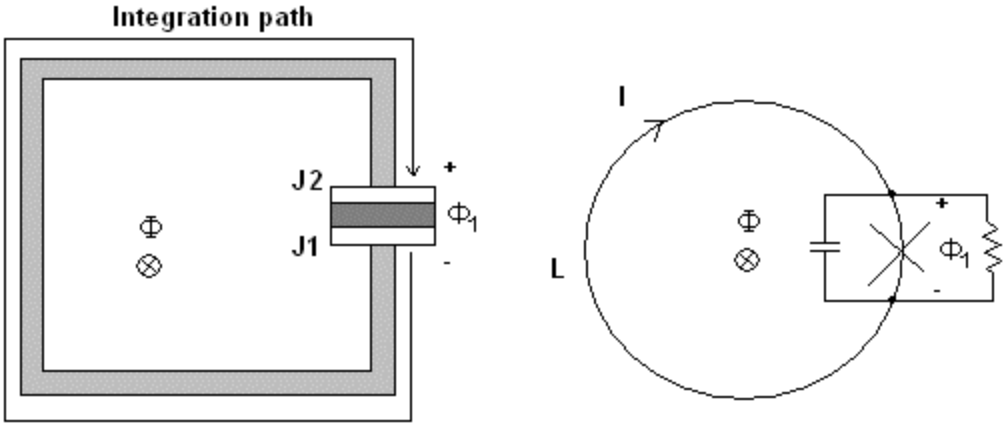

Figure 1.6: rf-SQUID and its equivalent schematic view

As mentioned in section 1.3.1, electron pairs in superconducting state are described by an order parameter, which is similar to a many body wave function.

$$y(r) = |y(r)|\, e^{iq(r)} \tag{1.10}$$

Considering the rf-SQUID shown in Figure 1.6, if we take the integral of the phase of the wave function around the superconducting loop clockwise, and using superposition, it is found that;

$$\int_{J1}^{J2} \nabla q . d\vec{l} = \oint \nabla q . d\vec{l} - \int_{J2}^{J1} \nabla q . d\vec{l} \tag{1.11}$$

The term on the left side of equation 1.11 is the integral on the loop except the discontinuity. This integral is a multiple of $2p$. The first integral on the right side is

taken on the loop including the discontinuity, and it should be the phase difference between the junction edges [4]. The right side of the equation can be adjusted as

$$(-\frac{2p\Phi}{\Phi_0}-(q_{J2}-q_{J1}))-\frac{2e}{\hbar}\int_{J1}^{J2}\vec{A}.d\vec{l} \tag{1.12}$$

where the phase gradient is written in terms of vector potential [17]. Then, equation 1.11 becomes [4], [12];

$$-2np+(q_{J2}-q_{J1})=-\frac{2p\Phi}{\Phi_0}-\frac{2e}{\hbar}\int_{J1}^{J2}\vec{A}.d\vec{l} \tag{1.13}$$

Also the gauge invariant phase across the junction is defined as [4];

$$f=q_{J2}-q_{J1}+\frac{2e}{\hbar}\int_{J1}^{J2}\vec{A}.d\vec{l} \tag{1.14}$$

and equation 1.13 becomes;

$$f=2np-\frac{2p\Phi}{\Phi_0} \tag{1.15}$$

In equation 1.15, Φ is flux inside the loop. If an external field is applied to the SQUID, the flux relation becomes;

$$\Phi=\Phi_{ext}+LI \tag{1.16}$$

where L is the effective inductance of the SQUID loop, and I is the total current flowing through the loop. If we adapt the last equations (1.15 and 1.16) into relevant positions of equation 1.8, the current through the loop becomes [4], [13];

$$I = I_c \sin(-2p\Phi / \Phi_0) \tag{1.17}$$

and the total flux inside the loop becomes [13];

$$\Phi = \Phi ext - LIc \sin(-2p\Phi / \Phi_0) \tag{1.18}$$

In equation 1.18, an important parameter for the operation of rf-SQUID can be extracted. This parameter is called the hysteresis parameter, pb_l, where b_l is given by;

$$b_l = \frac{2LI_c}{\Phi_0} \tag{1.19}$$

According to this parameter, rf-SQUID can be hysteretic ($pb_l > 1$) or non-hysteretic ($pb_l < 1$) [12]. In Figure 1.7, a plot of Φ_{ext} vs. Φ is shown for different hysteresis parameter values.

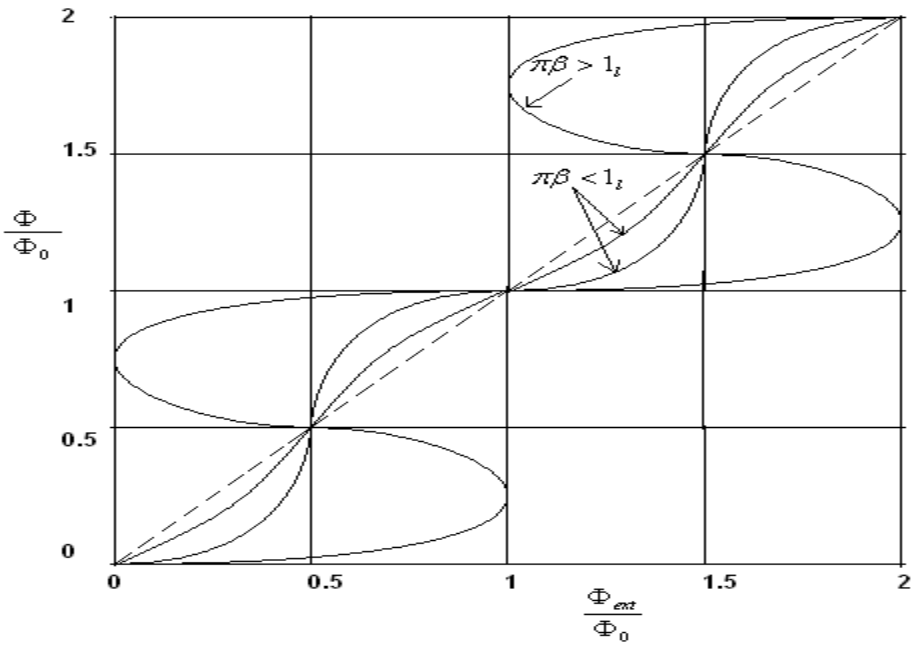

Figure 1.7: Total flux vs applied flux for different hysteresis parameter values

According to Figure 1.7, in hysteretic mode, total flux penetrating the rf-SQUID, has a negative slope in the curve as opposed to that in non-hysteretic case. Figure 1.8, taken from [12], shows the same curve in which the loop is closed. To see the effect of discontinuity, those two graphs (Figures 1.7 and 1.8) should be compared to each other. For more information about the theory and applications for SQUID, reader is encouraged to read [28].

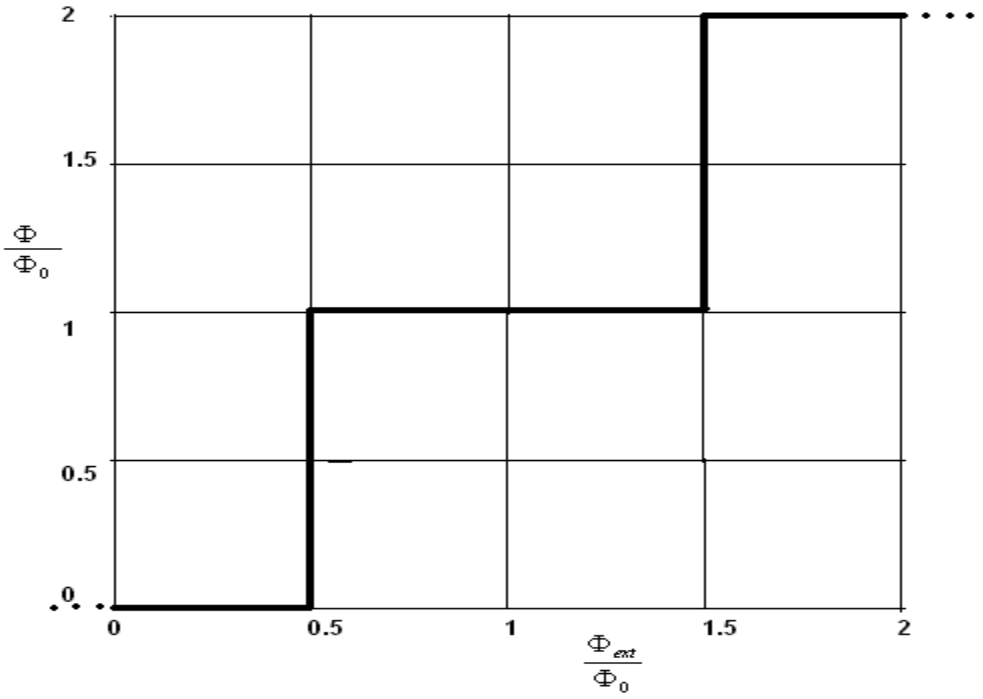

Figure 1.8: Total flux versus applied flux for a superconducting ring

Implementation of rf-SQUID (and dc-SQUID) is another area of interest. This subject is out of the scope of this report. Information about techniques and technologies in implementation of SQUIDs can be found in [18]-[22].

1.4 Conventional Read-Out Electronics

Read-out electronics for rf-SQUID is an area in which a hard challenge is going on between different superconductivity groups. The main challenges are

- Decreasing the noise (increasing SNR, so the dynamic range of receivers) contributing from the electronics and the tank circuits.

- Going to higher frequencies together with new resonator topologies. (The characteristics of rf-SQUID should be analyzed in microwave frequencies and various superconductivity groups carry out studies about this. But, at microwave frequencies, conventional tank circuits are not used and instead, resonator topologies for these frequencies are utilized.)

These purposes would inevitably lead to lower noise electronics with higher operating frequencies. Being the main subject of this thesis, the most common topology for the rf-SQUID readout electronics is shown in Figure 1.9, [13].

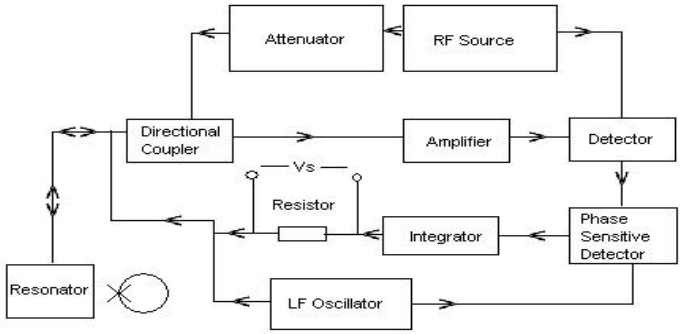

Figure 1.9: A typical schematic for rf-SQUID readout electronics (The output is V_s)

The system presented in Figure 1.9 is a typical transceiver circuit, but additionally transmitting low frequency signal to modulate the pumped rf power. The rf power is sent and received via a directional coupler. After the detector, the remaining signal is the amplitude modulation that SQUID adds to incoming rf power [13]. Phase sensitive detector compares the phases of the original low frequency signal with detector output to give a dc component, which is an error signal giving a measure of how far the SQUID is from the extrema in Figure 1.5. If a flux locked loop is implemented together with the integrator, the error signal will be integrated and fed back to SQUID to change SQUID's state to one of the extrema of Figure 1.5, at which the detector output will give 0 voltage (due to 2w frequency output (1.3.2)). In this condition, SQUID's condition would only change in flux fluctuations [4], [10], [13], [14], and [23]. Besides, the output signal (V_s) is taken on feedback resistor.

In this transceiver system, the transmitter has to provide enough amount of power to the rf-SQUID to get response without damaging rf-SQUID. This is because, for higher rf-powers, SQUID starts to absorb rf-energy and behave lossy. But the most important part of the electronics is the receiver, since some important parameters in SQUID signal detection can be derived here. For the receiver (and in all rf receivers), the most important parameters are as follows [24]:

- Sensitivity: Ability of a receiver to respond to weak signal levels.
- Selectivity: Receiver's ability to reject unwanted next channel signals.
- Spurious response rejection: minimization of the receiver's tendency to respond signals in other channels
- Intermodulation rejection: Receiver's tendency to generate unwanted signals from the signals in its band.

In the next chapter, the same considerations will be taken into account for our electronics.

There are also some further important parameters for receiver designs, which can be found in [25] and [26].

Chapter 2

DESIGN AND IMPLEMENTATION OF AN EXPERIMENTAL RF-SQUID READ-OUT SYSTEM

In this chapter, the steps for design and implementation of an experimental read-out system for rf-SQUID is explained. The manufacturer specifications for the devices and tools used in the implementation are included in the Appendix. Also, for abbreviations and unit conversions, please refer to the Appendix.

2.1 RF-SQUID Functioning

In section 1.3.2, some details about rf-SQUID were discussed. These details were mostly about electromagnetic characteristics of SQUID, which mainly implements a theoretical understanding of SQUID response to the applied flux changes. In this section, the study from the engineering point of view in understanding the SQUID response is carried out.

The first point, in understanding rf-SQUID response is to understand its response to a pumped rf signal. For this purpose a test set-up similar to the one in Figure 1.9, having only the rf-components can be assembled. The setup schematic is shown in Figure 2.1 [12].

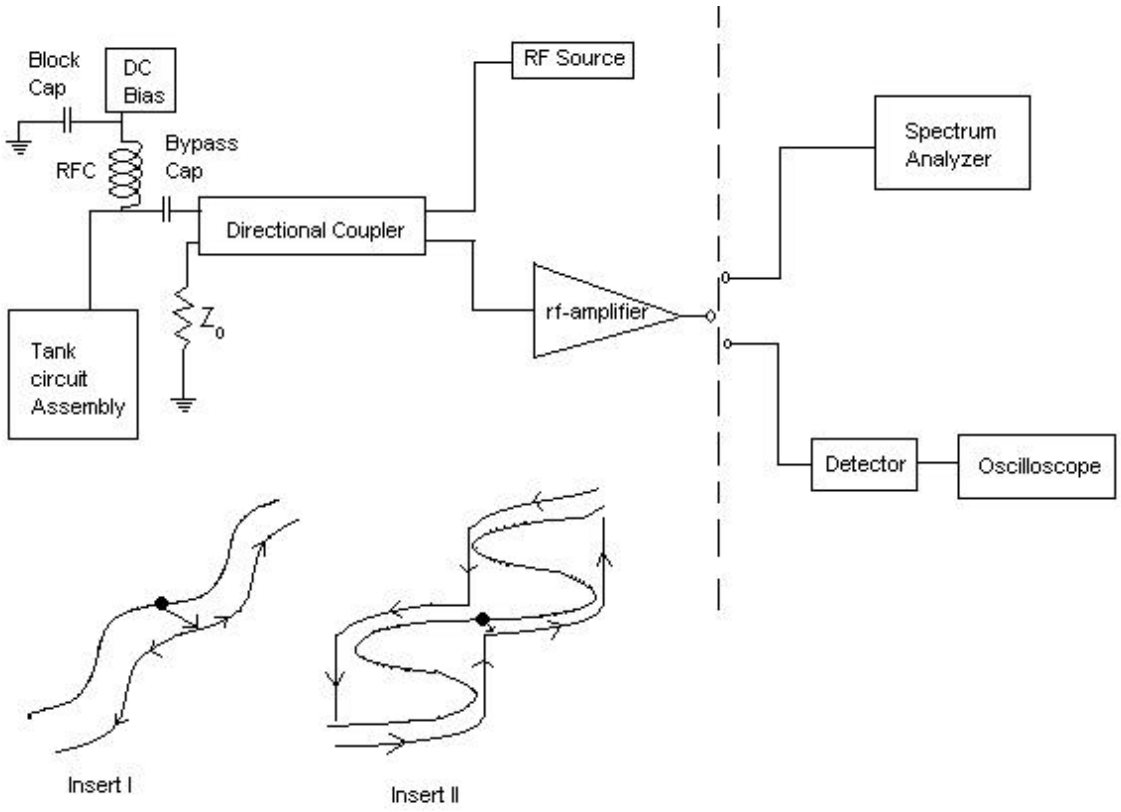

Figure 2.1: A set-up to understand the response of rf-SQUID to an applied rf-pump

In this setup, rf-source supplies the rf power to rf-SQUID tank-circuit assembly via a directional coupler having good isolation (preferably 15 dB larger than the return loss of the tank circuit assembly). The response signal coming from rf-SQUID is taken from the tank circuit assembly through the same coupler and amplified to a detectable level. For detection, a spectrum analyzer or a detector with an oscilloscope can be used. This experiment was also performed where the spectrum analyzer was used. As shown in the figure, there is also a DC-Bias applied to SQUID to change the flux [10], [12]. Two inserts are added in Figure 2.1. These inserts are about the behavior of rf-SQUID (whether hysteretic or not), the information about which are given in 1.3.2 [12].

Firstly, via DC bias, the working point of rf-SQUID is selected (thick dots on the inserts of Figure 2.1) for both hysteretic case and non-hysteretic case. An applied rf signal into the tank circuit will create rf flux on the SQUID and as indicated by arrows in the inserts of Figure 2.1, the SQUID working point moves. If the rf power is further increased, the extent of this movement gets wider.

For the hysteretic operation of rf-SQUID, if the rf power is increased, an excursion around one hysteresis loop takes place. The excursion is dissipative, thus the rf energy is absorbed by the SQUID at the hysteresis loops. After hysteresis loops, the envelope increases again. This increase (build-up) is slow depending on the Q of the tank circuit. As soon as the rf voltage reaches its former value, a new excursion around a hysteresis loop takes place. In Figure 2.2, the upper trace shows this case. When the applied rf-power is increased, the build up speed on the tank circuit increases as seen in the lower trace of Figure 2.2. When the rf power reaches a value at which the build up takes place only in one cycle, the SQUID goes into a second hysteresis loop and upper trace is seen again [12], [13].

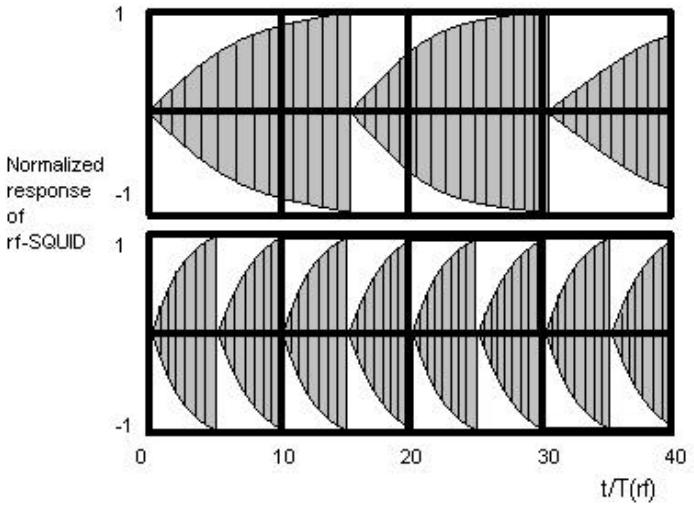

Figure 2.2: The envelope of SQUID response

In a hysteresis loop, the energy dissipated in the SQUID is [13],

$$\Delta E = \Phi_0 I_c = L I_c^2 \tag{2.1}$$

where L is the effective inductance of the SQUID and I_c is the critical current of the junction.

According to these results, the relation between the applied rf signal and the voltage response of rf-SQUID will look like a staircase pattern similar to the plot in Figure 2.3. At the plateau of steps, a hysteresis loop is traversed and on other parts, no modulation is added to the rf pump signal. Also according to the same figure, when the initial dc bias is changed, the staircase shifts (in Figure 2.3, two extreme cases of initial biases are shown) [12], [13].

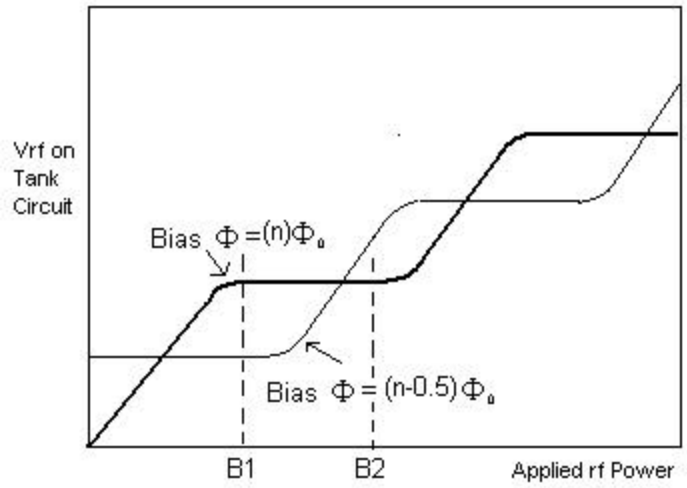

Figure 2.3: Staircase pattern for different DC biases

For the non-hysteretic case, a rigorous theoretical analysis results in the similar stair case pattern [27].

In another mode of operation, without any dc-bias, a low rf power (-60dBm to –90dBm) is applied to the SQUID, such that, during its cycle, no quantum transition takes place. For this purpose the critical rf magnetic flux cannot exceed

$$\Phi_{rf} = \frac{\Phi_0}{4} + L_s I_1 \qquad (2.2)$$

In equation 2.2, L_s is the effective inductance of the rf-SQUID and I_1 is the supercurrent in the loop. At this point an externally applied low frequency signal creates magnetic flux via a coupling coil on the tank circuit and the bias position of the rf-signal sweeps. This case is best understood from Φ_{ext} vs. Φ curve indicated in Figure 1.7. Similar figure with the effects of rf power and externally applied flux is shown in Figure 2.4. The extent of Φ_{ext} is much larger than Φ_{rf} and when applied together, Φ_{rf} sweeps over Φ_{ext} on the flux curve. According to Figure 2.3, an applied Φ_{ext} causes Φ_{rf} to sweep between the two staircase patterns [12], [13]. Thus an amplitude modulation is applied to the rf power whose envelope has a triangular-like relation with the applied external flux as indicated in Figure 2.5. On this figure, B1 and B2 refer to the biasing conditions indicated in Figure 2.3 [12].

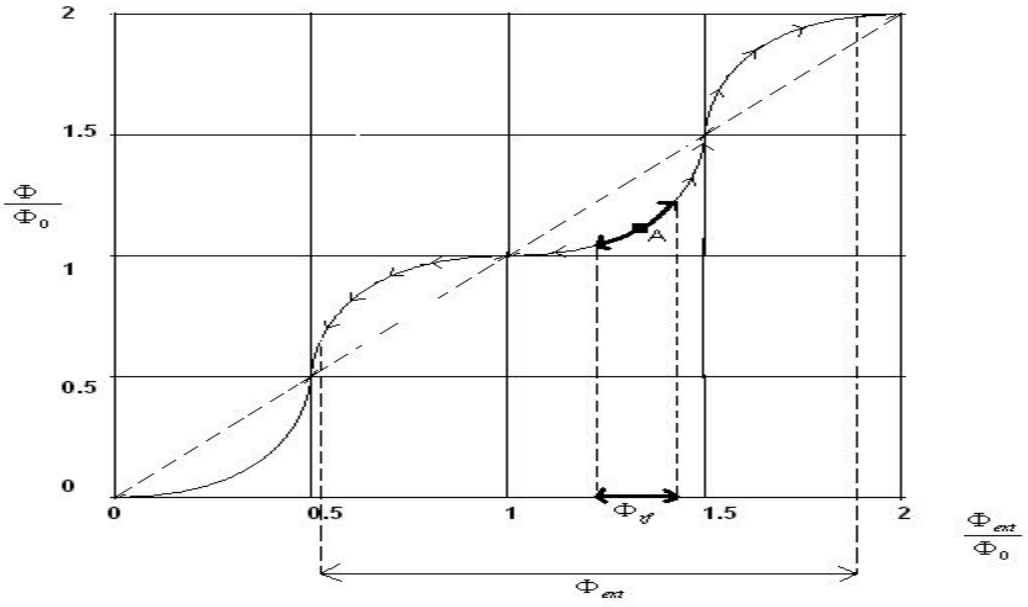

Figure 2.4: The effect of externally applied low frequency signal flux together with rf power flux

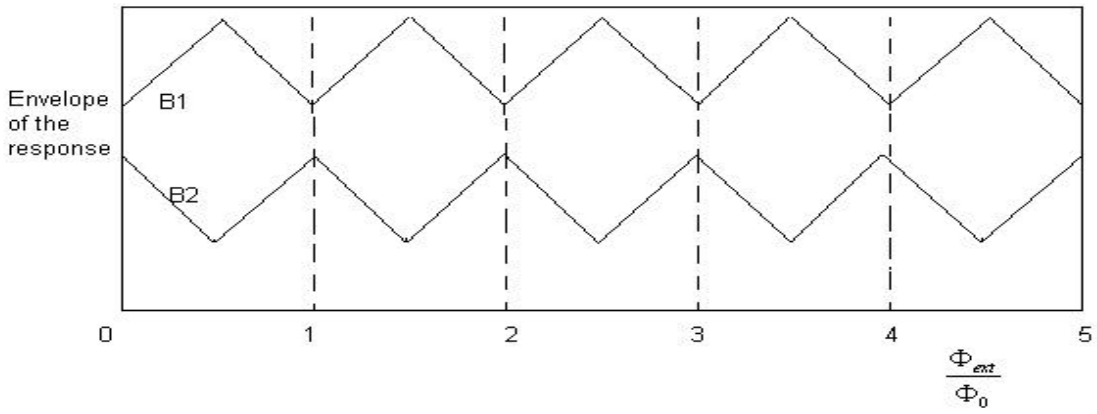

Figure 2.5: Envelope of the response of rf-SQUID vs. applied flux in second mode of operation for different initial biasing conditions, B1 and B2.

This last mode of operation is widely used, which is the mode of operation exploited in this work. A typical plot of implemented system is shown in Figure 2.6. The operation principle of this system is very similar to that indicated in Figure 2.1 but with some differences.

- In place of DC bias, a signal generator is used.
- Instead of a detector, a mixer is used (which is in fact a detector, but requiring in-phase rf-signal to acquire base-band envelope)

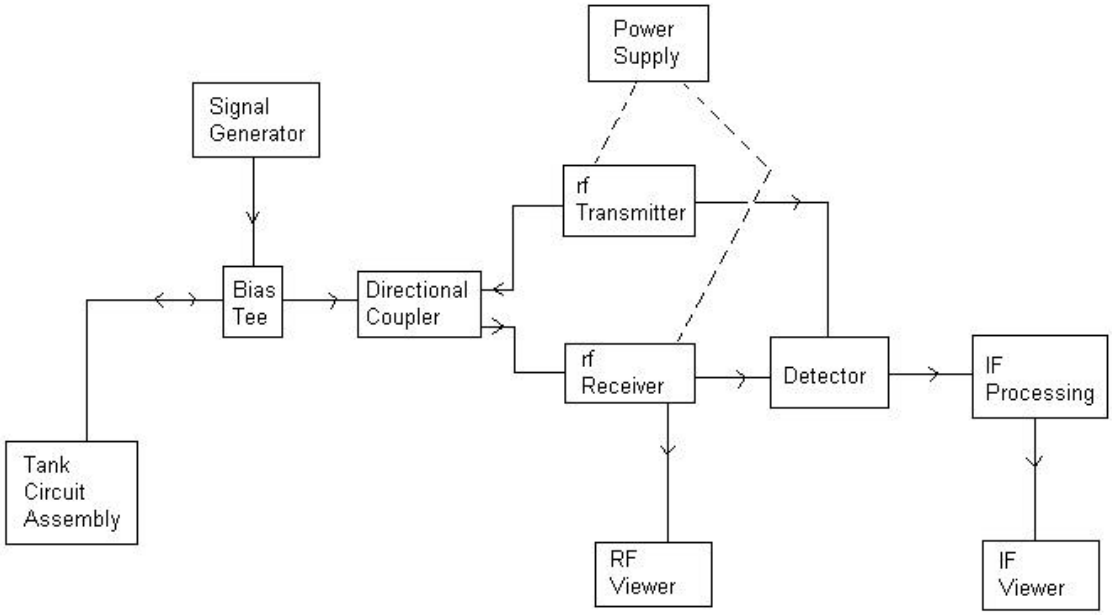

Figure 2.6: A typical plot of implemented system

2.2 Tank Circuit Assembly

RF-SQUID tank circuit is one of the main parts of a SQUID system, where the coupling is achieved through. It plays the role of an antenna in a microwave transmitter/receiver assembly.

The tank circuit is mainly a resonator resonating at a specified frequency. At this frequency, it pumps the flux created by RF wave coming from the transmitter subsystem into the rf-SQUID biasing it. At the biasing condition, the output voltage of the rf-SQUID is the periodic function of the flux [29].

In the literature on the rf-SQUID research, different types of resonators have been proposed. These resonators include planar and lumped element tank circuits. Planar resonators are produced on the fundamentals of coplanar waveguide technology and made of superconducting thin-films. One of the advantages of these resonators is their high quality factor (Q) whose effect will be shown. Information about coplanar resonators and their coupling to rf-SQUID can be found at [31].

For lower frequencies, several research groups have proposed different topologies for tank circuits [13]. In this work, the utilized tank circuit has a different topology as shown in Figure 2.7 [32].

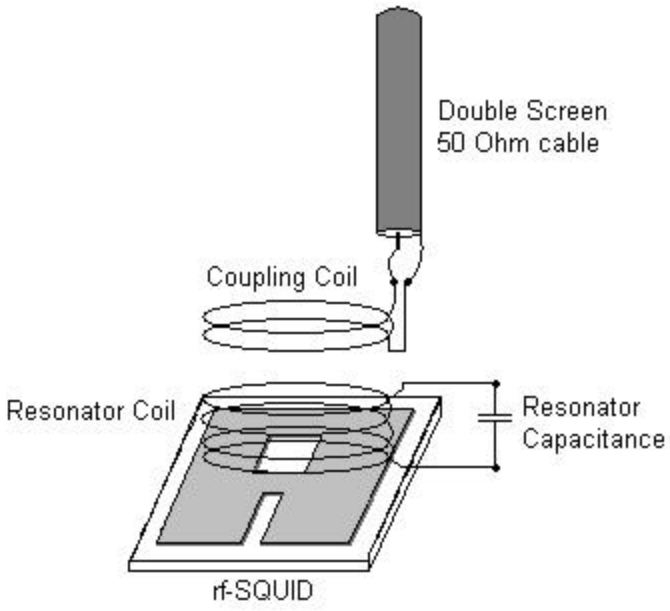

Figure 2.7: Utilized tank circuit topology

As stated before, there are two modes of operation of the rf-SQUID, hysteretic and non-hysteretic. In this section, the relation between the SQUID parameters and the tank circuit parameters are investigated for the non-hysteretic case. The same analysis for the hysteretic case is out of the scope of this work.

When an rf signal together with the low frequency signal are applied to the tank circuit, the low frequency signal is coupled to the SQUID via the coupling coil, and the rf power is coupled through the tank circuit resonating at a certain frequency. But the created flux by the signals applied to the tank circuit assembly affects the effective inductance of the rf-SQUID, L_{eff} , where,

$$L_{eff} = L_s\left[1+\frac{1}{b_l \cos f}\right] \tag{2.3}$$

In this equation, b_l is the hysteresis parameter, and f is the phase shift caused by the applied flux ($f = 2p\,\frac{\Phi}{\Phi_0}$) (Section 1.3.2). Since there is a transformer relation between the SQUID inductance and the tank circuit inductance, there would be a coupling between them, k, and the mutual inductance, M [29]. Then the equivalent inductance of the tank circuit becomes

$$L_T = L\left[1-\frac{k^2 L_s}{L_{eff}}\right] \tag{2.4}$$

in which L is the inductance of the coil. The relation between the coupling and the mutual inductance is $k^2 = \frac{M^2}{L_s L_{eff}}$ [34]. Having found the equivalent tank inductance, the tank circuit resonation frequency becomes

$$w = \frac{1}{\sqrt{L_T C}} = \frac{w_0}{\sqrt{\left(1-\frac{k^2 b_l \cos(f)}{1+b_l \cos(f)}\right)}} \tag{2.5}$$

where

$$w_0 = \frac{1}{\sqrt{LC}} \tag{2.6}$$

and C is the tank circuit capacitance [29]. If the Josephson junction used in the SQUID is not a 0-junction, an extra phase shift is required, x, and equation 2.5 becomes

$$w = \frac{1}{\sqrt{L_T C}} = \frac{w_0}{\sqrt{\left(1 - \frac{k^2 b_l \cos(f + x)}{1 + b_l \cos(f + x)}\right)}} \tag{2.7}$$

for the SQUID operation, the maximum extent of the frequency shift must be larger than the bandwidth of the tank circuit, which is

$$\Delta w_T = \frac{w_0}{Q} \tag{2.8}$$

then the maximum extent of the operating frequency of rf-SQUID from equation 2.7 is;

$$\frac{\Delta w}{w0} \approx \frac{k^2 b_l}{(1 - k^2)(1 - b_l{}^2)} \tag{2.9}$$

We need $\Delta w > \Delta w_T$ for proper operation of the tank circuit and this condition is provided by;

$$\frac{k^2 b_l Q}{(1 - k^2)(1 - b_l{}^2)} > 1 \tag{2.10}$$

According to this equation, higher Q and higher coupling coefficient between tank circuit inductance and the effective inductance of the rf-SQUID is required for rf-SQUID operation bandwidth to cover tank circuit bandwidth [29], [13].

Some of the important parameters of the tank circuit are as follow:

- As pointed out in equation 2.10, coupling mechanism is important, since it quantifies the magnetic flux linkage into the SQUID sensor. The inter-winding capacitance, winding method used, geometry of coils, spacing between coils, shielding and focusing of SQUID affect the coupling [34], [35]. Design of an effective transformer is a matter of experience [24].

- Reflection parameter (S11) of a tank circuit determines the amount of power that is sent into tank circuit assembly for a characteristic impedance of Z_0. It is also named as return loss, and formulated as the ratio of the reflected power (P_{in}^-) to the incident power (P_{in}^+).

$$RL = -10\log_{10}\left(\frac{P_{in}^-}{P_{in}^+}\right) \tag{2.11}$$

For a tank circuit to function properly, it should have a low RL to transfer all the power at its terminals into rf-SQUID [36]. The S11 of a tank circuit is shown in Figure 2.8.

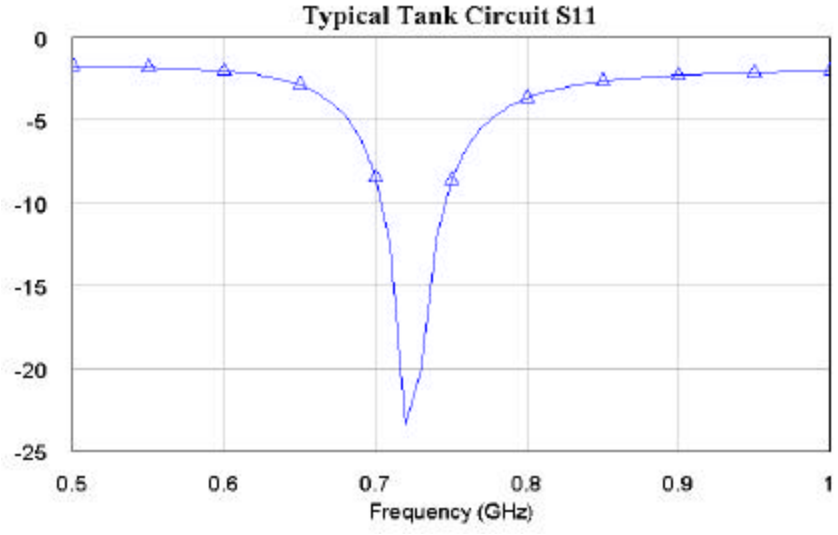

Figure 2.8: A typical plot of tank circuit S11

- Bandwidth or Q is another parameter, whose effect was demonstrated in equation 2.10. It defines the frequency extent of a circuit's response, at which the amplitude response at one extent is 3dB below its pass-band amplitude response. This is important in noise analysis, since it affects the selectivity (indirectly noise bandwidth) of the tank circuit [13].

- Electromagnetic shielding is also important for the tank circuit. Environmental in-band signals are amplified together with the main SQUID signal. They cause interferences in the receiver. In some cases, they might lead to oscillations, stealing rf-power from the main SQUID signal [24].

2.3 RF Subsystems Design

Section 2.1 describes the major points in rf-SQUID functioning and the modulation created by the rf-SQUID on the applied rf-power. For a proper detection, the rf-power must be sent in a controlled manner and the received power should be clearly transported to mixer. After mixer, the required amplification and filtering should be made to read rf-SQUID response in a clear manner.

In this work, the system in Figure 2.6 is established. The implemented system has mainly 2 parts, which are the transmitter and the receiver (including IF). The system is homodyne type, in which direct down-conversion to base-band is achieved via the same carrier signal.

2.3.1 Transmitter (Tx)

Transmitter is one of the important blocks in the system of Figure 2.6. Its main function is to send power into both rf-SQUID and the mixer. A local oscillator (LO) provides rf-signal and then it is divided to feed both rf-SQUID and the mixer. A block diagram of this part is shown in Figure 2.9.

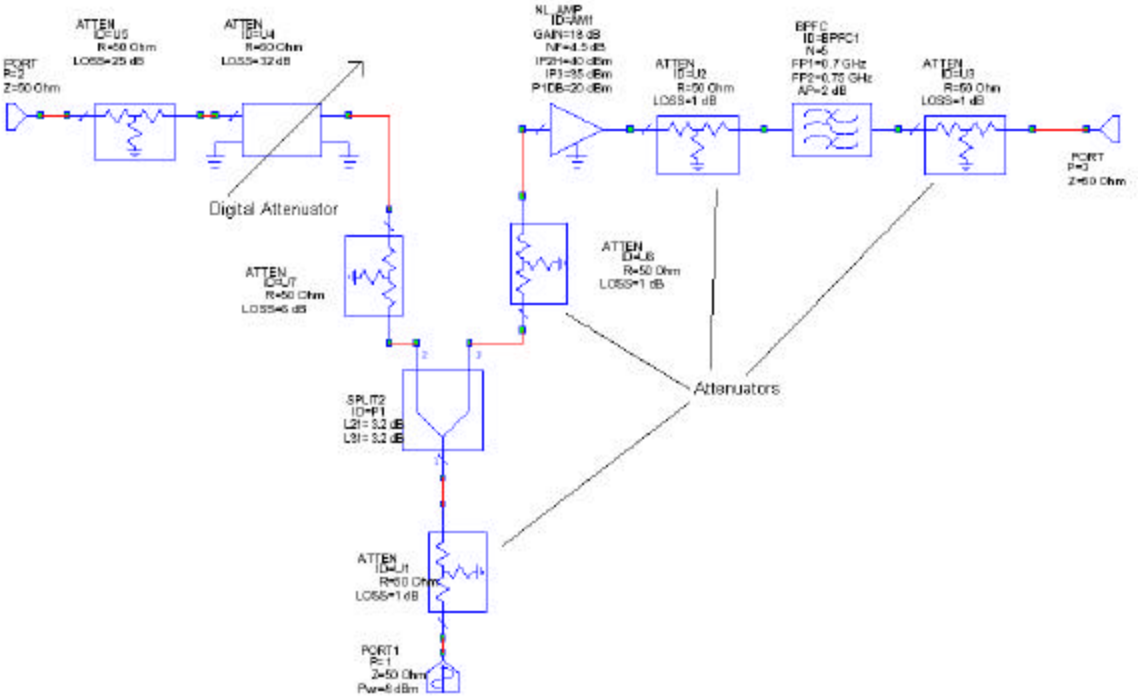

Figure 2.9: Transmitter Subsystem

The first important point to notice is the LO output. It is selected to be +8dBm (the used LO has this level of output power). Also, an attenuator is used as a buffer for the mismatches at the output of the LO, [35].

After the LO, there is a power divider with two channels. The channel on the left of Figure 2.9 sends rf-signal into rf-SQUID. This channel attenuates the rf-signal to lower values (-60dBm to –90dBm). For adjustment, a digital attenuator is added on the channel, and it has an attenuation range of –32dB to –64dB. In this manner the transmitted power can be adjusted to well defined values [12], [13].

In fact, this part of the circuit does not look like a conventional transmitter, at which the power is amplified. Also, since we do send only the carrier (no added modulation), there are no strict linearity constraints of the stages.

The channel on the right side of Figure 2.9 is the second part of the transmitter stage. Its function is to amplify the LO signal to a level required by the mixer (+17dBm). An amplifier and a filter are used on the strip together with the attenuators (for buffering). Here the filter is used to prevent the out of band signals going into mixer. The source of these signals might be the amplifier (2^{nd} order IP products or 3^{rd} order IM) [24] or environmental signals amplified by the amplifier (in inadequate shielding).

Figure 2.10 shows a simulation of the transmitter subsystem. On the figure, the power at the output of the two channels for a frequency of 720 Mhz is shown. For 64 dB of attenuation in the digital attenuator, the power going into rf-SQUID is –93 dBm.

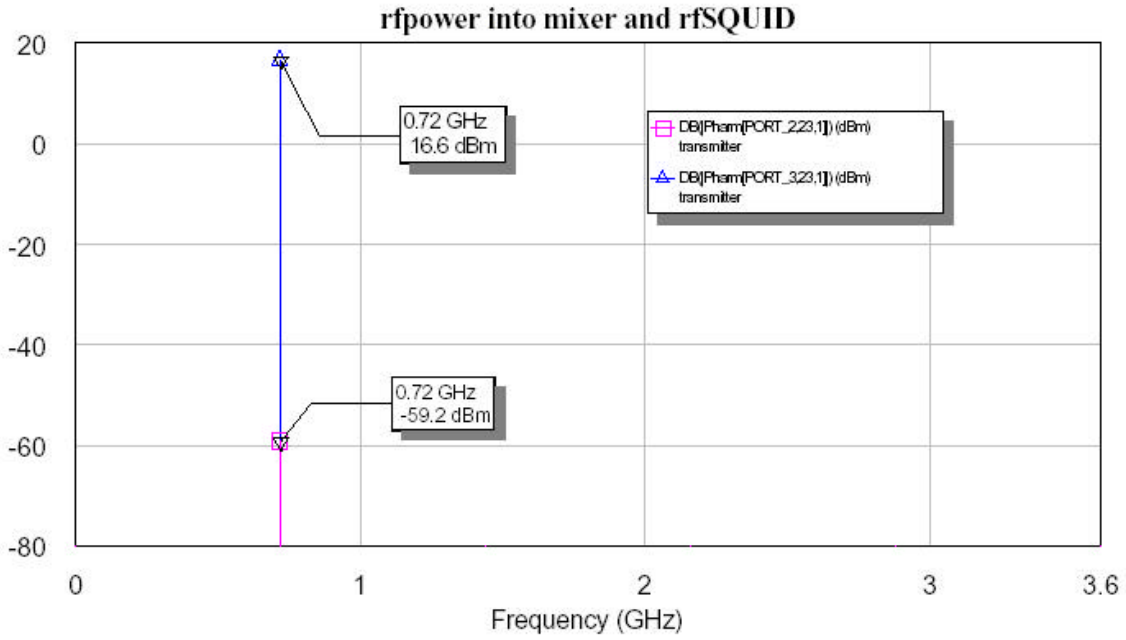

Figure 2.10: Rf power spectrum for 720 MHz frequency at the output of two channels of the transmitter subsystem

2.3.2 Receiver (Rx)

The most important block of the system is the receiver. This is a critical block since the received signal should be transported to the mixer and the IF stages with lowest possible distortion. It is shown in 2.1 that, SQUID's response is an AM modulated signal [13] and AM modulation requires linear processing [24], [37], [38]. In section 1.4, some properties of a typical receiver system are called and these properties are analyzed in this subsection.

Receiver's schematic circuit is shown in Figure 2.11. According to the figure, the power from the transmitter is sent into rf-SQUID assembly via the coupler. Also a bias-

tee is added between tank circuit assembly and the coupler to couple the low frequency flux into the rf-SQUID. The modulated rf-signal coming from the tank circuit assembly is sent into the receiver strip via the coupler and the signal is amplified. After this amplification, the signal is taken into the mixer together with the high power coming from the transmitter to get the base-band signal. Lastly, the base-band signal (the envelope on the rf signal) is filtered and amplified.

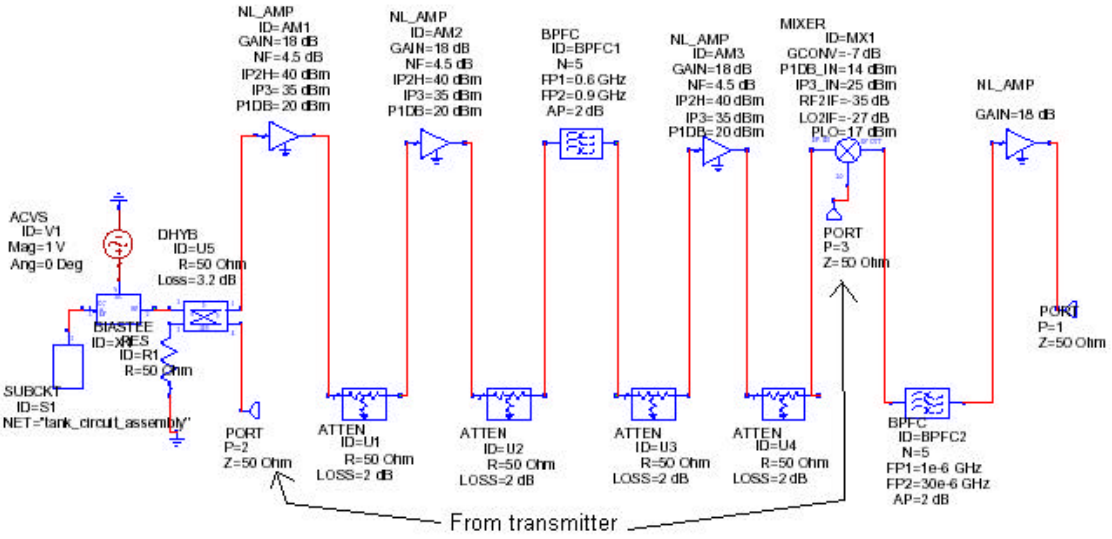

Figure 2.11: Receiver, Schematic View

Although detailed specification data sheets are added, some important characteristics of the utilized devices are shown in Table 2.1 - Table 2.4.

Amplifier	
Name	SCA-4
Frequency Range	0.1-3GHz
Power Gain	18dB
Output 1dB Compression Point	19dBm
Noise Figure	4.5dB
IP3	38dBm
Isolation	22dB
V_D	5V

Table 2.1:Amplifier Properties

Filter	
Bandwidth	0.6-0.9GHz
Loss	2 dB
Rejection	50 dB at 0.4GHz
	50 dB at 1.1 GHz
Power Rating (experienced)	20dBm

Table 2.2: Filter Characteristics

Mixer	
Name	ZFM-2H
Frequency Range	RF 5MHz-1GHz
	LO 5MHz-1GHz
	IF DC-1GHz
Conversion Loss	7dB

LO Power	17dBm
RF-LO Isolation	35dB
LO-IF Isolation	25dB
Input 1dB compression	14dBm
Input IP3	21 dBm

Table 2.3: Mixer properties

Also utilized coupler is a 3 dB coupler, the isolation of which is over 30 dB in the band of interest (600MHz-900MHz). Bias-Tee's loss can be neglected (very low) and the attenuators between each stage are used for increasing match between each device. The filter and the amplifier after the mixer are assembled in an instrument by SRS[1].

The important receiver parameters stated in section 1.4, and their effects are as follows:

- **Receiver Sensitivity**

Receiver sensitivity is a fundamental property for system performance. In this part, device gains and noise figures are treated separately to find total noise factor. In view of this analysis, receiver sensitivity is found [24].

The noise factor in a receiver is [24]

$$F_{IN} = F_1 + \frac{F_2 - 1}{G_1} + \frac{F_3 - 1}{G_1 G_2} + \ldots = 1 + \sum_{i=1}^{n} \frac{F_i - 1}{\prod_{j=0}^{i-1} G_j} \tag{2.12}$$

F_i : Noise factor of i^{th} stage (linear)

[1] The information for this instrument can be found in Appendix.

G_i : Gain of i^{th} state (linear)

After the calculation of the effective noise factor of the receiver, sensitivity of the receiver can be calculated from;

$$e = \sqrt{F_{IN} kTB(R-1)Z_0} \tag{2.13}$$

where the parameters are defined as:

E: receiver sensitivity (V)

k: Boltzmann's constant (J/K)

T: temperature (K)

B: Equivalent Noise Bandwidth (Hz)

R: 1+SNR at the input (linear)

Z_0: System impedance

For the analysis, following assumptions are made: The rf-power coming from rf-SQUID is around –70 dBm, the bandwidth of the system is 30 kHz (determined by the IF circuit), and all the stages are matched to each other. The results of the analysis are shown in Table 2.4 through Table 2.6.

Stage #	1	2	3	4	5	6	7	8	9	10	11	12
Stage	Dir. Coup.	Amp.	Atten.	Amp.	Att.	Filter	Att.	Amp.	Att	Mixer	filter	Amp.
Gain(dB)	-3.2	18	-2	18	-2	-2.5	-2	18	-2	-7	-1	50
NF(dB)	3.2	4.5	2	4.5	2	4.5	2	4.5	1	7	1	NA
Output IP3(dBm)	100	38	100	38	100	100	100	38	100	20	100	40
Output Power (dBm)	-73.2	-55.2	-57.2	-39.2	-41.2	-43.7	-45.7	-27.7	-29.7	-36.7	-37.7	12.3
Input Power (dBm)	-70	-73.2	-55.2	-57.2	-39.2	-41.2	-43.7	-45.7	-27.7	-29.7	-36.7	-37.7
Total Gain (dB)	-3.2	14.8	12.8	30.8	28.8	26.3	24.3	42.3	40.3	33.3	32.3	82.3

Table 2.4: Noise and Power in each stage of the receiver system

Input Power	-70 dBm
Analysis temperature	25 ^{o}C
Noise Bandwidth	30 KHz
Required S/N	10dB
Noise Source	290K

Table 2.5: Assumptions for calculations

Gain	32.3 dB for rf, adjustable IF
NF	7.79dB
Noise Temp	1454.3K
SNR	51.41dB
Sensitivity	-111dBm
Noise Floor	-166dBm/Hz
Input IP3	-42dBm
Output IP3	40dBm

Table 2.6: Results characterizing the receiver

According to the results, the receiver is able to respond signals at −111dBm level (on 50 Ohm, Z_0) with an SNR of 10dB.

- **Selectivity**

Receiver selectivity is another important parameter of the characteristics of the receiver. It quantifies the tendency of a receiver to respond to channels adjacent to the desired reception channel [24]. In this work, only one channel is utilized for rf-SQUID operation and there is no adjacent channel-filtering requirement. Thus, the IF filter's bandwidth was tuned to filter only the received modulation. In the future, for multi-channel rf-SQUID based systems and operation, the receiver selectivity will become important. Hence the related equations are also included in this report [24]. For selectivity we have;

$$Selectivity = -CR - 10\log[10^{(-IF_{sel}/10)} + 10^{(-Spurs/10)} + BWx10^{(SBN/10)}] \qquad (2.14)$$

where in equation 2.14 [24]

Selectivity	:	Amount of adjacent channel selectivity (dB)
CR	:	Co-channel rejection (dB)
IF_{sel}	:	IF filter rejection at the adjacent channel (dB)
Spurs	:	LO spurious signals in the if bandwidth at a frequency offset of channel spacing (dBc)
BW	:	IF noise bandwidth (dBc)
SBN	:	SSB phase noise of LO at channel spacing (dBc/Hz)

- **Receiver Spurious Responses**

These signals are unwanted signals but they again produce signals in the IF bandwidth. The mixer according to equation 2.15 mostly produces them [39], [40] as;

$$\pm m f_{rf} \pm n f_{LO} = \pm f_{IF} \tag{2.15}$$

where m and n are the integer multipliers of RF frequency and LO frequency. The created spurious frequencies are

$$f_{rf1} = \frac{n f_{LO} - f_{IF}}{m}$$
$$f_{rf2} = \frac{n f_{LO} + f_{IF}}{m} \tag{2.16}$$

Following these equations, the (m,n) indices that can be mapped near our IF frequency are as follows [24], [39], [40]:

- ❖ (-1,1) for low-side injection ($f_{LO}<f_{RF}$) and (1, -1) for high side injection ($f_{LO}>f_{RF}$). The effect of these products was analyzed in sensitivity analysis. They cause noise to be increased.
- ❖ (2, -2) for low-side injection and (-2,2) for high side injection. It causes $2f_{IF}$ to be appeared at the output of the mixer. For 20 KHz of IF frequency, 40 KHz signal can be viewed at the output which is limited by the IF filter used and the 2nd order intercept point (IP2) performance of the mixer.
- ❖ Higher order spurious signals resulting from higher order combinations of m and n. These are also limited by the IF filter directly following IF port of the mixer and the mixer performance for higher order products. Higher IF frequencies should be selected but in rf-SQUID operation, we are limited by the responses of rf-SQUID.
- ❖ If the LO is synthesized, spurious signals in its spectrum due to reference frequency and its harmonics may result. These signals can cause mixer to create close IF signals.

- **3rd Order Intercept Point (IP3)**

IP3 is a measure of system linearity. It is a theoretical point at which the desired signal and the third order distortion products are equal in amplitude. In Figure 2.12, a graphical description of intercept point and 3rd order intercept is shown [24], [36], [40], [41].

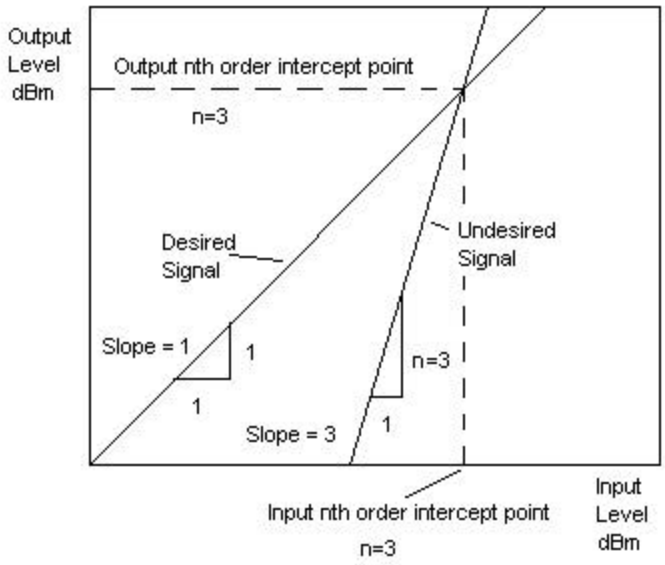

Figure 2.12: Intercept Point Definition and IP3

IP3 was found in the sensitivity analysis, for which equation 2.17 was used. In this equation all values are in terms of mW.

$$IP_{INPUT} = \frac{1}{\sum_{j=1}^{N} \frac{1}{IP_j}} \tag{2.17}$$

In our system, input IP3 is found as –32.3 dBm and the maximum signal returning from rf-SQUID is around –70 dBm (far from non-linearity).

2.3.3 Flux Feeding

Flux feeding is a key part of the operation of the system. According to Figure 2.11, an ac flux is given via a bias tee. The main aim of the ac flux is to change the biasing of rf-SQUID continuously as indicated in Figure 2.4 [13].

In Figure 2.7, there are two coils, one of which is the coupling coil. This coil together with the tank circuit coil helps resonance at the required frequency. Besides, it is this coil through which ac flux is fed to the rf-SQUID.

2.4 Implementation of rf-SQUID Read-Out System

Up to this point, system design of read-out electronics were investigated. The implementation of the system is made in blocks as indicated in Figure 2.6. Also the theoretical details about these subsystems are shown in Figure 2.9 and Figure 2.11. The specification sheets about the circuit elements are included in Appendix.

Before implementation, the measurements related to circuit elements (schematic view) and the subsystems are covered in this section. These measurements include

- S-parameters
- 1dB compression point, IP2 and IP3 (for the amplifiers)
- Coupling and isolation parameters (for the power dividers and couplers)

2.4.1 Measurements Related to Devices and Subsystems

- **Amplifier**

In the Appendix, the specifications of the used amplifier (SCA-4, MA-COM) are given. Some measurements are performed to verify these specifications. These measurements include S-parameters, 1dB compression point, 2nd order intercept point, and 3rd order intercept point.

Firstly S-parameters are measured. A network analyzer (Model Number : 8753D) is used for the measurement of the S-parameters of the amplifier.

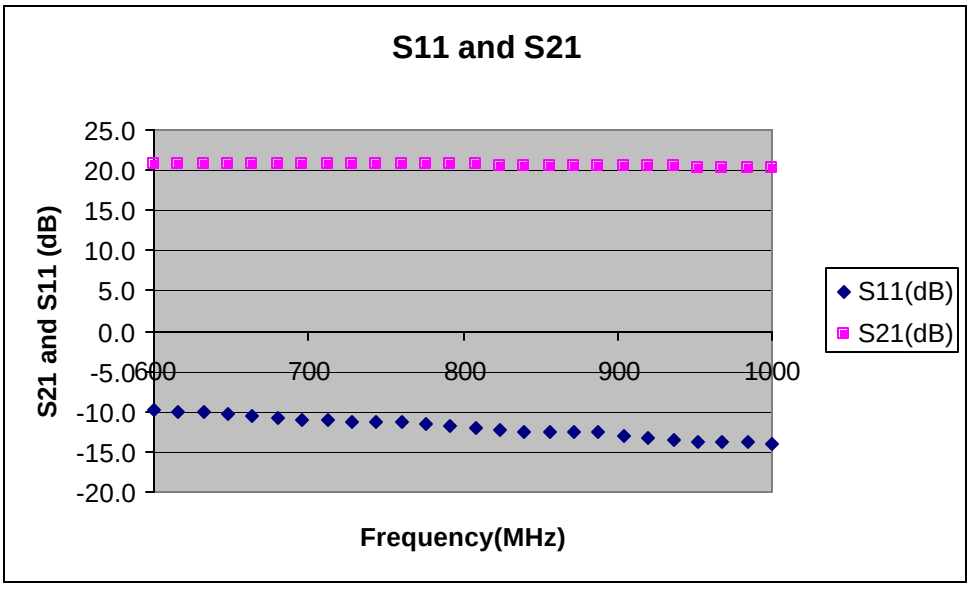

Figure 2.13: Amplifier S11 and S21

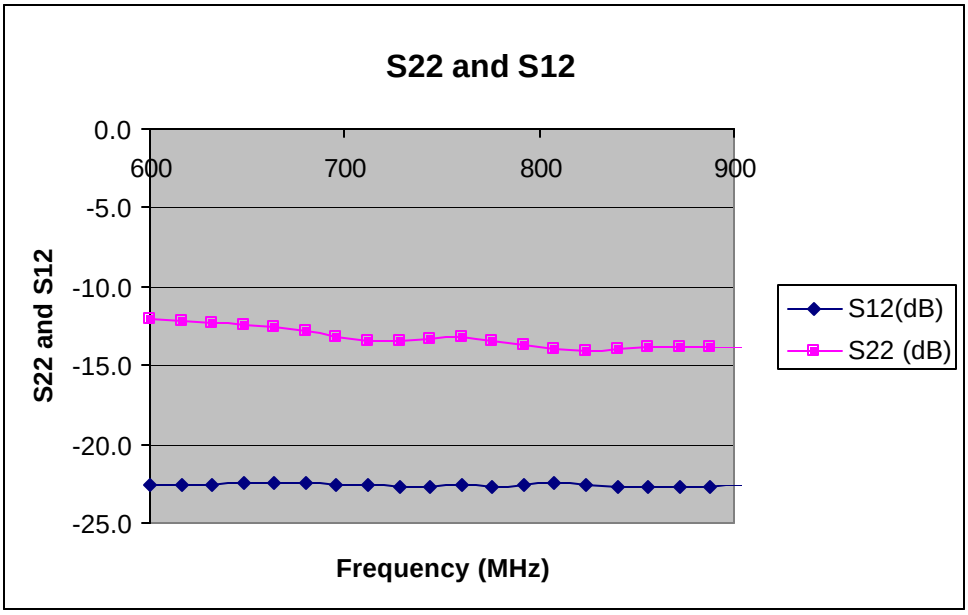

Figure 2.14: Amplifier S22 and S12

In Figure 2.13 and Figure 2.14, the measured S-parameters of amplifier are shown. S11 lower than –10 dB is compatible for the application. Together with the use of the attenuators between each device in the receiver (Figure 2.11), S11 and S22 can be improved. S21 is over 20 dB and S12, in other words the isolation of the amplifier, is around 23 dB.

Other parameters of interest are the 1dB compression point, IP2, and IP3. Figure 2.15 through Figure 2.18 show the measurements related to these parameters.

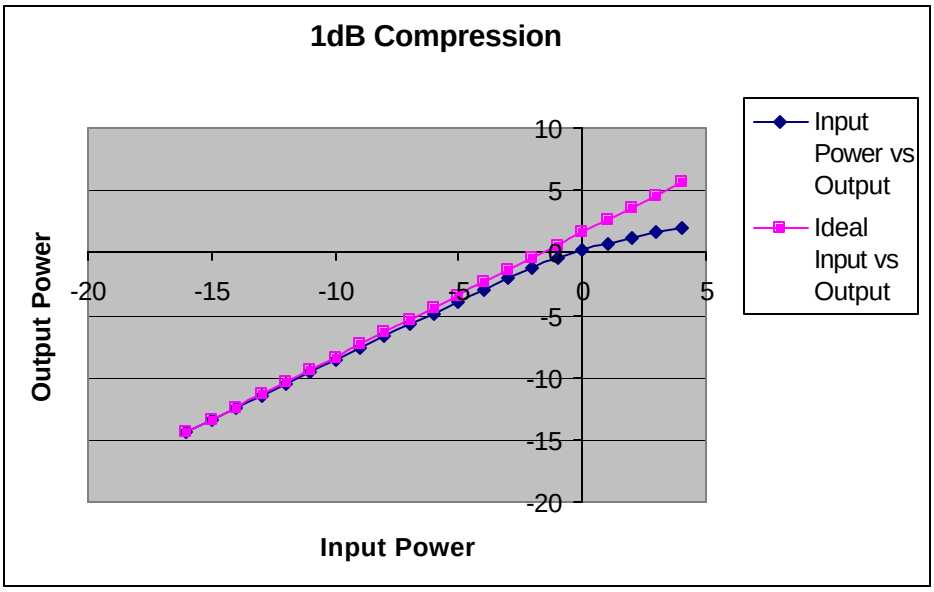

Figure 2.15: 1dB compression point of the amplifier

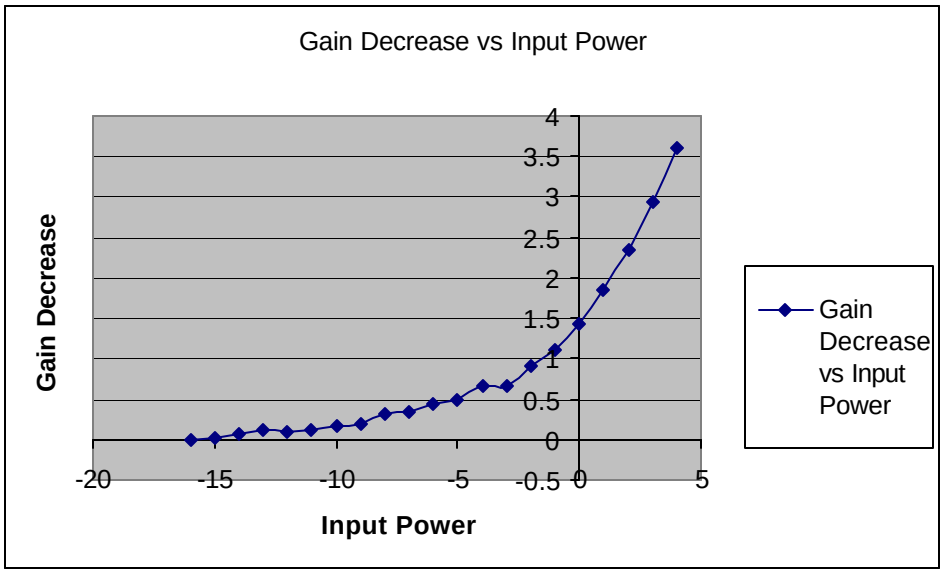

Figure 2.16: Gain decrease for the exact measurement of 1dB compression

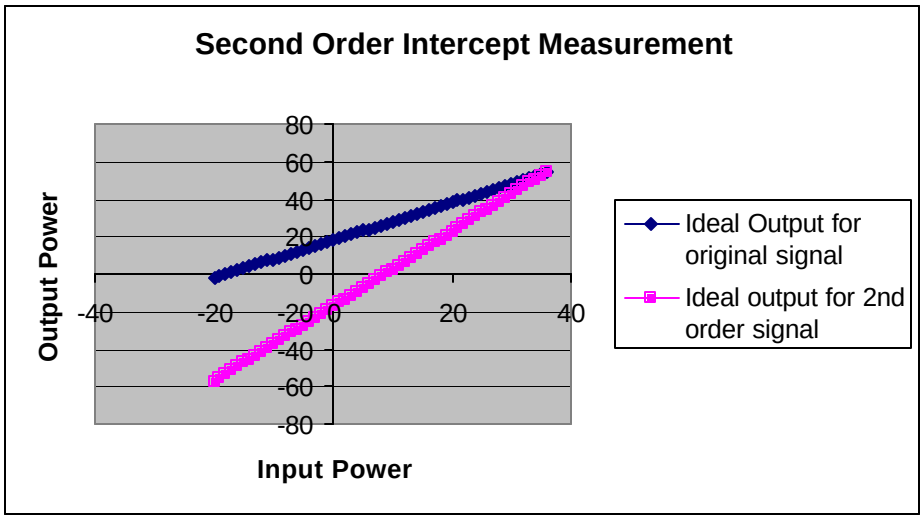

Figure 2.17: IP2 measurement

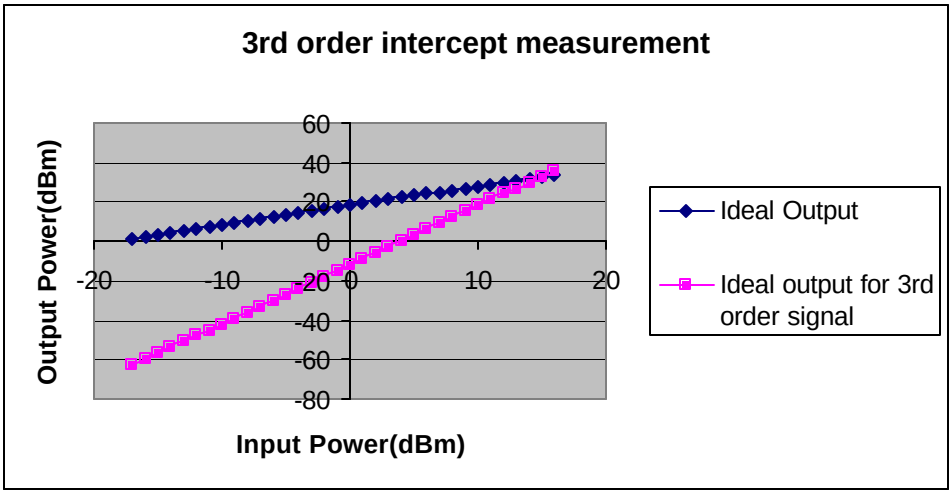

Figure 2.18: IP3 measurement

P1dB	-1 dBm at the input
IP2	35 dBm at the input
IP3	16dBm at the input

Table 2.7: Power measurements of amplifier

Also noise figure measurement of the amplifier was performed with a calibrated noise source and a 4.21 dB was measured.

- **Attenuator**

Attenuators are used between each device and the SQUID output of the transmitter. They are used to increase the match between the devices and regulate the power going into the rf-SQUID (A digital attenuator is used for this purpose having similar properties as other attenuators). A typical S parameter measurement of a 3dB attenuator is shown in Figure 2.19.

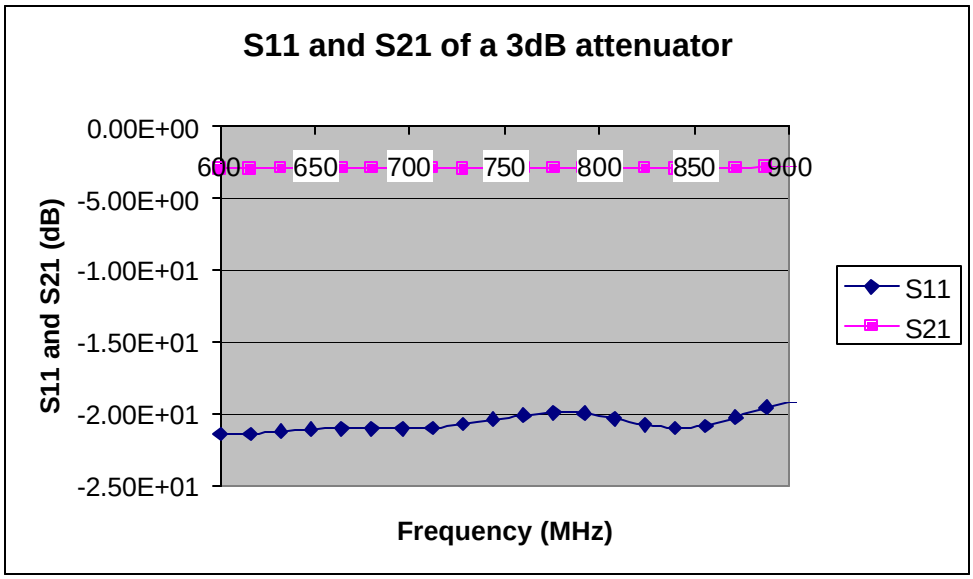

Figure 2.19: S parameter measurement of an attenuator

- **3dB Coupler**

In section 2.1 and 2.3, the role of the coupler in sending and receiving power from the rf-SQUID tank circuit assembly was discussed. The used coupler in this work is a 180

degrees coupler for which the through port and coupled port are 180 degrees out of phase. This property of coupler is not utilized in this work. The S parameters related to the coupler (coupled port S21, through S21, S11 (at the transmitter side) and isolation) are reported below.

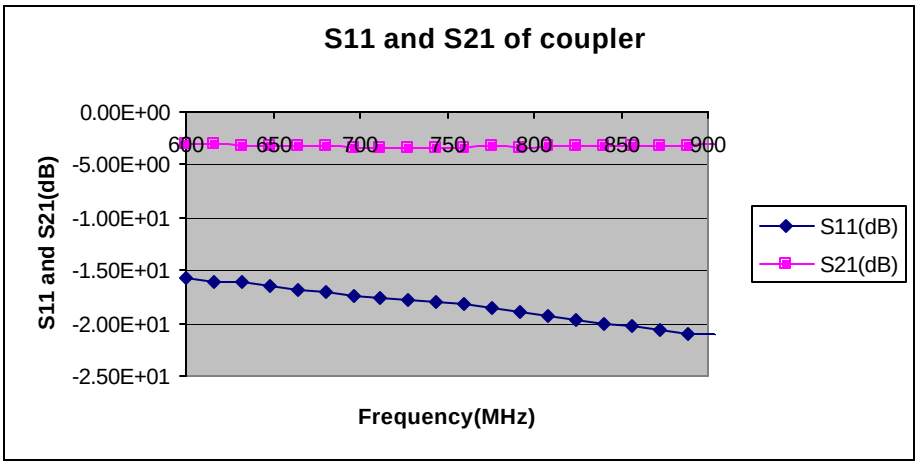

Figure 2.20: S11 and S21 of the coupler

In Figure 2.20, S21 parameter is found for the through port, where it is also similar for the coupling port except for the phase, which is 180 degrees out of phase.

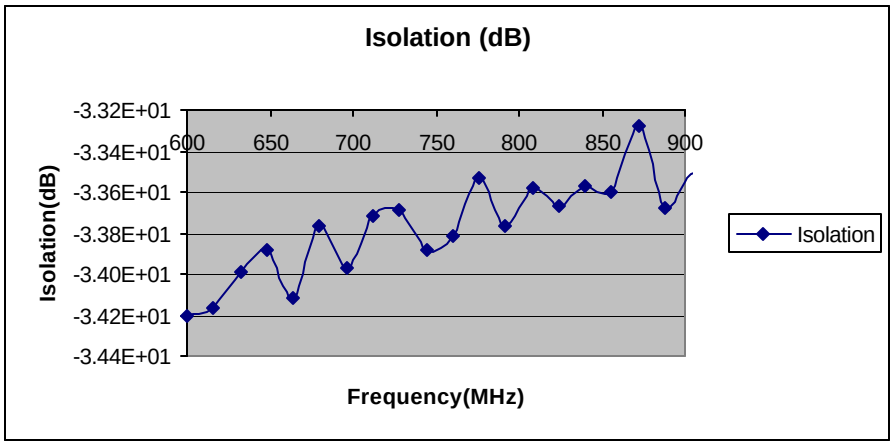

Figure 2.21: Isolation parameter of the coupler

According to Figure 2.6, the transmitter and the receiver sub-blocks are connected to the isolated ports of the coupler. So power coming from the transmitter is isolated from the receiver by the isolation parameter shown in Figure 2.21.

- **Power Divider**

Power Divider is used in some parts of the transmitter and the receiver. In Figure 2.9, transmitter has two arms and these two arms are connected to the mixer and the coupler. To achieve this, division in microwave frequencies is done with power dividers. A power divider with moderate isolation was designed for this work [39]. The measured S-parameters of it are as follows;

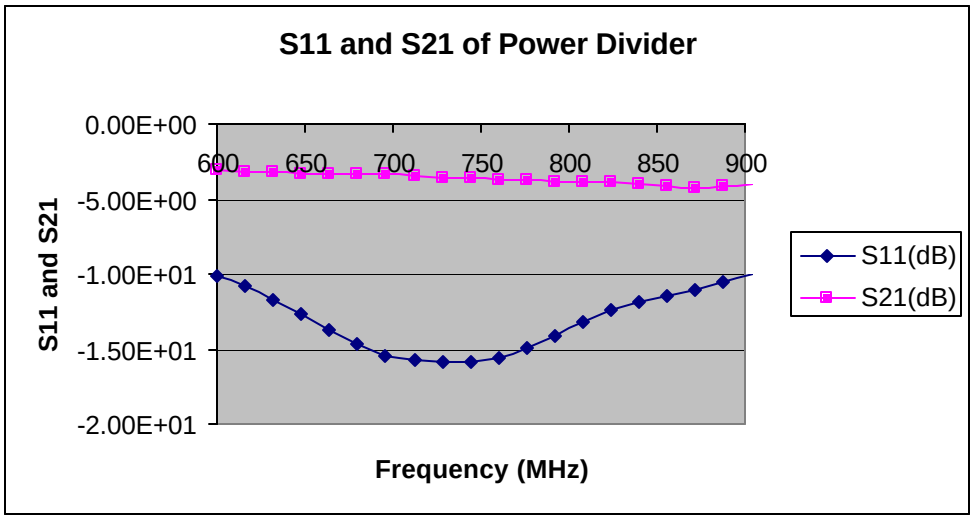

Figure 2.22: S11 and S21 related to designed power divider

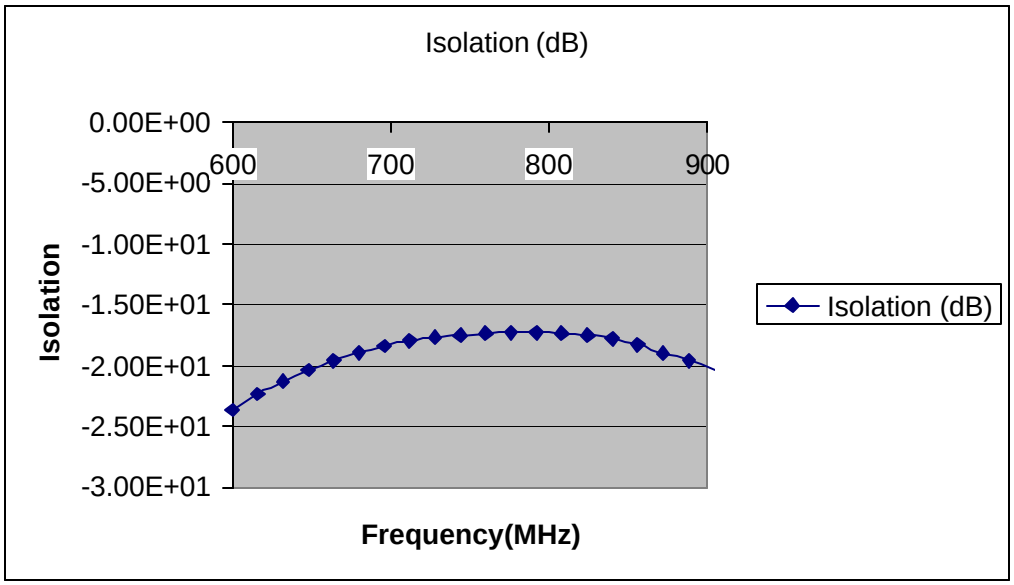

Figure 2.23: Isolation parameter of power divider

Figure 2.22 shows the S-parameters of only one arm. The second arm is symmetric to this arm and similar S-parameters result. Isolation is better than 15 dB as shown in Figure 2.23.

- **Filter**

Filter is a critical component in almost all rf-systems. It is used in three places in this work. In the receiver it decides the operating bandwidth, in transmitter it filters harmonics of LO signal that feeds the LO port of the mixer, and at the output of the LO for filtering out of band harmonics that can cause wrong measurements. The filter should be selective and have S11 < -10dB.

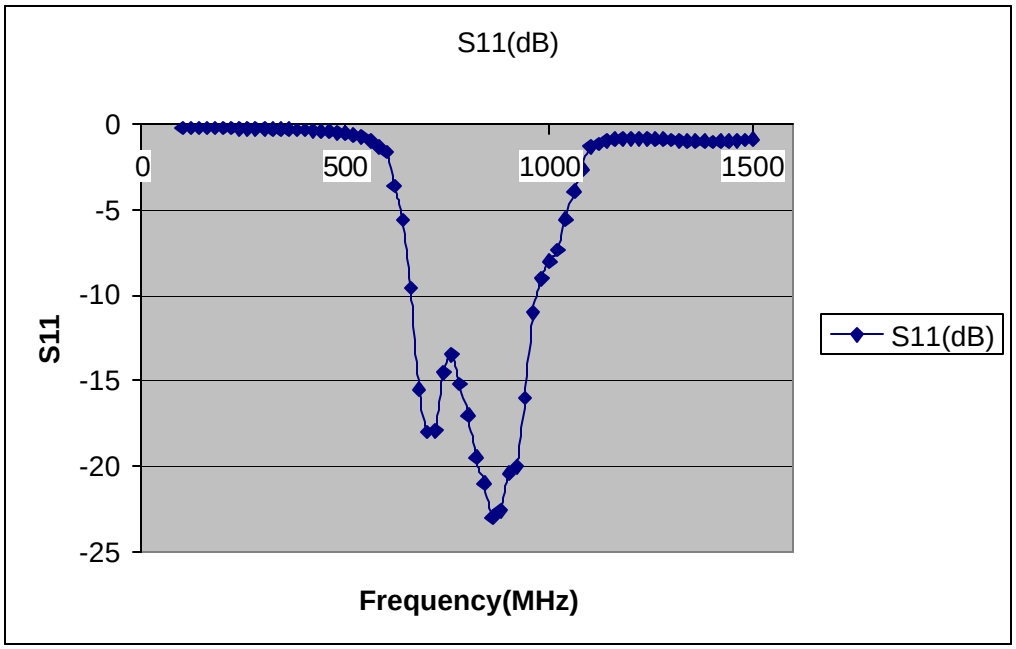

Figure 2.24: S11 parameter of filter

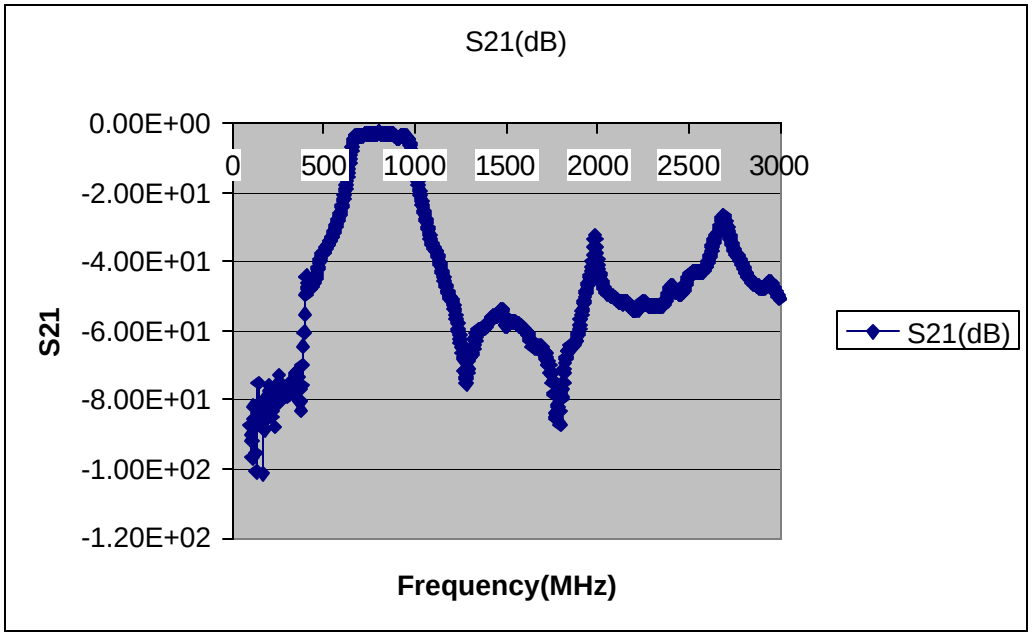

Figure 2.25: S21 of the filter

Figure 2.24 and Figure 2.25 show the S parameters of the filter. It should be pointed out that in S21, for higher frequencies, there are jumps, which are due to the box resonance. Different patterns with conducting materials should be implemented in the box to decrease the level of the resonance [24], [40].

- **Cables**

As pointed out earlier, the implemented system is an experimental system and during the work, modifications can be made for optimum performance. For this purpose, different devices were soldered on PCBs and boxed with copper foils. On each board, SMA connectors are soldered. The connection between each box is made by 50-Ohm rf cables. Thus, rf cables also become a part of the system, whose S parameters are shown in Figure 2.26. The measured cable is 10 inches long.

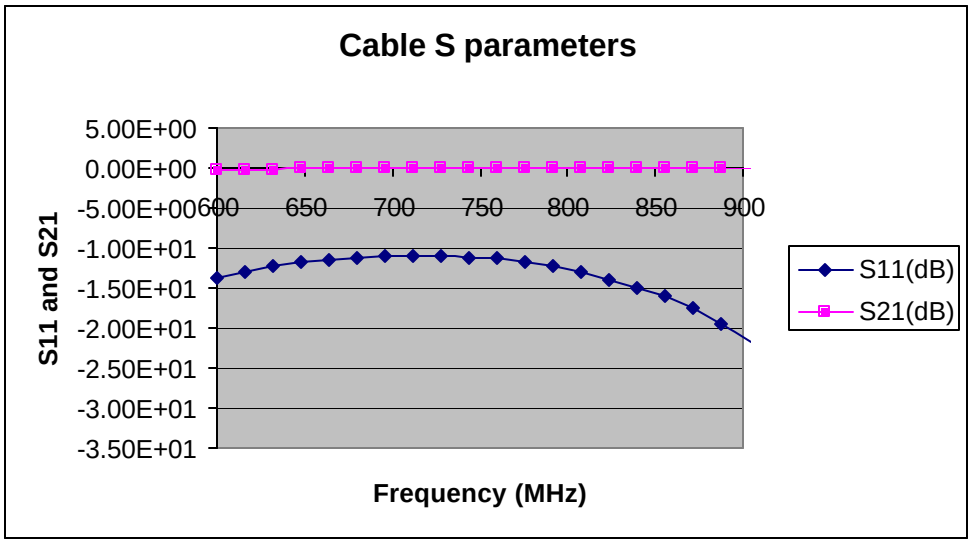

Figure 2.26: 10 inch cable S-parameters

In this figure, it is clear that these cables are not strictly 50 Ohm, but have good enough characteristics for this application.

- **Mixer**

The mixer of the system is tested for the conversion loss associated with it. For this test, HP 8656B and HP 8657B signal generators are used on a same time basis. HP 8590L spectrum analyzer is used to view the spectrum at the IF port of the mixer. The experiment setup is shown in Figure 2.27.

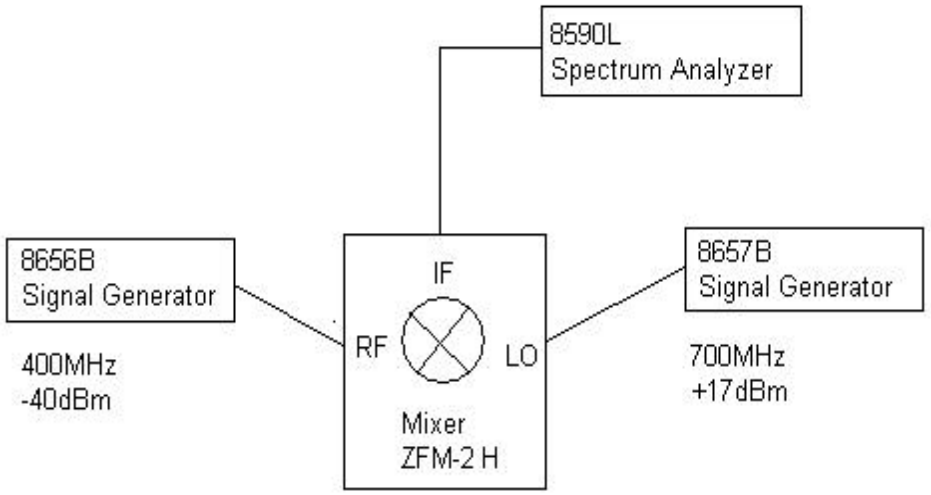

Figure 2.27: Established Setup to measure mixer

RF	400MHz	-40dBm	
LO	700MHz	+17dBm	
Spectrum			
1	300MHz	-46dBm	LO-RF
2	400MHz	-61dBm	RF
3	700MHz	-12.4dBm	LO
4	1.1GHz	-46dBm	LO+RF
5	1.4GHz	-24dBm	2LO
6	1.7GHz	-57dBm	3LO-RF
Conversion Loss	6dB		

Table 2.8: The spectrum at the if port of mixer after a sample mixing action

Table **2.8** shows the spectrum data at its IF port at a mixing action. The signals in the spectrum can be analyzed using equation 2.15. This test (not only for this mixer but also for all mixers) warns rf designer to be careful about the outputs of the mixer. The spectrum can be cleaned by using filters at the IF output of mixer [24]. In this work SR560 from Stanford Research Systems is used to filter the output of the mixer.

- **Tank Circuit Assembly**

In section 2.2, the specifications, characteristics and sensitivities of the operation of tank circuit in the system was discussed. A detailed plot of the tank circuit assembly is shown in Figure 2.28.

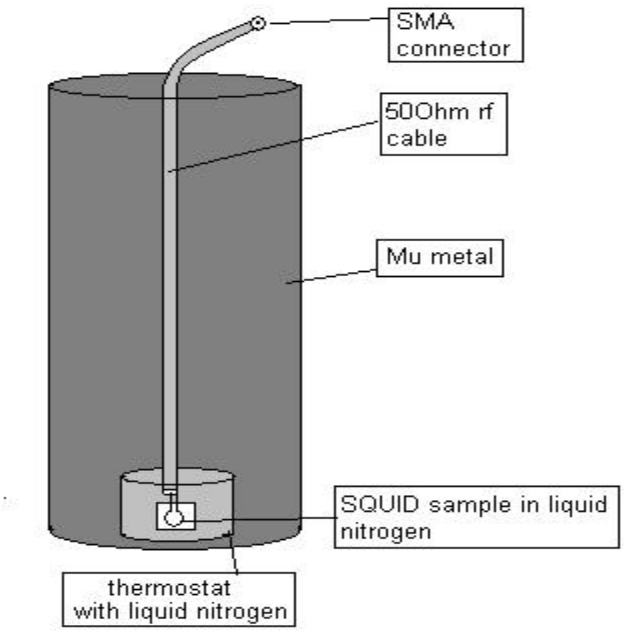

Figure 2.28: Tank circuit assembly setup

As shown in the figure, tank circuit is placed into a thermostat containing liquid nitrogen. The thermostat is placed into a Mu-metal shield to exclude external flux from the rf-SQUID. The cable used to get the signal from the tank circuit is a double screen (electromagnetically shielded) 50-Ohm rf-cable where at the tip of the rf-cable, SMA connector is used. The tank circuit resonance frequency measurement is made in this configuration. In Figure 2.29, measured S11 of a sample tank circuit is shown, which resonates at 842MHz.

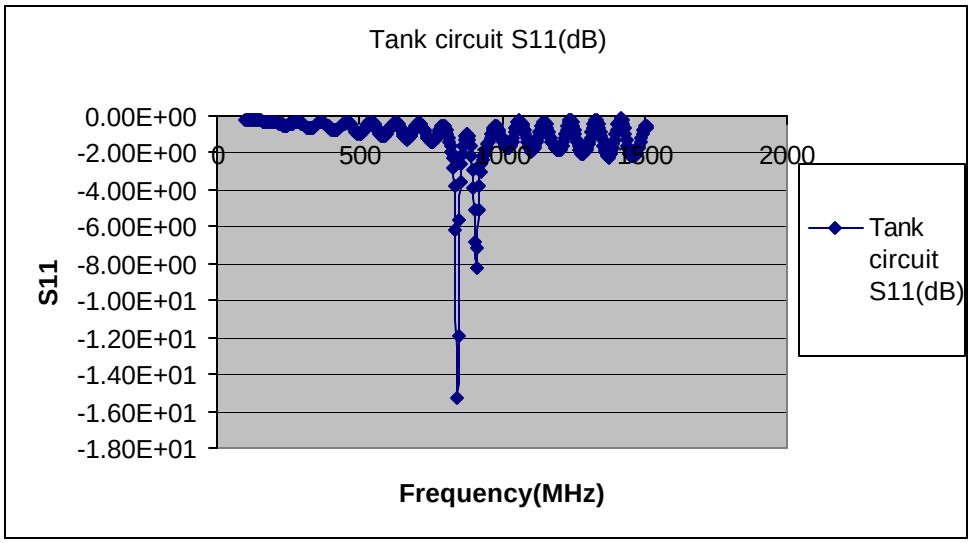

Figure 2.29: Tank Circuit S11

More information on the tank circuit design and implementation can be found in [34].

- **Receiver**

The S-parameters of the receiver are measured up to the rf port of the mixer. Also, 20 dB attenuator is used in the measurement to protect the network analyzer's preamplifier and limiter against saturation or even crack. Additionally, low power was given from the network analyzer.

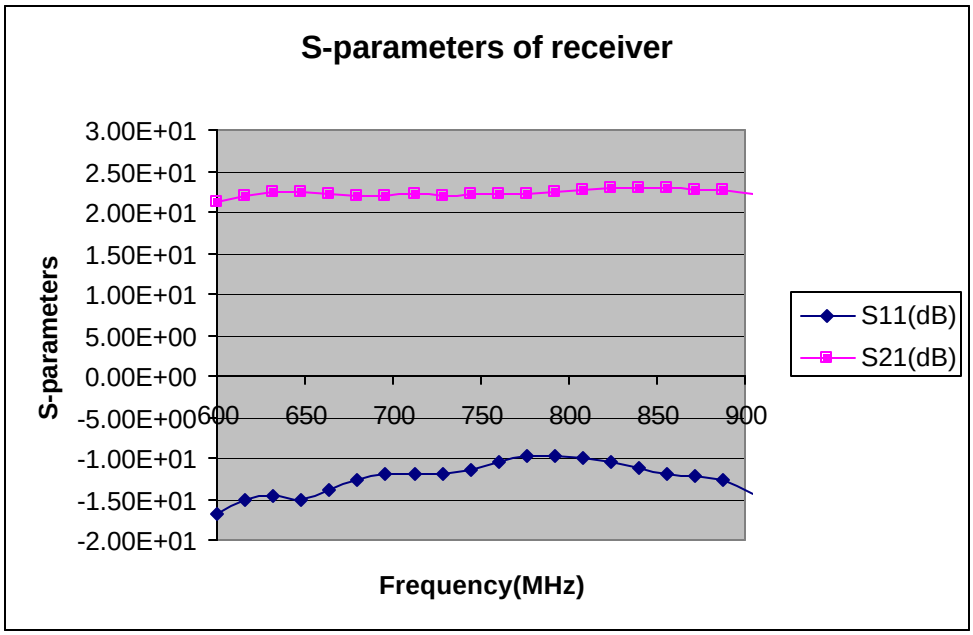

Figure 2.30: S-parameters of the receiver

Together with the 20 dB attenuator, receiver had more than 40 dB of S21. Besides, S11 parameter of the receiver was below 10 dB, which was enough for the application.

Another measurement related to the receiver was the 1dB compression point measurement. Figure 2.31 demonstrates the acquired data for this measurement. The measured 1 dB compression point is –29 dBm from input (+12dBm from output).

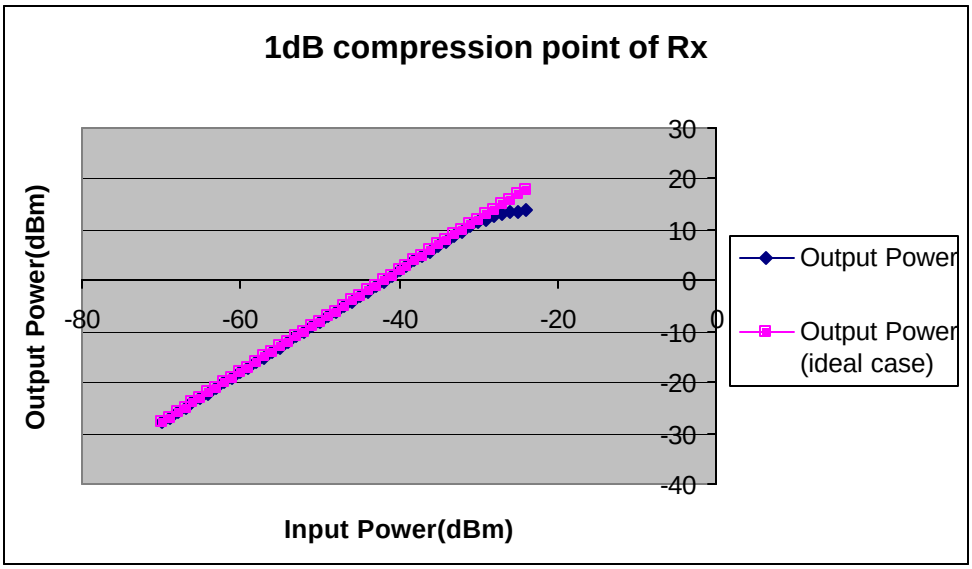

Figure 2.31: 1 dB Compression Point of Receiver

- **Transmitter**

The S parameters related to the transmitter were measured in two configurations due to the two arms in the transmitter. While measuring an arm, the other arm needed to be terminated with a load.

In Figure 2.32, the LO arm of the transmitter is shown. It has an S11 better than –8 dB, and its S21, is around 10 dB. In this work, a signal generator[2] connected from outside was used to supply +8dBm power for the system. Together with these S-parameters, transmitter can supply +17 dBm power to the LO port of the mixer.

[2] In the system, an oscillator is placed inside the transmitter box, but for the sake of seeing the frequency, a signal generator is used as an oscillator.

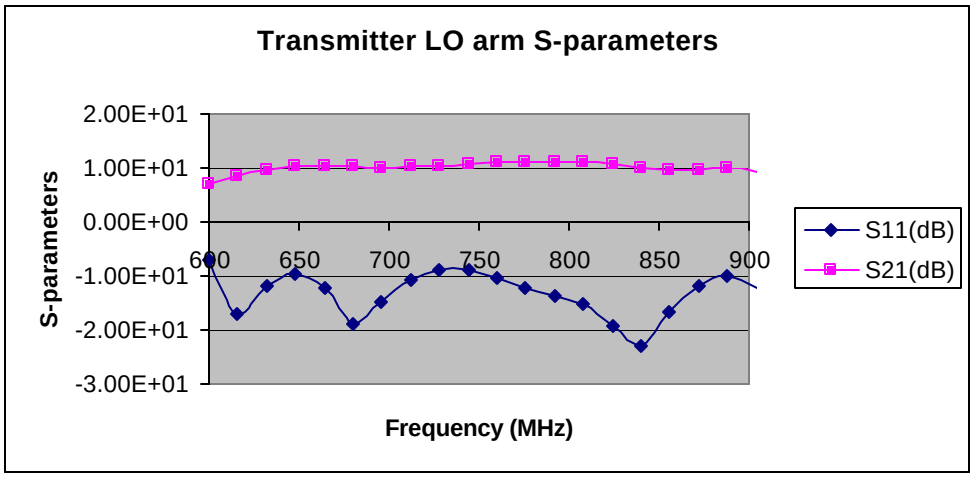

Figure 2.32: Transmitter LO arm S-parameters

In Figure 2.33, S-parameters of transmitter's SQUID arm is shown, for 0 dB of attenuation. According to the figure, there is a large ripple in the gain and in Chapter 3, the effect of this case will be analyzed. The ripple is due to the cables and connectors.

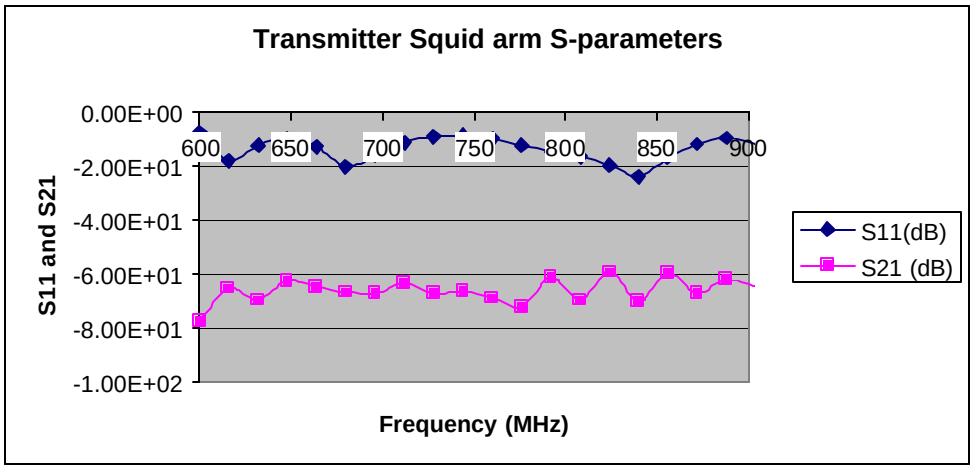

Figure 2.33: Transmitter SQUID arm S-parameters

2.4.2 Practical Issues in Implementation

After the design and the characterizations of the devices and the subsystems, integration of subsystems was done, where some important issues needed to be taken into account during the implementation.

All devices (including cables) needed to be shielded with a conductor foil to prevent interference between each device and from the environment. This is important since signals interfering from outside world are amplified with the main signal decreasing the sensitivity of the receiver. Another measure to fight against the interferences is to twist the cables with odd number of turns. Box resonance [43] can also be a problem in the receivers. It can exist in the band or out of the band but it absorbs energy of the main signal, lowering the power. If it is in-band, serious sensitivity problems may arise. Absorbers and various patterns made with conductors (at the same potential with box) can prevent box resonance. Lastly, the potential between the grounds of each subsystem should be zero to guarantee appropriate grounding.

In this work, we used copper sheets to accomplish boxing of each device. In Figure 2.34 and Figure 2.35, sample pictures taken from the receiver and the transmitter are shown. In these pictures, it should be noted that all the devices except cables are shielded using copper foils and aluminum boxes. The cables are double-screened cables and extra shield is not applied on them [44].

The shielded subsystem blocks were put into a bigger box. Bigger box helps us to gather all the subsystems into a compact space, which guarantees extra prevention from environmental in-band signals. After connections of the cables were made to these bigger boxes, the connectors were covered with aluminum and copper foils. This is due to connectors' being outside and being open to environmental signals.

An absorber is glued on the cover of the main box, which is able to absorb possible box resonance. Besides, the placement topology of the devices in the box can prevent box resonance.

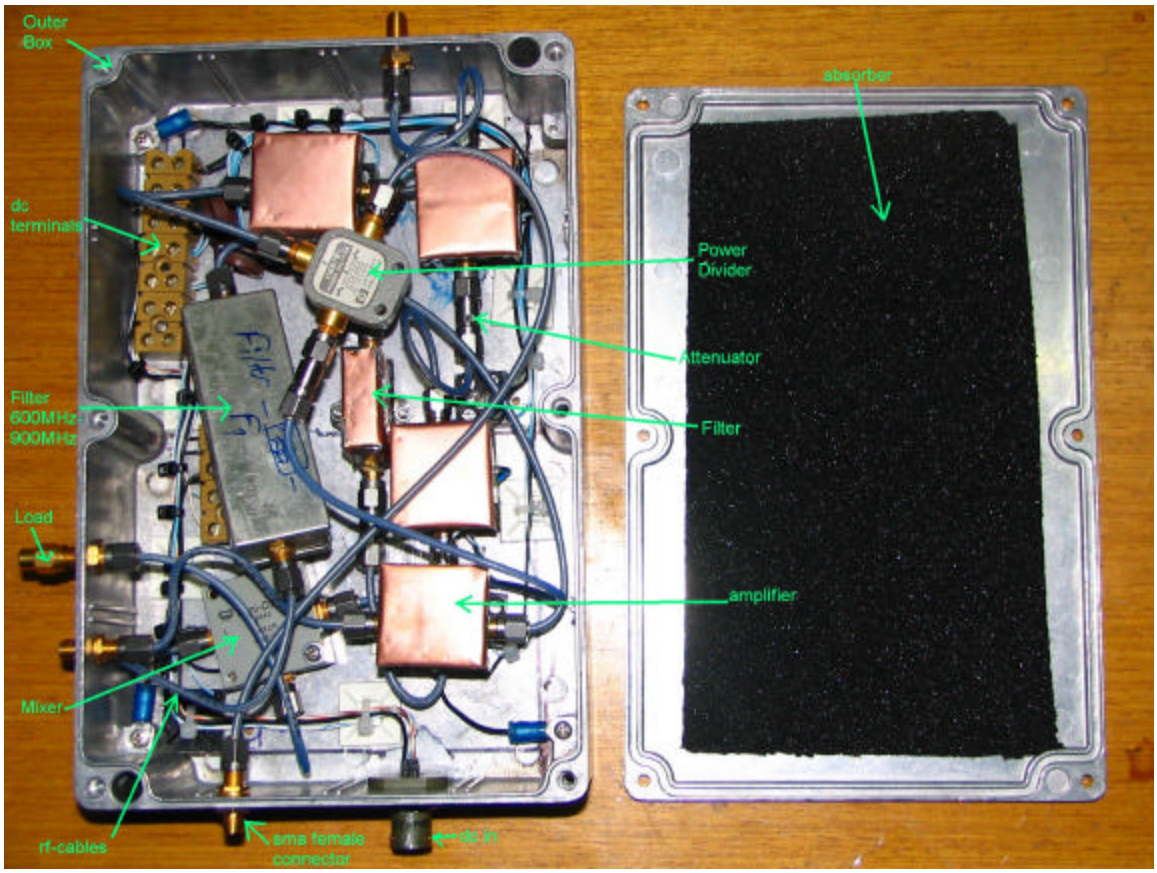

Figure 2.34: A picture of receiver system

After packaging the devices and subsystems into the boxes, the system was integrated. Besides the transmitter and receiver, there are measurement devices and power supply as indicated in Figure 2.6. After integration, the potentials between the grounds of each block were measured both DC-wise and AC-wise. To bypass the grounding problems, chassis of each device were connected to a common ground (earth ground) via large diameter copper cables. For continuing problems in grounding, problematic points of the blocks were shielded with aluminum foil and copper foil.

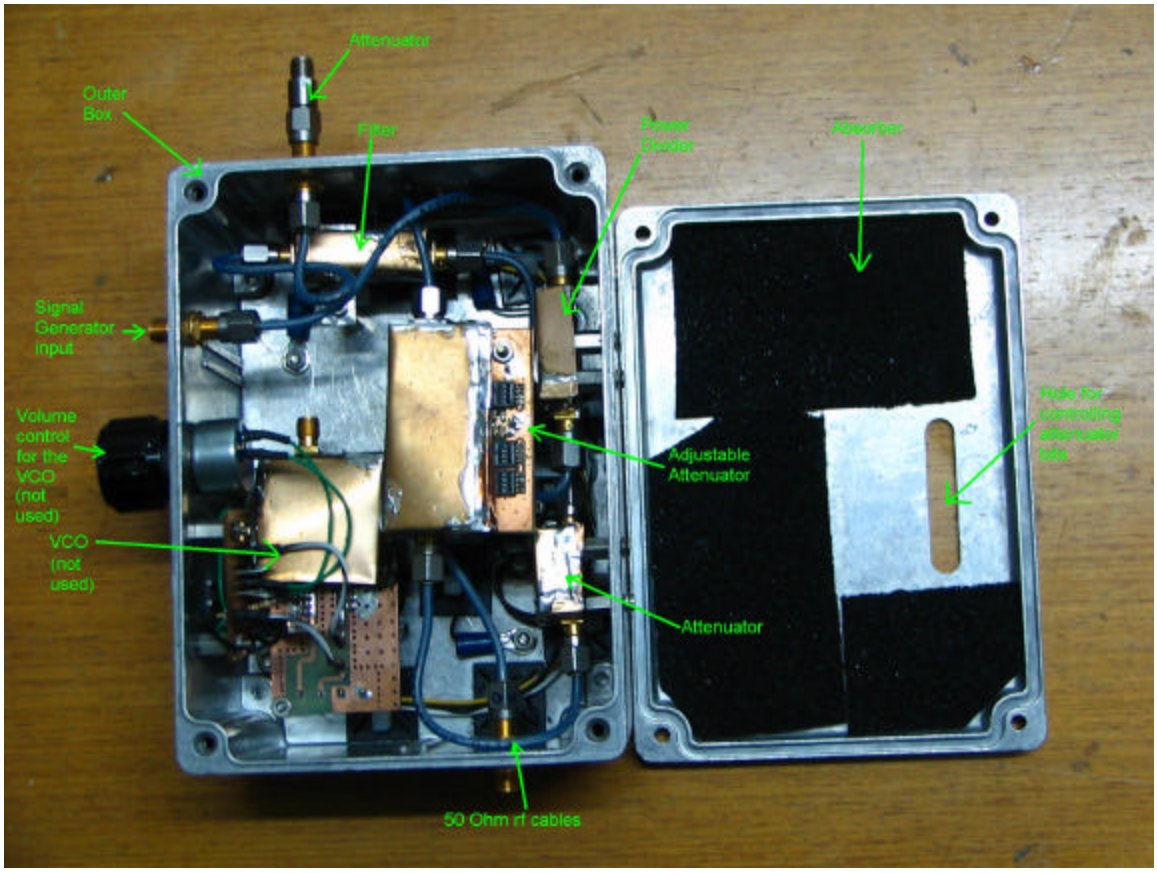

Figure 2.35: A picture of transmitter system

The connection cable between the tank circuit and the receiver was also shielded properly as shown in Figure 2.36. This cable and its connectors are open to environment and any picked signal interfering will be amplified in the receiver along with the main signal.

Figure 2.36: Tank Circuit Assembly

2.4.3 Implemented System and Sample Measurements

Proper design and implementation stages led us to the setup seen in Figure 2.37. Each part in the system is given a name on the figure and connections are made according to Figure 2.6. Besides, in Table 2.9, the devices and the subsystems used in the setup are shown.

Parts	NAME	COMPANY
Receiver	Designed in SERL	
Transmitter	Designed in SERL	
Tank Circuit Assembly	Designed in SERL	
IF Filter and Amplifier	SR560	SRS
Power Supply	E3616A	HP
Spectrum Analyzer	8590L	HP
Signal Generator	8657B	HP
Waveform Generator	GW	GW

Table 2.9: Devices and subsystems used in the setup

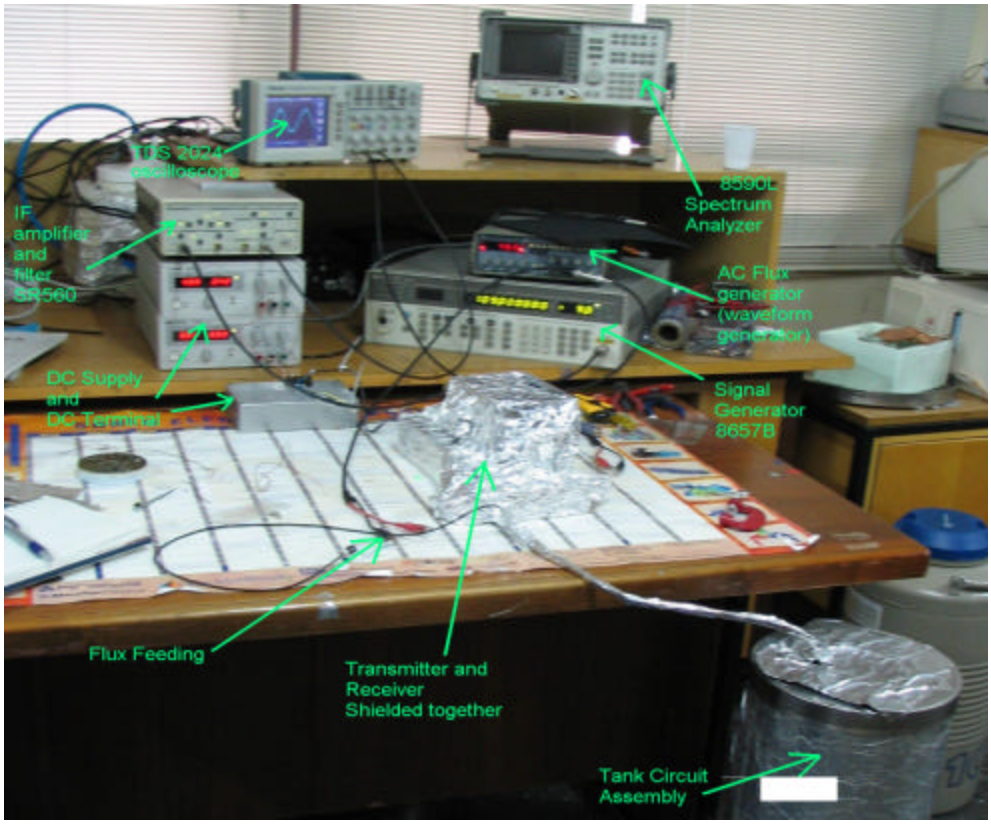

Figure 2.37: Implemented System

Using the system, some measurements were performed. More details about these measurements are explained in the next chapter. Here, only sample measurements are shown in Figure 2.38 and Figure 2.39.

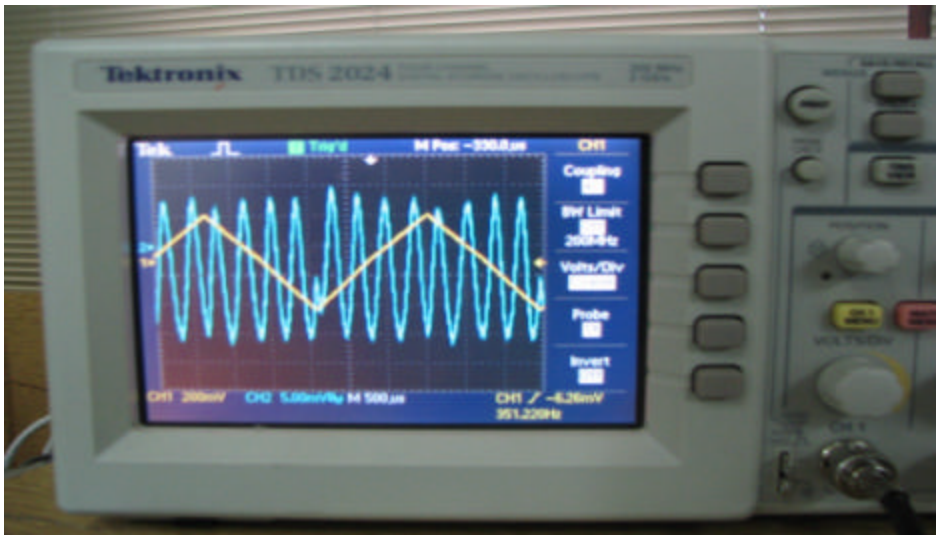

Figure 2.38: Measurement of applied flux and SQUID response on TDS 2024 oscilloscope in Y-T mode

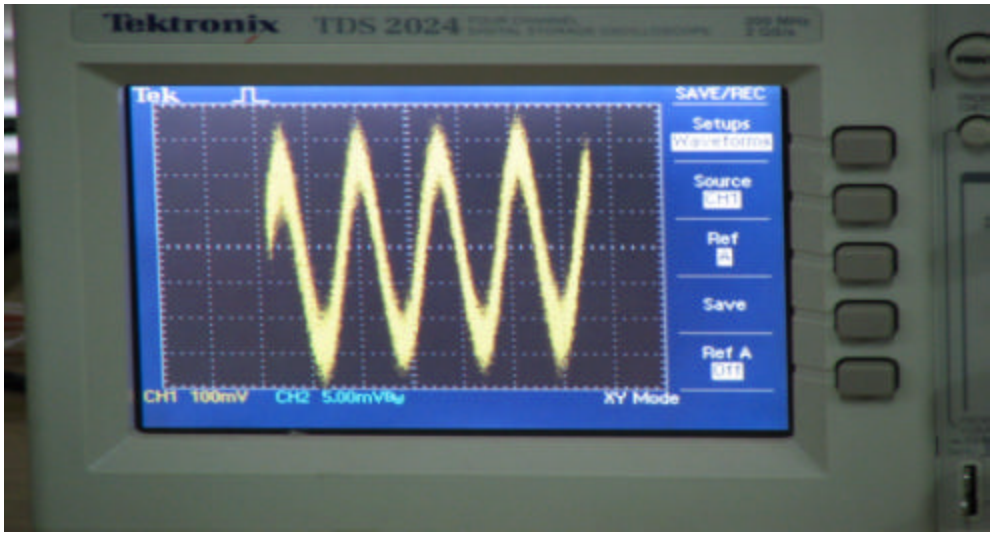

Figure 2.39: Measurement of applied flux and SQUID response on TDS 2024 in X-Y mode

Chapter 3

EXPERIMENTS AND RESULTS

Upon implementation of rf-SQUID readout electronics and the setup, several experiments were performed to characterize rf-SQUID response versus applied rf frequency and rf amplitude as variables. Besides, rf spectrum before the mixer is also analyzed at specific rf attenuation levels in this section.

3.1 Preliminary Work and Device Settings

Before experiments, to automate the measurements, a program in lab-view was developed. This program controls the signal generator and the oscilloscope. A picture of the user interface of the program is shown in Figure 3.1.

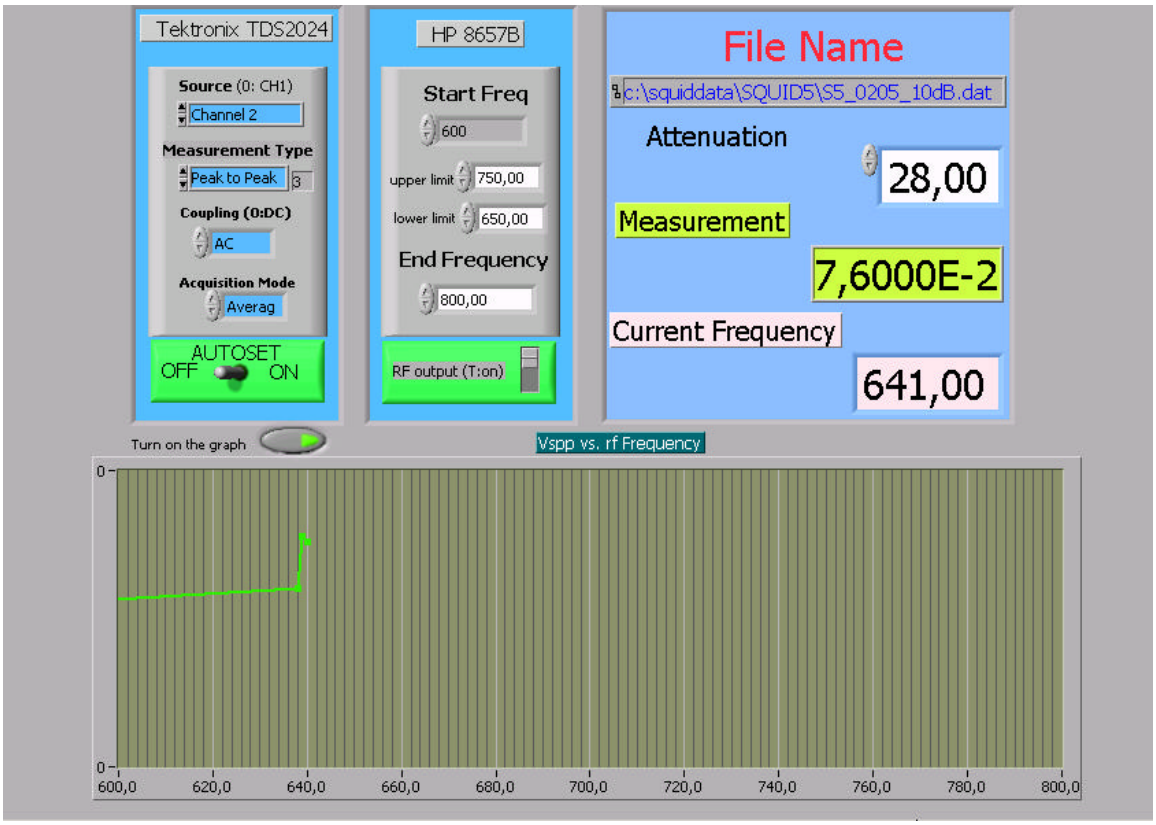

Figure 3.1: A program written in labview to automate measurements

The program adjusts the sweep frequencies and the initial settings of the oscilloscope for the measurements. At the same time, it plots the data on-line and demonstrates current conditions of the measurement. After a measurement, the measured data is saved to a disk with a specified name for further data processing.

The utilized devices are listed in Table 2.9. The required initial values for these devices were set before the measurements. The settings are listed for the signal generator and the spectrum analyzer in Table 3.1 and Table 3.2

.

Signal Generator	
Frequency	600MHz-800MHz sweep
Amplitude	+8dBm

Table 3.1: Signal Generator Settings

Spectrum Analyzer	
Center Frequency	750MHz
Span	300 MHz
RBW	1MHz
VBW	1MHz
Attenuation	10dB
Reference Level	-20dBm
Scale	5dB

Table 3.2: Spectrum Analyzer Settings

Lastly 2 rf-SQUID gradiometers with a tank circuit resonating at 720 MHz were used in these measurements. Gradiometers are made of Y-Ba-Cu-O film deposited on $LaAlO_3(100)$ substrate. For more information on the fabrication techniques and the characteristics of the SQUIDs, please refer to [45] and [46].

3.2 Rf-SQUID Output Response (V_{spp}) and Spectrum Measurements

Upon preliminary work, data were taken from rf-SQUID by changing frequency and rf-amplitude on two rf-SQUIDs. For these SQUIDs, acquired 3-D data are shown in Figures 3.2-3.7.

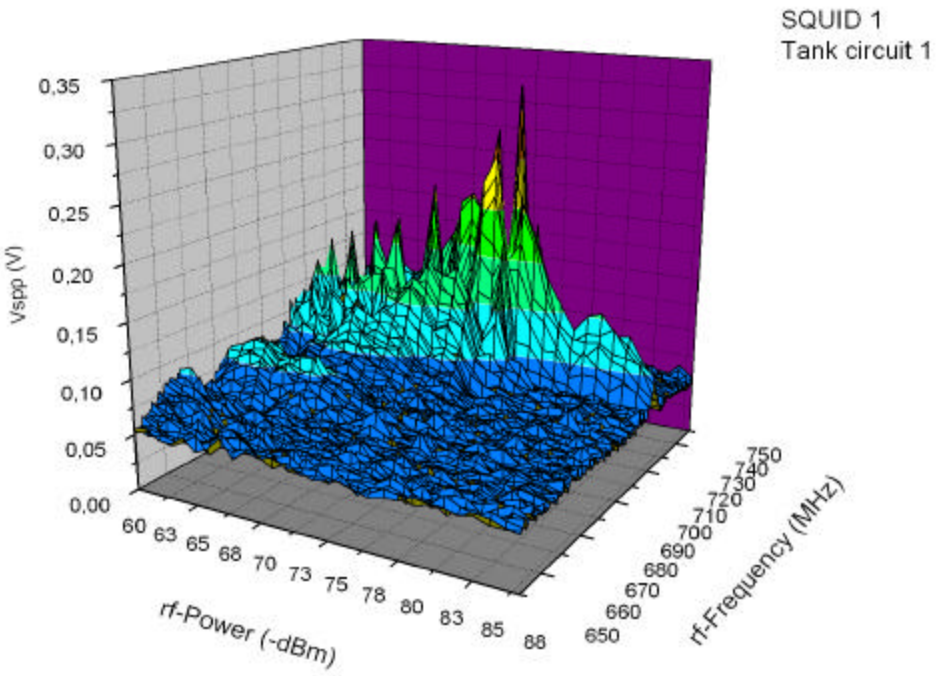

Figure 3.2: 3D plot of rf-SQUID peak to peak response for changing frequency and rf pump amplitude-SQUID1

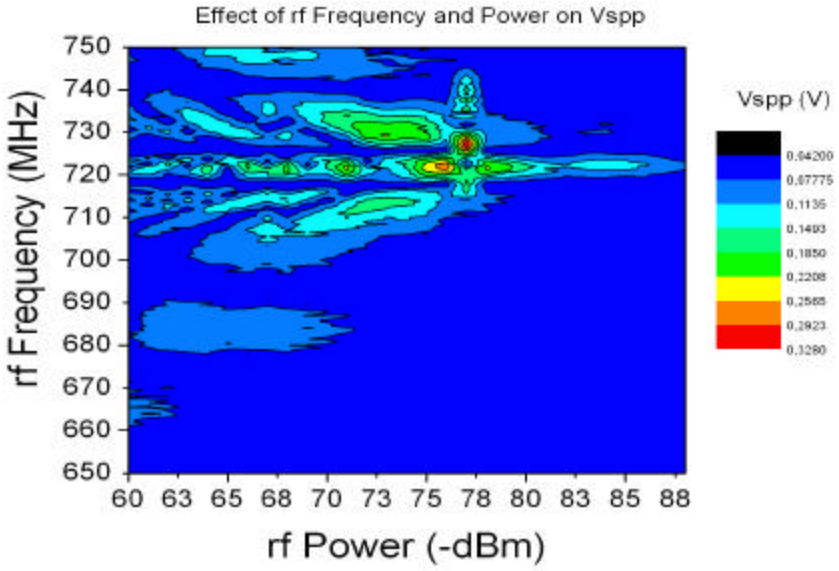

Figure 3.3: Contour plot of rf-SQUID peak to peak response for changing frequency and rf pump amplitude-SQUID1

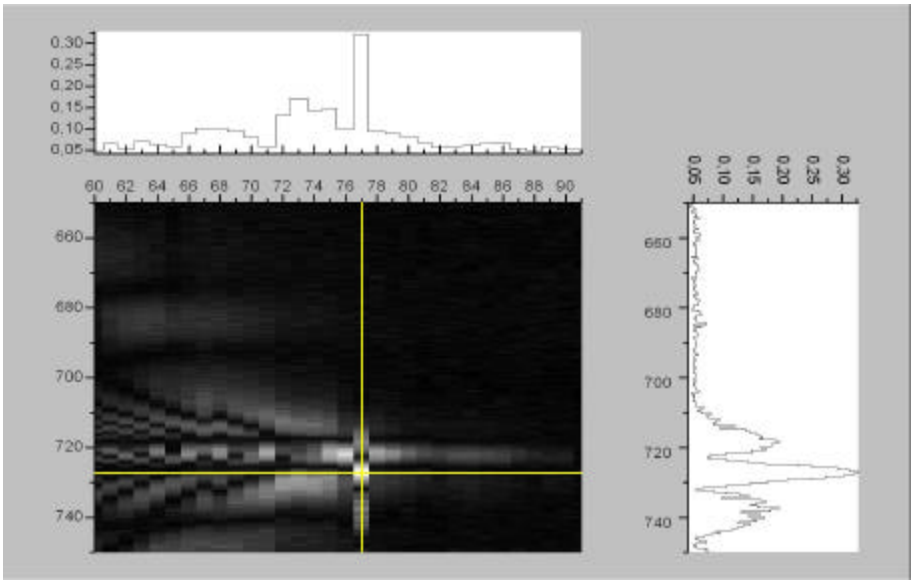

Figure 3.4: Grayscale profile plot of rf-SQUID peak to peak response for changing frequency and rf pump amplitude.-SQUID1

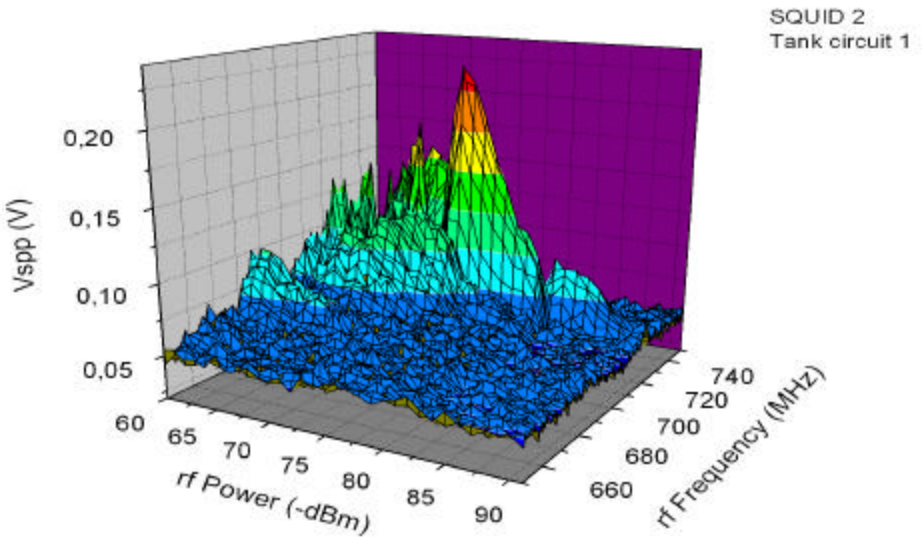

Figure 3.5: 3D plot of rf-SQUID peak to peak response for changing frequency and rf pump amplitude-SQUID2

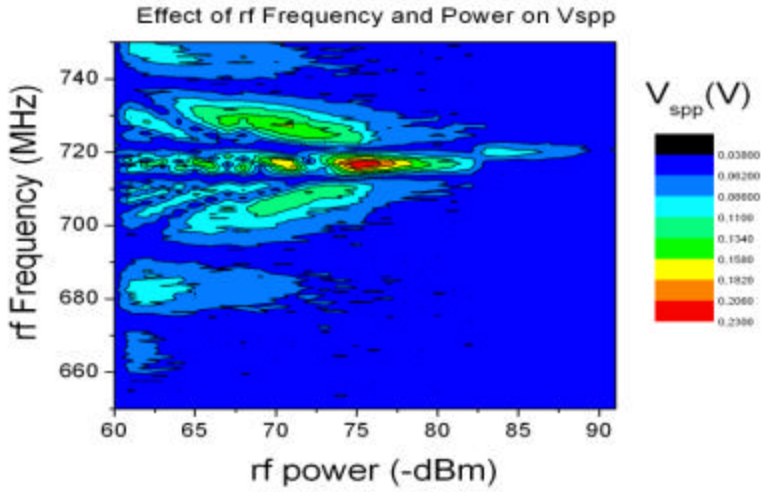

Figure 3.6: Contour plot of rf-SQUID peak to peak response for changing frequency and rf pump amplitude-SQUID2

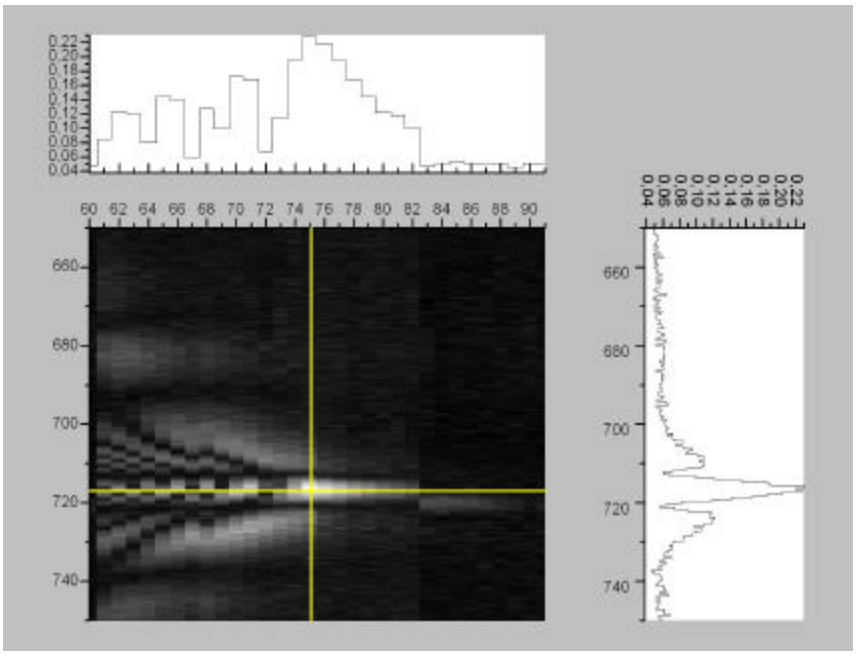

Figure 3.7: Grayscale profile plot of rf-SQUID peak to peak response for changing frequency and rf pump amplitude.-SQUID2

First observation about the graphs is that two SQUID gradiometers display similar characteristics in terms of the applied frequency and power amplitude. This is because they were fabricated on the same substrate with same techniques. Small differences in the patterns are likely to be due to fabrication or device adjustment while placing SQUID on the tank circuit.

Upper inserts in Figure 3.4 and Figure 3.7 shows that, lowering pumping power increases the amplitude of SQUID response with its peak around –76 dBm power. Similarly, the right inserts of these figures show that the peak-to-peak voltage of rf-SQUID response with respect to frequency is observed to follow a sinc-like curve. In Figure 3.8, this curve is shown clearly, where there is 15 dB of attenuation in the rf-power (attenuation is applied on –60 dBm power. Thus 15 dB attenuation means –75 dBm pumped power). Besides, according to Figure 2.11, the spectrum power at the rf

input of the mixer is demonstrated in Figure 3.9[3] . At the circled points, rf-SQUID has large interferences.

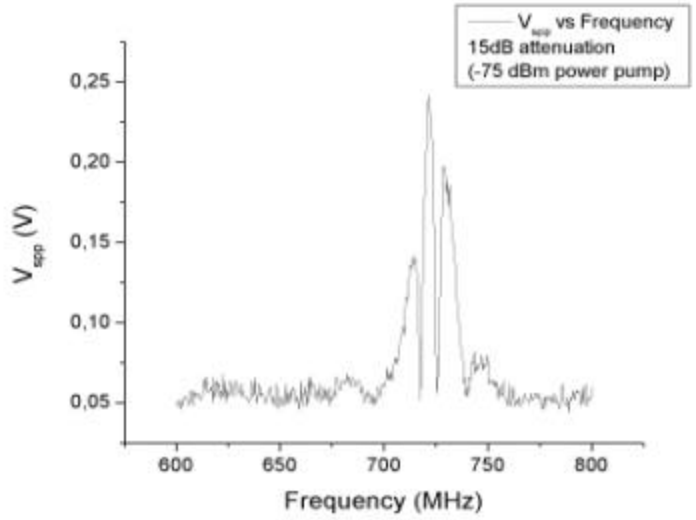

Figure 3.8: SQUID1 V_{spp} measurement with 15dB attenuation

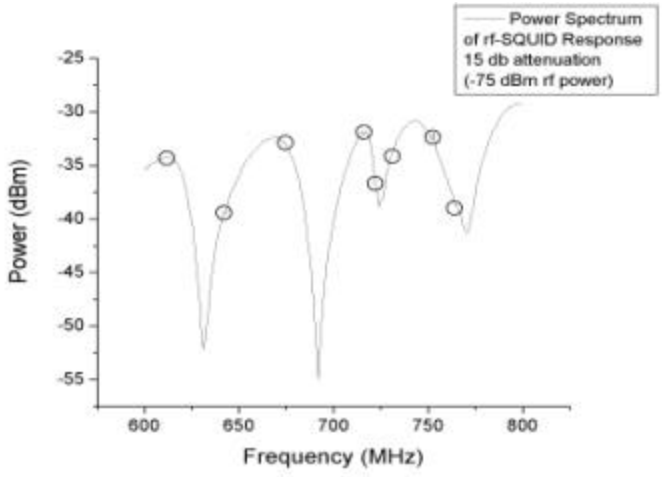

Figure 3.9: SQUID1 spectrum measurement: Circled points are the places where there are peaks in the rf-SQUID response (Figure 3.8)

[3] Here the resolution bandwidth of spectrum analyzer is adjusted to 1 MHz. So all SQUID signal (AM modulation) is averaged in 1MHz and only one signal's amplitude is found at the output.

These figures show that, when there is a SQUID response, the continuity of spectrum power is affected and sudden changes in the slope in spectrum power are observed. At these points, rf power is modulated (increased side lobes of AM signal) and sent back to the receiver and high interferences occur. Thus, spectrum power can be monitored to find out the frequencies at which SQUID responds. In Figure 3.10, both spectrum power and V_{spp} measurements are placed onto the same graph to better visualize the points where there is SQUID interference. Graphs for the second SQUID are plotted in Figure 3.11 and Figure 3.12.

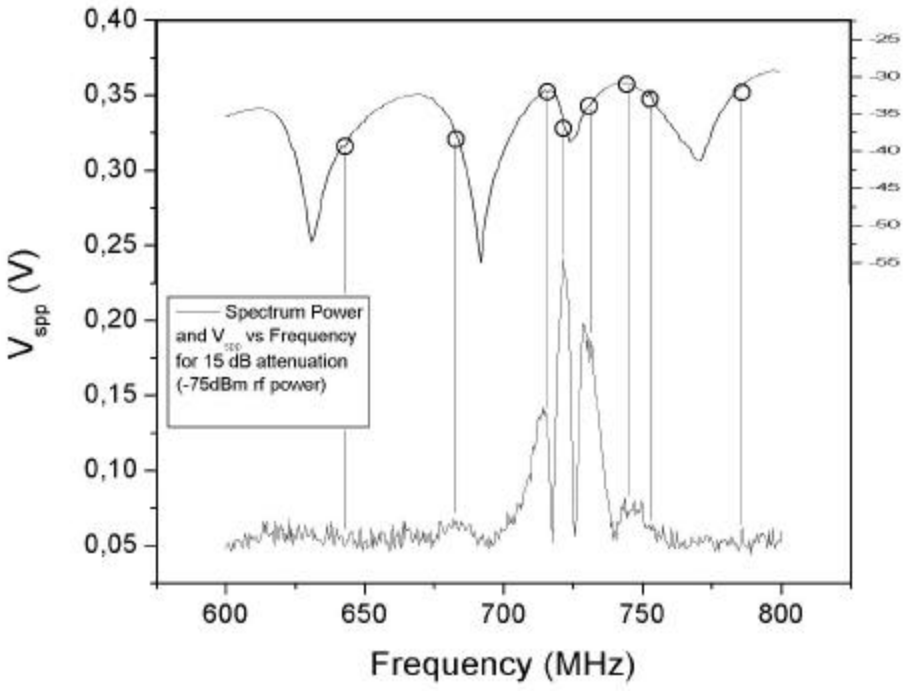

Figure 3.10: Spectrum and Vspp measurement for SQUID1 with 15 dB attenuation level

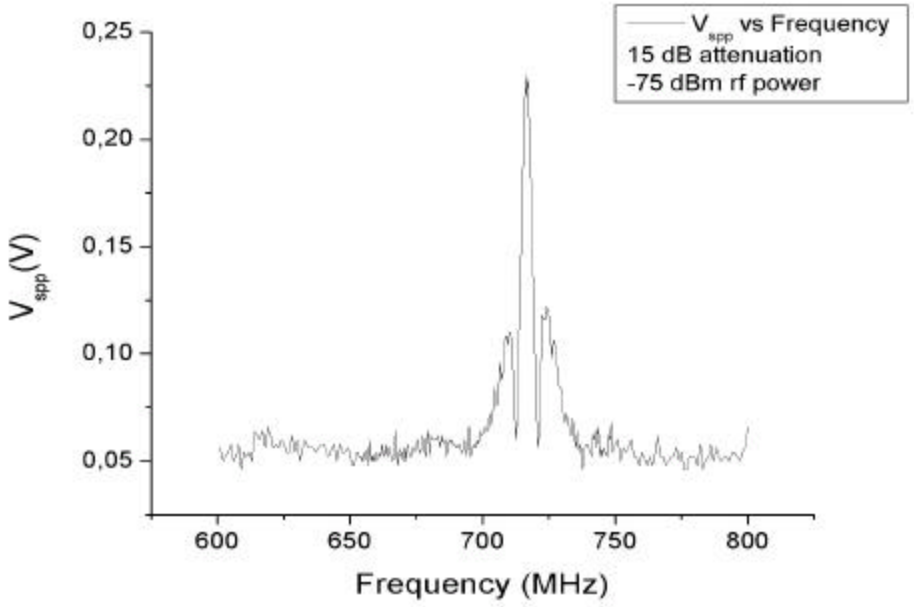

Figure 3.11: SQUID2 V_{spp} measurement with 15dB attenuation

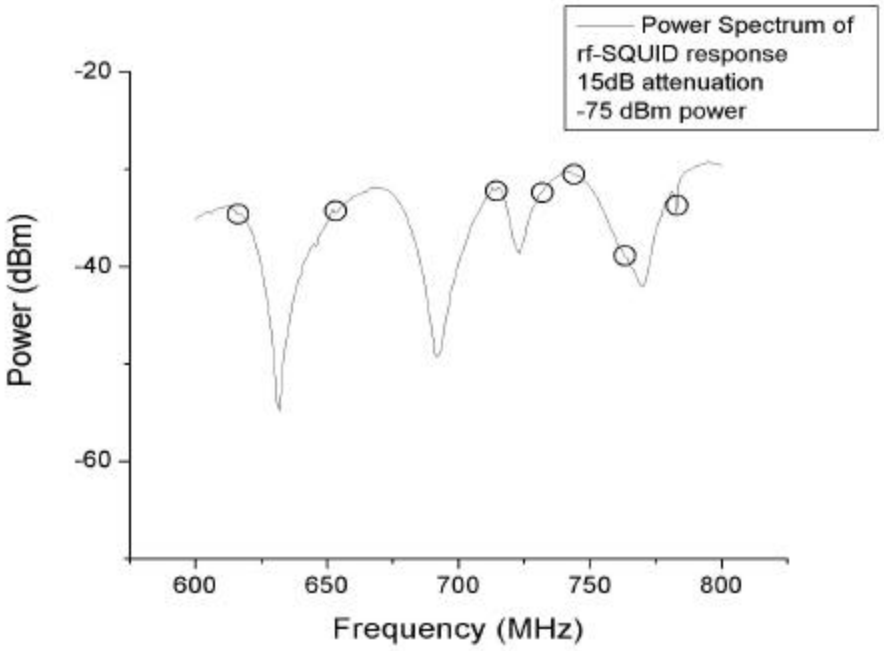

Figure 3.12: SQUID2 spectrum measurement

An important point to note in these graphs is that there exist deep notches in the rf spectrum of the signal for both SQUIDs. These notches are interpreted to be due to the tank circuit characteristics with the SQUID in liquid nitrogen. When the amplitude of the pumped rf signal is increased, changes in V_{spp} and rf spectrum are observed. For SQUID1, the results are shown in Figure 3.13 and Figure 3.14.

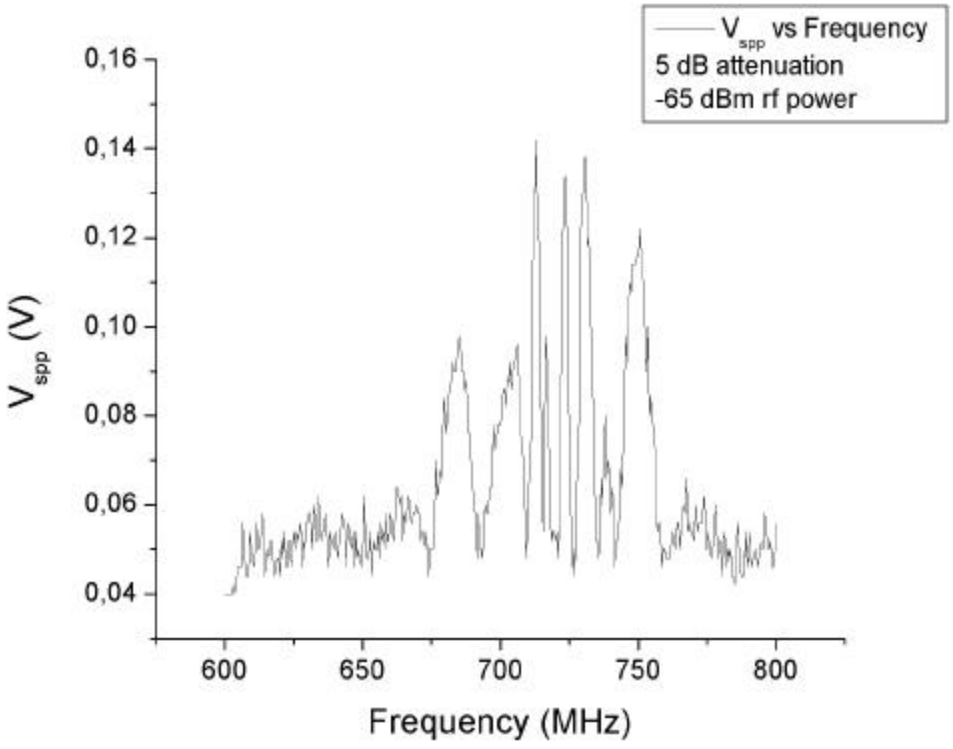

Figure 3.13: SQUID1 Vspp measurement with 5 dB attenuation

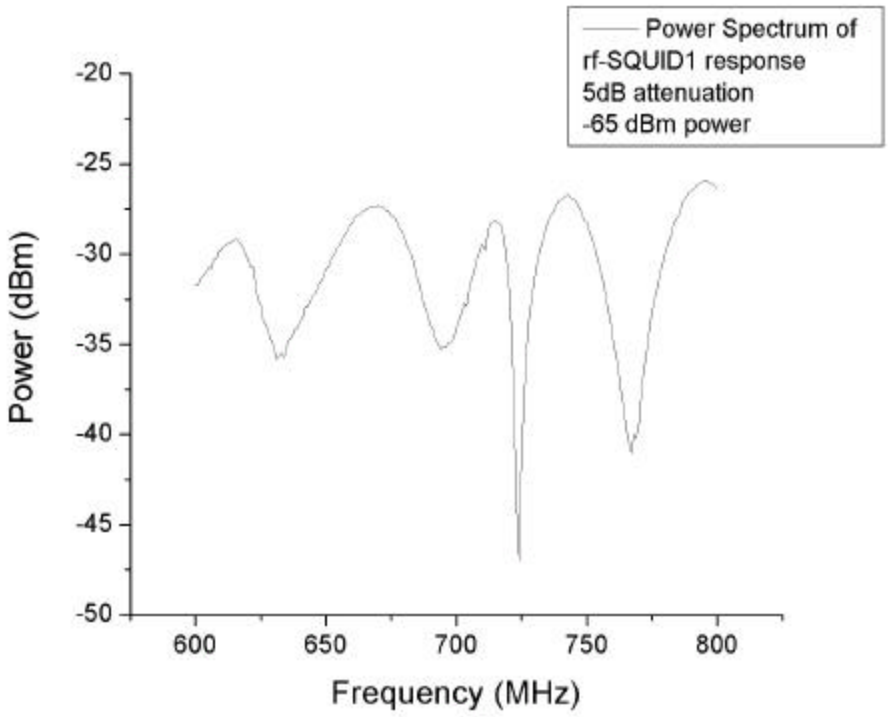

Figure 3.14: SQUID1 spectrum measurement

According to these graphs, with higher amplitude rf signal pump, the number of large rf-SQUID interferences increase around the resonance point of the tank circuit. But the level of these interferences are lower than that with low amplitude rf signal pump. The spectrum of this case is similar to the one with lower amplitude rf pump as shown in Figure 3.9. There are two main differences. Firstly, there is increase in all levels, which is due to higher amplitude rf power going into tank circuit. Secondly, the levels of depth of the notches in the spectrum are changed. This is due to the higher rf power, which affects the Q of the tank circuit (due to SQUID effective inductance change) at the frequencies where there are notches.

Similar graphs for SQUID 2 are included in Figure 3.15 and Figure 3.16.

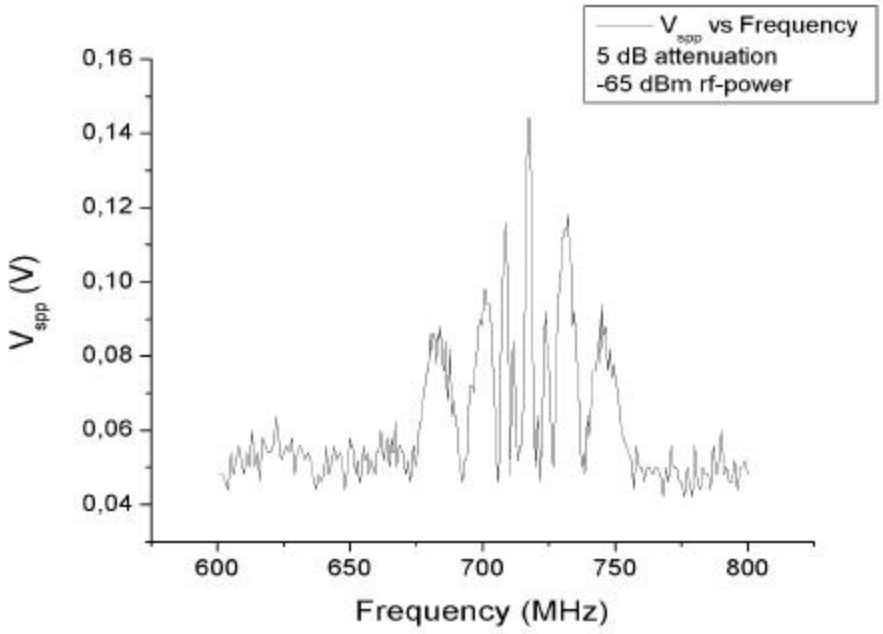

Figure 3.15: SQUID2 V_{spp} measurement with 5 dB attenuation

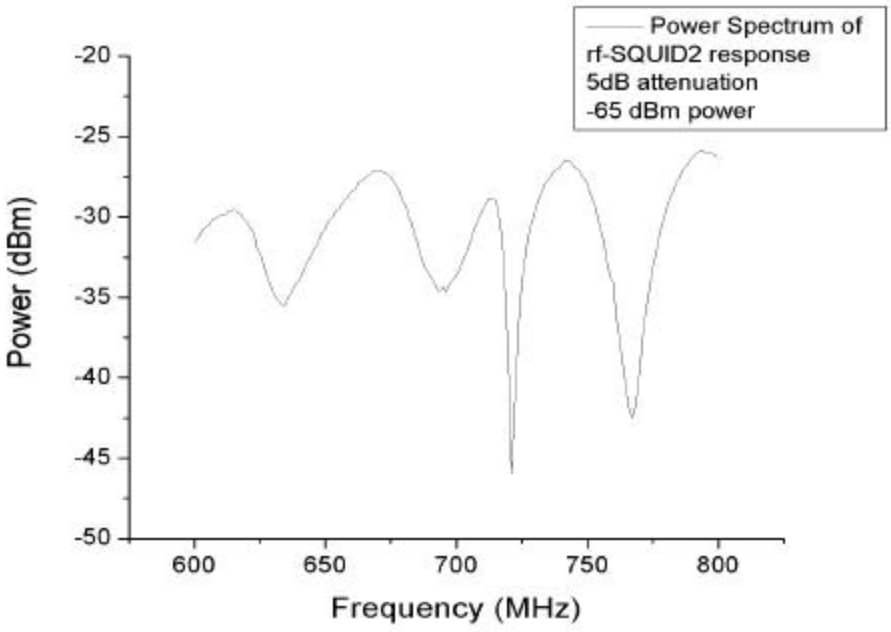

Figure 3.16: SQUID2 spectrum measurement

The frequency behavior of rf-SQUID should be analyzed with more experiments with different SQUIDs. Thus, different parameters in implementation of SQUIDs and their frequency responses can be related.

Chapter 4

CONCLUSIONS AND FUTURE WORK

In this work, an experimental transmit-receive system of homodyne type working in the frequency range of 600MHz-900MHz has been designed and implemented for rf-SQUID characterization and magnetometry. This system utilizes the flux properties of rf-SQUID and outputs the amplitude modulation added by the rf-SQUID on rf input signal due to an externally applied flux.

Following the design and implementation of the system, experiments to characterize rf-SQUID response were performed. In these experiments, the applied rf signal's frequency and amplitude were changed and output peak to peak voltage was observed and reported versus these parameters.

During the design and the implementation, several points were noticed to adjust for a better performance of the implemented transceiver. When looked as a whole, the receiver should be converted to super heterodyne type. This means adding another IF and increasing the number of mixers, although mixers are pathetic devices. This change also requires a frequency synthesizer at which all created signals have the same time-base. The virtue in using super heterodyne lies in the fact that, designer can select the first IF frequency freely. Besides, the necessity to down-convert from high frequencies to a few KHz, which is hard for a mixer working at the frequencies of interest, becomes

obsolete by true selection of the first IF and proper filtering. Such a system becomes harder to implement but can offer better results.

During noise figure derivations listed in Table 2.4 through Table 2.6, the loss associated with the coupler (3dB due to power division) was unfortunately added directly to the noise figure of the receiver. Instead of using a 3dB coupler, couplers with 10 dB or lower coupling values can be utilized, which decreases the receiver noise figure and the attenuation requirement in the transmitter. Additionally, using a lower noise amplifier as the first stage of the receiver could definitely decrease the noise figure to much lower values.

Characterization of rf-SQUIDs in terms of rf frequency and amplitude is essential at present condition. Until now, two gradiometers were tested and properties of them are reported. Various types of rf-SQUIDs should be analyzed in the same manner to acquire frequency and amplitude characteristics of their signals. These properties can be related to the fabrication methods and the physical parameters of them to further improve the SQUID and resonater assembly designs.

For rf-SQUID operation at higher frequencies (>1GHz), the architecture of the receiver would be better to be super-heterodyne, since direct detection of modulation signal at these frequencies will become harder. 2 IF stages, second of which is similar to ours, would be adequate to detect modulation. As mentioned above, synthesizers are required for local oscillator and they are capable of creating unwanted harmonics of the base frequencies, which cause noise to increase [40]. Another challenge at higher frequencies is the resonator, which requires other technologies in the implementation.

APPENDIX A

A.1 Power Conversions

In this study, dBm conventions are used to define the power. The conversion between mW and dBm together with voltage on system impedance (50 Ohm) are shown in equation 5.1 and **Table A.1**.

$$P(dBm) = 10\log_{10}(P(mW)) = 10\log_{10}(\frac{V_{rms}^{2}}{50}1000) \quad \text{(A.1)}$$

Vrms (υV)	Power(mW)	Power(dBm)
0.223606798	1	0
0.125743343	0.316227766	-5
0.070710678	0.1	-10
0.039763536	0.031622777	-15
0.02236068	0.01	-20
0.012574334	0.003162278	-25
0.007071068	0.001	-30
0.003976354	0.000316228	-35
0.002236068	0.0001	-40
0.001257433	3.16228E-05	-45
0.000707107	0.00001	-50
0.000397635	3.16228E-06	-55
0.000223607	0.000001	-60
0.000125743	3.16228E-07	-65
7.07107E-05	0.0000001	-70
3.97635E-05	3.16228E-08	-75
2.23607E-05	0.00000001	-80
1.25743E-05	3.16228E-09	-85
7.07107E-06	0.000000001	-90

Table A.1: Conversion between power conventions and voltage for Z_0=50

A.2 Device and Instrument Information

In this subsection, the manufacturer data sheets for devices and instruments are placed.

- **AMPLIFIER**

Manufacturer : Stanford Microdevices

Manufacturer's Specification : Wireless Products Catalog

Manufacturer's Type Number: SCA-4

Description :DC-3GHz Cascadable GaAs MMIC Amplifier

Electrical Specifications (T_a=25°C)(Id = 100mA and Z_0=50 Ohm)

Symbol	Parameters & Test Conditions: Id=50mA, Zo=50Ω		Min	Typ	Max	Units
G_p	Power Gain	f=0.1-2.0 GHz	16	18		dB
		f=2.0-3.0 GHz		17		
Gf	Gain Flatness	f=0.1-2.0 GHz		+/-1		
	Gain Flatness over any 100 MHz			+/-0.1		
P1dB	Output Power at 1dB Compression	f=0.9 GHz		20.5		dBm
		f=1.9 GHz		19.8		
		f=2.5 GHz		18.8		
NF	Noise Figure	f=0.1-3.0 GHz		4.5		dB
IP3	Third Order Intercept Point Output Tones @ 0 dBm 10 MHz Apart	f=0.9 GHz	35.5	37.5		dBm
		f=1.9 GHz	36	38		
		f=2.5 GHz		36.5		
T_D	Group Delay	f=1.9 GHz		120		psec.
ISOL	Reverse Isolation	f=0.1-3.0 GHz		22		dB
V_D	Device Voltage	V_D=+5V	4.3	5.2	5.7	V
dV/dT	Device Voltage Temperature Coefficient			-5		mV/degC
dG/dT	Device Gain Temperature Coefficient			-0.0027		dB/degC

Table A.2: Electrical Specifications

APPENDIX A

Absolute Maximum Ratings:

Device Current	:120 mA
Power Dissipation	:660mW
RF Input Power	:200mW
Junction Temperature	:+200^{o}C
Operating Temperature	:-45^{o}C to +85^{o}C
Storage Temperature	:-65^{o}C to +150^{o}C

Outline Drawing

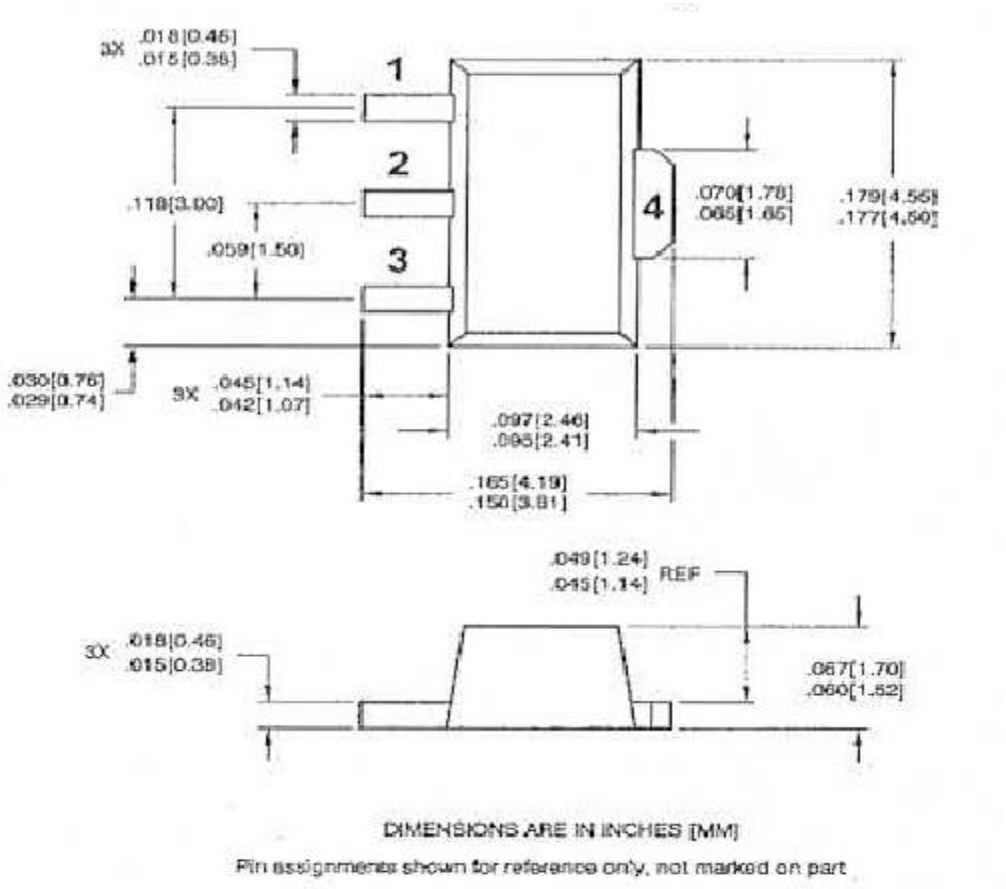

Figure A.1: Outline Drawing of SCA-4 Amplifier

Pin Designation	
1	RF in
2	GND
3	RF out and Bias
4	GND

Table A.3: Pin Arrangement

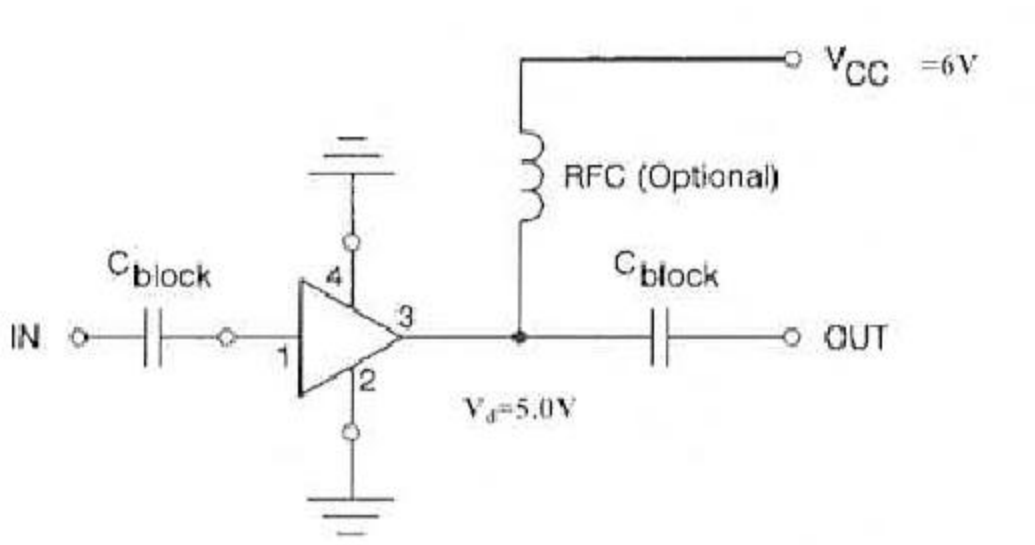

Figure A.2: Biasing configuration of SCA-4

- **MIXER**

Manufacturer : Mini Circuits

Manufacturer's Type Number: ZFM-2H

Detailed Catalogue : http://www.minicircuits.com

APPENDIX A

Electrical Specifications:

ZFM-2H LO Power Level 17 dBm

Frequency MHz		Max. Conversion Loss dB		Min. LO-RF Isolation dB			Min. LO-IF Isolation dB		
LO/RF	IF	Mid-Band	Total Range	L	M	U	L	M	U
5.00-1000	DC-1000	7.0	10.0	40	30	20	40	25	17

Table A.4: Electrical Specifications for ZFM-2H

Absolute Maximum Ratings

RF Power : 200mW

Peak IF Current : 40mA

Outline Drawing

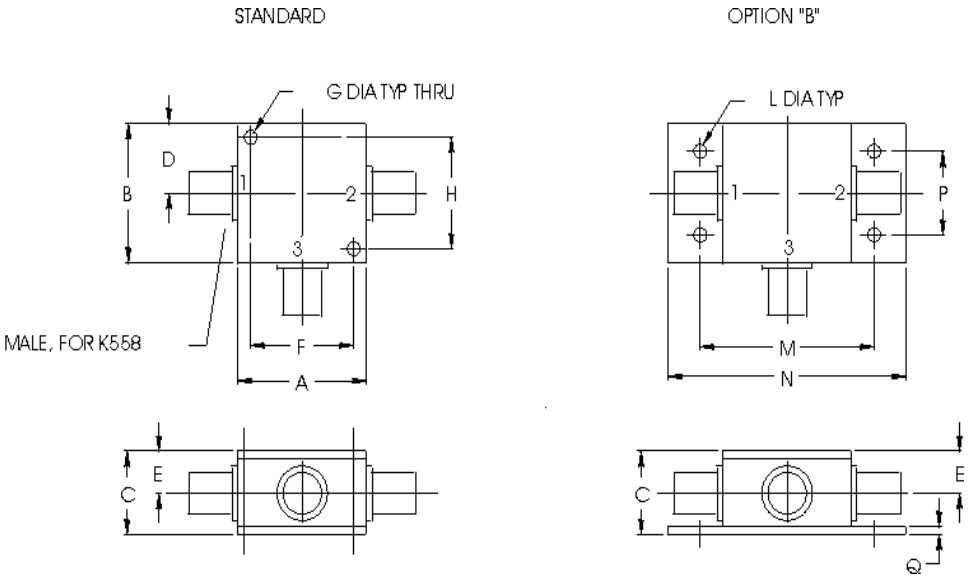

Figure A.3: Outline Drawing of ZFM-2H

Case Style - K18 (inch,mm) weight: 70.00 grams.

A	B	C	D	E	F	G	H	J
1.25	1.25	.75	.63	.38	1.000	.125	1.000	
31.750	31.750	19.050	16.002	9.652	25.400	3.175	25.400	

K	L	M	N	P	Q	R	S	T
	.125	1.688	2.18	.75	.07			
	3.175	42.875	55.372	19.050	1.778			

Table A.5: Dimensions

Connector : SMA female

Performance data tables are included in the following pages.

APPENDIX A

Typical Performance Data

ZFM-2H		Conversion Loss (dB)			ISO	Isolation L-R (dB)			Isolation L-I (dB)		
RF MHz	LO MHz	LO +14 dBm	LO +17 dBm	LO +20 dBm	LO (MHz)	LO +14 dBm	LO +17 dBm	LO +20 dBm	LO +14 dBm	LO +17 dBm	LO +20 dBm
5.000	35.000	6.20	5.75	5.56	5.000	74.00	73.03	70.67	67.29	64.57	63.07
35.152	65.150	6.28	5.75	5.54	35.152	54.22	53.95	53.39	51.18	50.91	50.42
65.304	95.300	6.51	5.78	5.55	65.304	48.20	47.75	46.75	45.62	44.94	44.11
125.610	95.610	6.40	5.83	5.54	125.610	46.20	45.94	44.83	43.25	42.85	42.09
185.910	155.910	6.56	5.88	5.63	185.910	43.09	41.73	40.19	39.67	38.74	37.98
216.060	186.060	6.55	5.87	5.68	216.060	41.78	40.07	38.85	38.01	37.26	36.64
276.370	246.370	6.22	5.70	5.55	276.370	38.57	37.49	36.91	35.45	34.59	34.48
336.670	306.670	5.97	5.62	5.52	336.670	35.95	35.70	36.13	33.67	32.97	33.08
396.980	366.980	6.09	5.78	5.59	396.980	35.04	35.50	35.59	32.50	32.29	32.34
457.280	427.280	6.48	6.15	5.93	457.280	33.88	33.92	33.86	30.42	30.55	30.59
517.580	487.580	6.37	5.88	5.61	517.580	33.96	34.70	34.90	29.63	29.07	29.34
547.740	517.740	6.24	5.91	5.66	547.740	33.82	35.38	35.32	29.51	29.45	29.80
608.040	578.040	6.57	6.36	6.18	608.040	32.52	34.75	34.17	28.25	28.29	28.63
668.340	638.340	6.78	6.50	6.10	668.340	32.38	34.53	32.34	27.59	27.06	26.63
728.650	698.650	7.19	6.30	5.86	728.650	32.32	33.69	32.40	26.83	25.41	24.95
849.260	819.260	9.23	7.56	6.21	849.260	32.91	32.23	31.42	25.91	24.28	23.11
909.560	879.560	9.88	8.59	7.12	909.560	33.24	32.46	31.95	25.89	23.91	22.92
969.860	939.860	9.62	8.55	7.56	969.860	32.85	32.66	32.72	25.75	24.30	23.22
1000.000	970.000	9.60	8.57	7.71	1000.000	32.43	32.20	32.53	25.10	24.05	22.04

Table A.6: Typical Performance Data - 1

APPENDIX A

RF/LO	VSWR RF port			VSWR LO port			IF	VSWR IF port			Ø detection		
FREQ. (MHz)	LO +14 dBm	LO +17 dBm	LO +20 dBm	LO +14 dBm	LO +17 dBm	LO +20 dBm	FREQ. (MHz)	LO +14 dBm	LO +17 dBm	LO +20 dBm	,FREQ. MHz	max.DC output mV	DC offset mV
5.000	1.37	1.24	1.21	1.27	1.51	2.45	5.000	2.28	2.05	1.80	5.00	-946.00	-0.04
35.121	1.24	1.10	1.03	1.11	1.53	2.39	35.121	2.22	2.01	1.77	35.15	-938.10	-0.02
65.242	1.24	1.10	1.03	1.13	1.52	2.48	65.242	2.27	2.04	1.80	65.30	-949.90	0.00
95.364	1.23	1.09	1.03	1.16	1.44	2.26	95.364	2.28	2.06	1.80	95.46	-985.50	0.09
155.610	1.23	1.09	1.04	1.17	1.43	2.30	155.610	2.33	2.10	1.83	155.76	-936.30	0.06
185.730	1.23	1.10	1.04	1.16	1.39	2.08	185.730	2.34	2.10	1.82	185.91	-950.60	0.23
245.970	1.24	1.11	1.05	1.21	1.38	2.10	245.970	2.47	2.20	1.90	246.22	-990.70	0.93
306.210	1.25	1.11	1.06	1.23	1.40	2.16	306.210	2.61	2.28	1.95	306.52	-1007.30	0.88
366.450	1.26	1.12	1.07	1.21	1.37	2.14	366.450	2.64	2.30	1.97	366.82	-905.20	1.17
426.700	1.27	1.13	1.08	1.21	1.36	2.04	426.700	2.68	2.34	2.00	427.13	-847.70	2.27
486.940	1.29	1.15	1.09	1.18	1.37	2.00	486.940	2.84	2.44	2.07	487.43	-867.60	2.06
517.060	1.29	1.15	1.08	1.16	1.39	2.03	517.060	2.94	2.51	2.09	517.58	-892.00	1.26
577.300	1.30	1.16	1.08	1.17	1.38	2.00	577.300	2.93	2.52	2.11	577.89	-927.80	1.97
637.550	1.33	1.17	1.10	1.17	1.38	1.93	637.550	2.91	2.50	2.13	638.19	-867.70	4.69
697.790	1.36	1.20	1.12	1.20	1.36	1.93	697.790	2.89	2.48	2.14	698.50	-753.40	4.48
758.030	1.38	1.22	1.15	1.13	1.45	1.94	758.030	2.69	2.35	2.06	758.80	-693.90	5.71
818.270	1.42	1.26	1.20	1.06	1.49	2.01	818.270	2.60	2.25	1.99	819.10	-667.60	4.22
878.520	1.51	1.34	1.29	1.03	1.52	2.05	878.520	2.62	2.25	1.97	879.41	-684.00	5.20
938.760	1.64	1.46	1.41	1.06	1.54	2.03	938.760	2.69	2.26	1.96	939.71	-675.30	6.68
1000.000	1.80	1.62	1.55	1.09	1.53	1.99	1000.000	2.63	2.22	1.92	1000.00	-664.10	7.63

Table A.7: Performance Data-2

APPENDIX A

- **TUNABLE ATTENUATOR**

Manufacturer : MA/COM

Manufacturer's Type Number: AT20-0263

Description : Digital Attenuator, 31dB, 5 Bit, TTL Driver, DC-2GHz

Detailed Catalogue : http://www.macom.com

Electrical Specifications (TA = 25°C)

Parameter	Test conditions		Units	Min.	Typ.	Max.
Reference Insertion Loss	DC-0.5GHz DC-1.0GHz DC-2.0GHz		dB dB dB		2.0 2.2 2.5	2.4 2.8 3.0
Attenuation accuracy	Any single bit Any combination of bits	DC-2.0GHz DC-2.0GHz	±(0.25+3% of attenuation setting in dB)dB ±(0.25+3% of attenuation setting in dB)dB or ±0.45dB, whichever is greater			
VSWR	DC-2.0GHz					1.6:1
Trise, Tfall Ton, Toff Transients	10% to 90% 50% Control to 90/10% RF In band (peak to peak)		nS nS mV		50 150 50	
1dB Compression	Input power Input power	0.05GHz 0.5-2.0GHz	dBm dBm		+20 +28	
Input IP3	For two-tone input power up to +5dBm	0.05GHz 0.5-2.0GHz	dBm dBm		+40 +48	
Input IP2	For two-tone input power up to +5dBm	0.05GHz 0.5-2.0GHz	dBm dBm		+45 +68	
V_{CC} V_{EE}			V V	4.5 -8.0	5.0	5.5 -5.0
I_{CC}	V_{CC}=4.5 to 5.5V Vctl=0 to 0.8V, or Vcc-2.1V to Vcc		mA			5.0
I_{EE}	V_{EE}=-5.0 to -8.0V		mA			1.0

Table A.8: Electrical Specifications of AT20-0263

Absolute Maximum Ratings

Maximum Input Power

0.5GHz :+27dBm Power

0.5-2GHz :+34dBm

APPENDIX A

Supply Voltage

Vcc	:+5.5V
Vee	:-8.5V
Control Voltage	:-0.5V to Vcc+0.5V
Operating Temperature	:-40°C to +125°C
Storage Temperature	:-65°C to +150°C

Functional Schematic (Top View)

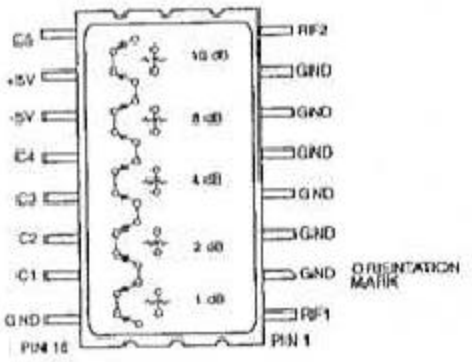

Figure A.4: Functional Schematic and Pin Assignments of AT20-0263

Truth Table

CONTROL INPUTS					
C5	C4	C3	C2	C1	Attenuation
0	0	0	0	0	Reference
0	0	0	0	1	1dB
0	0	0	1	0	2dB
0	0	1	0	0	4dB
0	1	0	0	0	8dB
1	0	0	0	0	16dB
1	1	1	1	1	31dB

0=TTL Low 1=TTL High

Table A.9: Truth Table

Package Dimensions

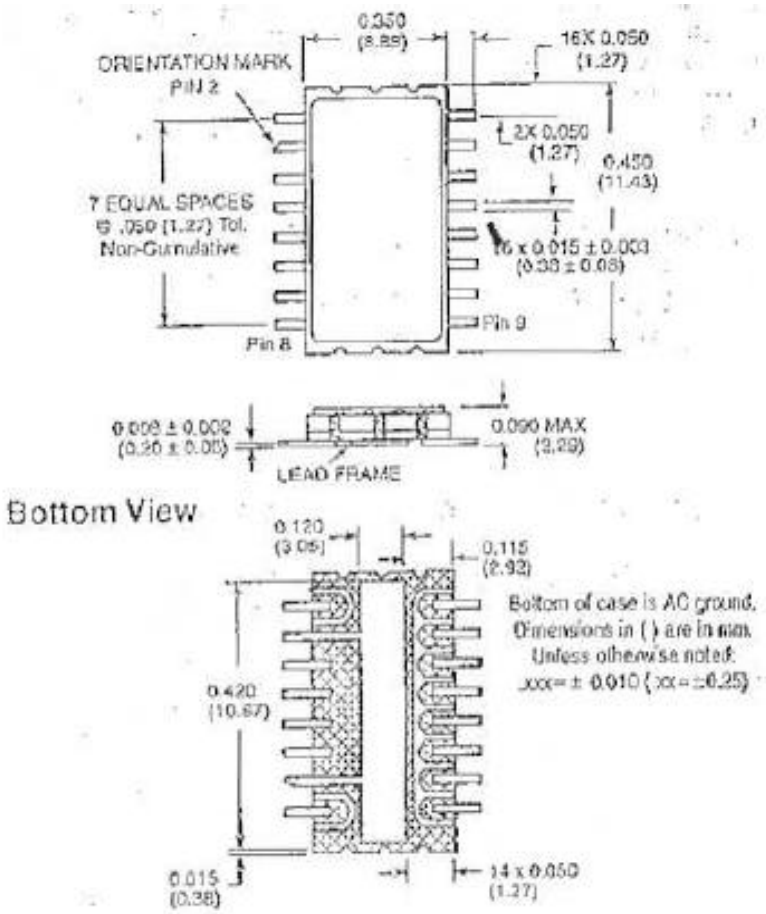

Figure A.5: Package Dimensions

- **FILTER**

Filter is designed for this work and schematic view is shown in Figure A.6.

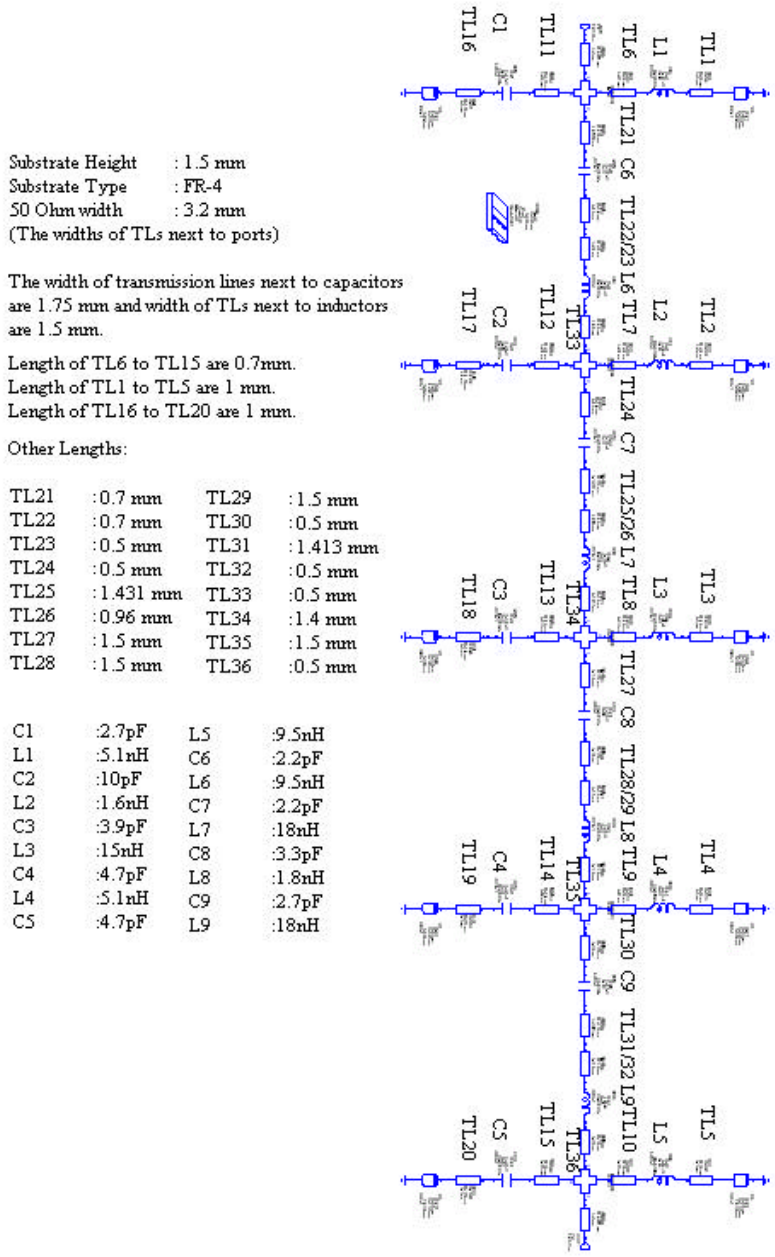

Figure A.6: 600MHz - 900MHz Filter Schematic View

APPENDIX A

Specifications

Frequency Range : 600MHz – 900 MHz

Power Rating : +20 dBm

Design Details : [42]

S-parameters were included in measurements.

- **POWER DIVIDER**

A power divider (Wilkinson) is designed for this study and schematic view is shown in Figure A.7.

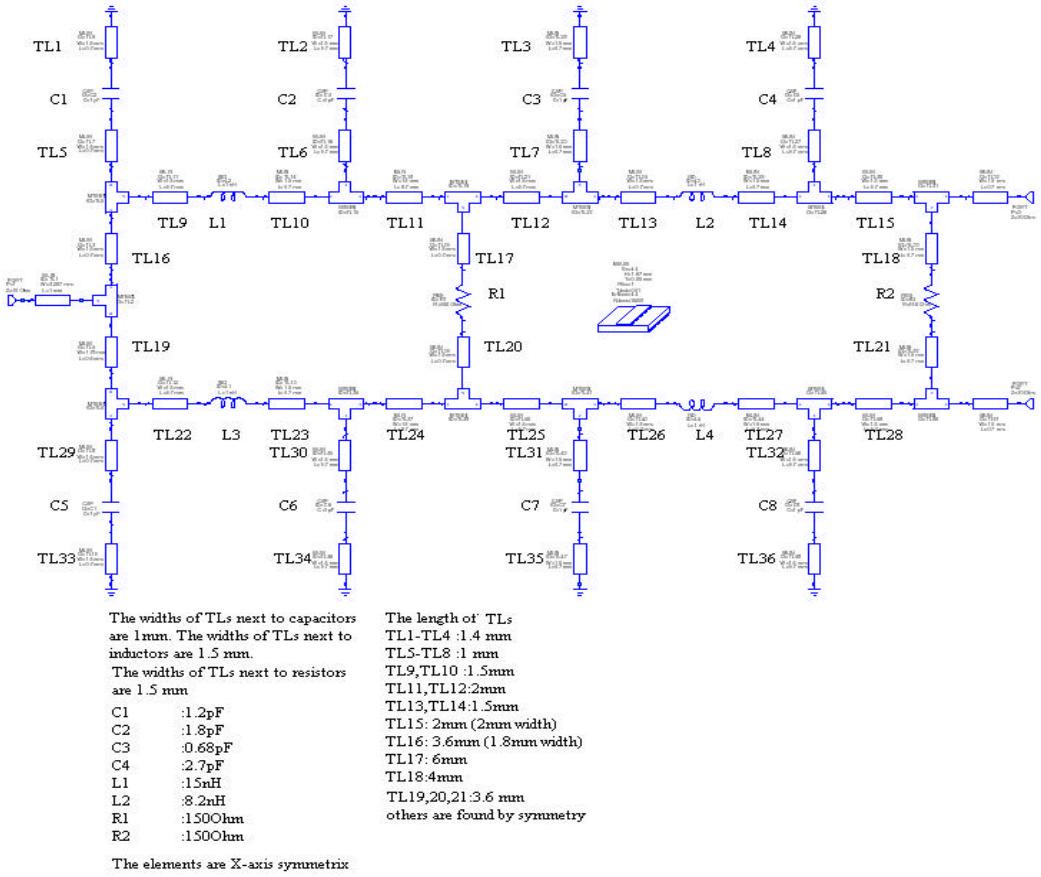

Figure A.7: Schematic view of power divider

APPENDIX A

Frequency Range : 600MHz – 900 MHz

Power Rating : +20 dBm

S-parameters were included in measurements.

Design Details : [24]

- **VOLTAGE CONTROLLED OSCILLATOR**

Manufacturer : Mini Circuits

Manufacturer's Type Number: JTOS 1025

Detailed Catalogue : http://www.minicircuits.com

Electrical Specifications

JTOS-1025

Freq. MHz		Power Output dBm		Tuning Voltage V		Phase Noise dBc/Hz SSB at offset frequencies: Typ.					Pulling MHz pk-pk @ 12 dBr	Pushing MHz/V	Tuning Sensitivity MHz/V	Harmonics dBc		3dB Modulation Bandwidth kHz	Power Supply	
Min.	Max.	Typ.	Aux.	Min.	Max.	100 Hz	1 kHz	10 kHz	100 kHz	1 MHz	Typ.	Typ.	Typ.	Typ.	Max.	Typ.	Voltage V	Current mA Max
685 - 1025.0		8.6		1.0 - 16.0			- 70.000	- 94.000	- 114.000	- 134.000	5.0	0.60	21.0 - 36.0	- 28.0	-20.0	100.0	12	22

Table A.10: Specifications of JTOS 1025

Outline Drawing

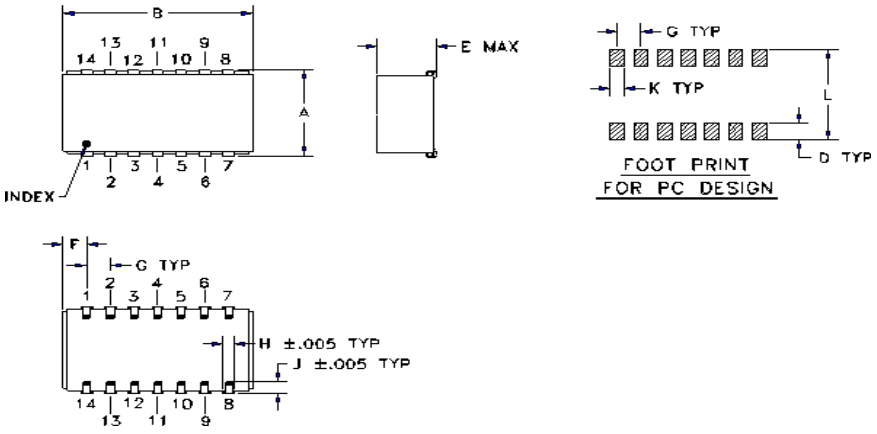

Figure A.8: Outline Drawing of JTOS-1025

Pin Connections

Pin Connections				
Port	RF OUT	V-CC	V-TUNE	GND EXT
jc	13	2	5	1,3,4,6,7,8,9,10,11,12,14

Table A.11: Pin Assignments

Dimensions

Case Style - BK377 (inch,mm) weight: 3.00 grams.

A	B	C	D	E	F	G	H	J
.505	.800		.100	.250	.100	.100	.047	.065
12.827	20.320		2.540	6.350	2.540	2.540	1.194	1.651

K	L	M	N	P	Q	R	S	T
.065	.525							
1.651	13.335							

Tolerance: .x ± .1 .xx ± .03 .xxx ± .015 inch.

Table A.12: Dimensions

APPENDIX A

Performance Data

Tuning Characteristics MHz/V			Power Output dBm			Harmonics Suppression dBc		
V-Tune	Frequency (MHz)	Tuning Sensitivity	-55°C	+25°C	+85°C	F2	F3	F4
1.0	625.30	77.10	6.66	6.22	4.82	-23.40	-35.60	-30.60
2.0	673.60	48.30	8.22	7.67	6.75	-25.70	-35.70	-37.10
3.0	708.60	35.00	8.85	8.66	7.99	-25.60	-42.60	-42.50
4.0	738.60	29.90	8.36	8.21	8.04	-23.60	-41.90	-48.90
5.0	765.30	26.80	8.06	7.83	7.50	-21.00	-35.00	-42.60
6.0	791.20	25.90	8.10	7.97	7.40	-22.50	-33.20	-43.50
7.0	822.20	31.00	8.31	7.94	7.57	-27.40	-34.60	-43.60
8.0	853.60	31.40	8.59	8.40	7.83	-28.60	-35.10	-43.70
9.0	882.60	29.00	9.06	9.10	8.69	-28.60	-37.30	-45.80
10.0	913.60	31.00	8.88	8.83	8.69	-29.00	-41.50	-48.40
11.0	947.70	34.10	8.98	8.90	8.75	-29.50	-46.50	-48.70
12.0	978.90	30.50	9.15	9.29	8.94	-30.30	-47.10	-46.80
13.0	1005.50	27.30	9.49	9.44	9.04	-32.20	-45.70	-46.20
14.0	1029.70	24.20	10.16	9.95	9.51	-34.60	-45.70	-45.60
15.0	1051.00	21.30	10.30	9.89	9.91	-38.50	-47.70	-44.70
16.0	1069.70	18.70	9.69	10.17	9.98	-42.40	-49.70	-45.20

Table A.13: Performance Data 1

	Frequency (MHz) Varies With Temperature			Freq. Pushing (MHz/V) (Referred To Vcc)
V-Tune	-55°C	+25°C	+85°C	12V
1.0	628.98	625.29	619.33	2.12
2.0	677.46	673.58	666.63	0.34
3.0	712.87	708.62	701.19	0.04
4.0	743.18	738.55	730.37	0.25
5.0	769.79	765.32	756.55	0.34
6.0	795.71	791.21	783.06	0.36
7.0	827.70	822.18	814.32	0.57

8.0	859.42	853.56	844.82	0.21
9.0	888.68	882.60	873.53	0.02
10.0	920.11	913.62	905.36	1.02
11.0	954.59	947.74	938.26	0.82
12.0	985.45	978.88	967.90	0.47
13.0	1012.98	1005.53	994.57	0.27
14.0	1037.61	1029.75	1018.16	0.09
15.0	1059.36	1051.05	1038.79	0.09
16.0	1078.54	1069.71	1056.70	0.29

Table A.14: Performance Data 2

Phase Noise	
Carrier Offset (Hz)	SSB Phase Noise (dBc/Hz)
1000	-70
10000	-94
100000	-114
1000000	-134

Table A.15: Phase Noise

- **COUPLER**

Manufacturer :M/A-COM

Description : Hybrid, Broadband, 180 degrees phase shift.

Connector : SMA

No detailed data is present. For S parameters, refer to measurements.

- **ATTENUATOR**

Manufacturer : Huber Suhner

Manufacturer Type Number : 66XX.19.AB

XX = value of attenuation (3dB => XX = 03)

Detailed Catalogue : http://www.hubersuhner.com

Electrical Specifications

Nominal Impedance : 50Ohm

Attenuation Values : 1 to 30dB

Frequency Range : DC to 12.4GHz

Power Rating : 2 W average power to 30 ^{o}C ambient temperature, linearly derated to 0 W at 130 ^{o}C ambient temperature.

Power Coefficient : 0.001 dB/dB/W

Temperature Coefficient : 0.0001 dB/dB/^{o}C

Mechanical Specifications

Dimensions : (h/w/l) 7.1/7.1/22.04 (mm)

Weight : 0.004 Kg / 0.14 oz

- **CABLES**

Manufacturer : Astrolab INC.

Manufacturer Type Number : Minibend-X, where X is the length in inches.

Description : Flexible coaxial cable

APPENDIX A

Electrical Specifications

Assembly No.	Ref. No.	DIM. "L"	2.0 GHz VSWR	2.0 GHz LOSS, dB	12.4 GHz VSWR	12.4 GHz LOSS, dB	18.0 GHz VSWR	18.0 GHz LOSS, dB	24.0 GHz VSWR	24.0 GHz LOSS, dB
minibend-2.5	32081-2-29094C-2.5	2.50 (63.5)	1.20	0.18	1.25	0.36	1.37	0.50	1.45	0.57
minibend-3	32081-2-29094C-3	3.00 (76.2)	1.20	0.19	1.25	0.40	1.37	0.55	1.45	0.64
minibend-3.5	32081-2-29094C-3.5	3.50 (88.9)	1.20	0.21	1.25	0.44	1.37	0.60	1.45	0.70
minibend-4	32081-2-29094C-4	4.00 (101.6)	1.20	0.23	1.25	0.48	1.37	0.65	1.45	0.75
minibend-4.5	32081-2-29094C-4.5	4.50 (114.3)	1.20	0.24	1.25	0.54	1.37	0.70	1.45	0.82
minibend-5	32081-2-29094C-5	5.00 (127.0)	1.20	0.26	1.25	0.57	1.37	0.75	1.45	0.87
minibend-5.5	32081-2-29094C-5.5	5.50 (139.7)	1.20	0.27	1.25	0.62	1.37	0.80	1.45	0.93
minibend-6	32081-2-29094C-6	6.00 (152.4)	1.20	0.29	1.25	0.65	1.37	0.85	1.45	0.99
minibend-6.5	32081-2-29094C-6.5	6.50 (165.1)	1.20	0.30	1.25	0.70	1.37	0.90	1.45	1.04
minibend-7	32081-2-29094C-7	7.00 (177.8)	1.20	0.32	1.25	0.74	1.37	0.95	1.45	1.10
minibend-7.5	32081-2-29094C-7.5	7.50 (190.5)	1.20	0.34	1.25	0.78	1.37	1.00	1.45	1.16
minibend-8	32081-2-29094C-8	8.00 (203.2)	1.20	0.35	1.25	0.82	1.37	1.05	1.45	1.22
minibend-9	32081-2-29094C-9	9.00 (228.6)	1.20	0.38	1.25	0.91	1.37	1.15	1.45	1.35
minibend-10	32081-2-29094C-10	10.00 (254.0)	1.20	0.41	1.25	0.98	1.37	1.24	1.45	1.46
minibend-10.5	32081-2-29094C-10.5	10.50 (266.7)	1.20	0.43	1.25	1.03	1.37	1.29	1.45	1.52
minibend-11	32081-2-29094C-11	11.00 (279.4)	1.20	0.44	1.25	1.07	1.37	1.34	1.45	1.58
minibend-12	32081-2-29094C-12	12.00 (304.8)	1.20	0.47	1.25	1.15	1.37	1.42	1.45	1.68
minibend-13	32081-2-29094C-13	13.00 (330.2)	1.20	0.50	1.25	1.23	1.37	1.53	1.45	1.81
minibend-14	32081-2-29094C-14	14.00 (355.6)	1.20	0.53	1.25	1.30	1.37	1.62	1.45	1.92
minibend-15	32081-2-29094C-15	15.00 (381.0)	1.20	0.57	1.25	1.40	1.37	1.73	1.45	2.04
minibend-16	32081-2-29094C-16	16.00 (406.4)	1.20	0.60	1.25	1.47	1.37	1.82	1.45	2.15

Table A.16: Electrical Specifications for Minibend cables

- **IF AMPLIFIER AND FILTER (INSTRUMENT)**

Manufacturer : Stanford Research Systems
Manufacturer type number : SR560

Detailed Catalogue :

http://www.thinksrs.com/downloads/PDFs/Catalog/SR560c.pdf

A.3 Abbreviations

Abbreviations used through this work and their meanings are shown in **Table A.17**.

Abbreviation	Meaning
SQUID	Superconducting Quantum Interference Device
RF	Radio Frequency
LO	Local Oscillator
IF	Intermediate Frequency
Vspp	Peak to Peak SQUID Voltage
S parameter	Scattering Parameter
IP2	Second order intercept point
IP3	Third order intercept point
Spur	Spurious Responses
CR	Cochannel Rejection
BW	Bandwidth
Q	Quality Factor
F	Noise Factor
RL	Return Loss
IL	Insertion Loss
SERL	Superconducting Electronics Research Laboratory

Table A.17: Abbreviations and their meanings

Bibliography

[1] Online material, http://www.chemsoc.org

[2] A. Braginski, J. Clarke, "SQUID Handbook : Volume 1 : Fundamentals and Technology of SQUIDs and SQUID Systems", Chapter 1, Weinheim: Wiley-VCH Verlag GmbH & Co. KgaA, 2004.

[3] R. Akram, "HTSC Superconducting Edge-Transition Infrared Detectors; Principles, Fabrication and Characterization", Master's Thesis, Bilkent University, January 2000.

[4] T. V. Duzer, C. W. Turner, "Principles of Superconductive Devices and Circuits", New Jersey: Prentice Hall, 1999.

[5] M. Tinkham, "Introduction to Superconductivity", New York: McGraww-Hill, Inc., 1996.

[6] J.G. Bernorz and K.A. Müller, "Possible High T_c Superconductivity in the Ba-La-Cu-O System", Z. Phys. B, Vol.64, pp. 189-193, January 1986

[7] Burns, Gerald, "High Temperature Superconductivity: An Introduction", Boston: Academic Press, 1992.

[8] Blatt, John M., "Theory of Superconductivity", San Diego: Academic Press, 1964.

[9] Parks, R. D., "Superconductivity", New York: M. Dekker, 1969.

[10] W. G. Jenks, S. S. H. Sadeghi and J. P. Wiksko Jr, "SQUIDs for Nondestructive Evaluation", Appl. Phys. 30 (1997) 293-323.

[11] Kulik, Igor Orestovich, "The Josephson Effect in Superconducting Tunneling Sructures", Jerusalem: Israel Program for Scientific, 1972.

[12] W. Göpel, J. Hesse, J. N. Zemel, "Sensors, A Comprehensive Survey", Vol 5, Chapter 10, Physikalisch-Technische Bundesanstalt, Berlin, 1989.

[13] H. M. Mück, "Developments and Characterization of low noise rf-SQUIDs", Justus Liebig Universität Gießen, 1995.

[14] Wolaver Don H., "Phase-Locked Loop Circuit Design", New Jersey: Prentice Hall, Inc., 1991.

[15] Tesche, C. D. , Clarke, J., J. Low Temperature Physics 29 (1977), 301-331.

[16] A. I. Braginski, H. –J. Krause and J. Vrba , "SQUID Magnetometers (A volume of "Handbook of Thin Film Devices: Frontiers of Research, Technology and Applications")", submitted April 27, 1999; to be published 1999 by Academic Press, San Diego.

[17] S. Ramo, J. R. Whinnery, and T. Van Duzer, "Fields and Waves in Communication Electronics", New York: John Wiley & Sons, 1994, p.91.

[18] Rizwan Akram, "Development of Superconducting SQUID Magnetic Sensor for Scanning SQUID Microscope Applications", Ph.D. Thesis, Bilkent University, will be submitted in July 2005.

[19] M. Fardmanesh, J. Schubert, R. Akram, M. Bick, W. Zander, Y. Zhang, M. Banzet, and J.-H. Krause, "Asymmetric multi-junction YBCO rf-SQUID magnetometer and gradiometer designs on bi-crystal substrates and the noise and

junctions characteristics", in International Superconductive Electronics Conference (ISEC), Osaka, Japan, 2001.

[20] Fleming D., Gershenson M., Schneider R., Sweeny M., "Hybrid DC SQUID Fabrication and Characterization", IEEE Transactions on Magnetics, Volume 19, Issue 5, 1983.

[21] A. I. Braginski, in: H. Weinstock (Ed.), "SQUID Sensors: Fundamentals, Fabrication and Applications", Nato ASI Series, Kluwer Academic, Dordrecht, 1996.

[22] Online Document, http://www.coolchips.sfsu.edu/student_talks_Sept_2002/Yien_talk_done.pdf

[23] Online Document, http://www.jsquid.com/

[24] Peter Vizmuller, "RF Design Guide: Systems, Circuits and Equations", 1st Edition, Artech House Publishers, 1995.

[25] Meehan, M. D., and J. Purviance, "Yield and Reliability in Microwave and Circuit and System Design", Norwood. MA: Artech House, 1993.

[26] Smith, P. G., and D. G., Reinertsen, "Developing Products in Half the Time", New York: Van Nostrand Reinhold, 1991.

[27] Erne, S. N. et al., J. Applied Physics, 47, (1976), 5440-5442.

[28] A. Barone, G. Patérno, "Physics and Applications of Josephson Junctions", New York: John Wiley and Sons, 1982.

[29] Y.D. Dai, S.G.Wang and S.W. Du , "Probing Paring Symmetry of Superconductors by using r.f. SQUID", Solid State Communications, Vol.108, No. 4, pp251-254, 1998.

[30] F. Yoshihara, I Kanno, K. Shinada, "Rf-SQUID Microcalorimeter", Superconductor Science and Technology, Vol.16 (2003), 1257-1261.

[31] H.R. Yi, Y. Zhang, H. Bousack, and A. I. Braginski, "High Frequency Coupling Coefficient between the Coplanar Resonator and Radio Frequency SQUID", IEEE Transactions on Applied Superconductivity, Vol.9 , Issue 2, 4400-4403.

[32] D.F. He, X.H. Zeng, H.J. Krause, H. Soltner, F. Rüders, and Y. Zhang, "Radio Frequency SQUIDs Operating at 77K with 1 GHz Lumped-Element Tank Circuits.", Appl. Phys., Lett., vol.72, pp. 969-971, Feb. 1998.

[33] D. K. Cheng, "Field and Wave Electromgnetics", Second Edition, Massachusetts, Addison-Wesley Publishing Company, 1989.

[34] R. Kazazoglu, "The Design and Implementation of an Optimized Tank Circuit for rf-SQUID Electronics with an Operating Frequency of 2GHz at Liquid Nitrogen Temperature", Senior Design Project, Bilkent University, 2003.

[35] C. Bowick, "RF Circuit Design", USA: Howard W. Sams & Company, Inc., 1982.

[36] R. Ludwig, P. Bretchko, "RF Circuit Design", New Jersey: Prentice Hall, 2000.

[37] Schwartz Mischa, "Information Transmission, Modulation & Noise; A Unified Approach to Communication Systems", New York: McGraw Hill, Inc., 1970.

[38] Simon Haykin, "Communications Systems", New York: Wiley, 2000.

[39] K. Chang, "Handbook of Microwave and Optical Components", Volume 1, New York, Wiley-Interscience Publication, 1989.

[40] J. Bao, Y/ Tsui, "Microwave Receivers with Electronic Warfare Applications", New York: John Wiley & Sons, Inc., 1986.

[41] D. M. Pozar, "Microwave Engineering", 2nd Edition, New York: John Wiley & Sons, Inc., 1998.

[42] R. W. Rhea. "HF Filter Design and Computer Simulation", Atlanta: Noble Publishing, 1994.

[43] Balanis, Constantine A., "Advanced Engineering Electromagnetics", New York : Wiley, 1989.

[44] Paul, Clayton R., "Introduction to Electromagnetic Compatibility (EMC)", New York: John Wiley & Sons Ltd., 1992.

[45] M. Fardmanesh, J. Schubert, R. Akram, M. Bick, Y. Zhang, M. Banzet, W. Zander, H.-J. Krause, H. Burkhart, and M. Schilling, "1/f Noise Characteristics of SEJ Y-Ba-Cu-O rf-SQUIDs on $LaAlO_3$ Substrate and the Step Structure, Film, and Temperature Dependence", IEEE Transactions on Applied Superconductivity, Vol 11, No.1, March 2001.

[46] M. Fardmanesh, J. Schubert, M. Banzet, W. Zander, Y. Zhang, J. Krause, "Effects of the Step Structure on the Yield, Operating Temperature, and the Noise in SEJ rf-SQUID Magnetometers and Gradiometers"., Physica C., 2001, pp. 40-44.